REVISTA DE LA REAL ACADEMIA DE CIENCIAS Exactas Físicas Químicas y Naturales DE ZARAGOZA

Serie 2.ª
Volumen 67

2012

ÍNDICE DE MATERIAS

Rev. Real Academia de Ciencias. Zaragoza. **67:** 7–49, (2012).
ISSN: 0370-3207

Optimization of spatial and temporal discretization schemes for Computational Aero Acoustics problems

L. Rández

Departamento de Matemática Aplicada - IUMA

Universidad de Zaragoza. c/ Pedro Cerbuna 12, 50009 Zaragoza, SPAIN.

Premio a la Investigación de la Academia 2012. Sección de Exactas

Abstract

In this paper new finite difference (FD) and Runge–Kutta schemes for Computational Aero Acoustics (CAA) that minimize the total dispersion and dissipation errors arising in the spatial and temporal discretization process are derived. The available parameters in the spatial discretization as well as in the time marching Runge–Kutta scheme are selected so that they minimize a measure of the total dispersion and dissipation errors for linear wave propagations. These schemes are fourth-order accurate in space with finite differences and a resolution with number of points greater or equal to nine together with fourth-order six-stage low storage Runge–Kutta methods for the time integration. The new schemes are tested on a one dimensional convection equation involving long-range sound propagation, and on one-dimensional Euler problems. The numerical results obtained with these test problems indicate an important improvement in accuracy and in numerical efficiency when they are compared with other low dispersive and low dissipative explicit schemes recently published.

Key Words: Computational Aero Acoustics; Low dispersion and dissipation; Finite difference schemes; Low storage Runge–Kutta methods; Optimization
AMS classification: 65C20; 65M20; 76Q05

1 Introduction

In the field of Computational Aero-Acoustics (CAA) the prediction of sound far from its source implies the need of accurate and stable numerical algorithms. As it has been widely recognized [3, 19, 21] stable and high order convergent schemes do not guarantee

a good behavior in the numerical approximation of aero acoustics problems. The main reason is that acoustic waves are non-dispersive and non-dissipative in their propagation and can travel long distances in all directions. Consequently, the numerical schemes must be designed by minimizing the dispersion and dissipation errors in long-time integrations. Note that in standard computational fluid dynamics (CFD) codes a dissipation (in many cases artificial) is included to stabilize the schemes and therefore such schemes are not suitable for CAA problems. In addition, to minimize the dispersion and dissipation errors for the required range of frequencies, large stability limits of the time advancing scheme are also necessary to control the error propagation and also low storage algorithms to improve the efficiency of high dimensional problems must be taken into account.

The construction of optimized time advancing Runge–Kutta (RK) schemes have been considered by several authors [1, 4, 5, 6, 10, 12, 13, 20] which propose a number of low dispersive and low dissipative RK algorithms in standard or in low storage form.

Concerning the spatial discretization, standard schemes have at least second or fourth-order of accuracy and for symmetric stencils they pay special attention to dispersion error. So, in a number of papers [10, 16, 17, 18, 22] Pade or compact type, finite volume (FV) and finite difference (FD) schemes have been proposed by choosing the available parameters so that they minimize the dispersion error. Recently, Bogey and Bailly [3] have optimized central FD schemes with a number of points greater or equal to nine for spatial derivation by minimizing their dispersion and dissipation errors in a range of wavenumbers. Such optimal schemes have algebraic order four and permit calculate linear waves with about four points per wavelength for an accuracy limit, and they are shown to be more accurate and efficient than the standard FD schemes of high order. These authors also have optimized RK algorithms with five and six-stages for time advancing by minimizing their dispersion and dissipation errors for the same range of wavenumbers. These optimized RK algorithms have algebraic order two, and they are shown to be more efficient than the standard fourth-order RK method. Next, Berland *et al.* [2] have optimized a fourth-order six-stage low storage RK algorithm that has similar properties to RK algorithms given in [3] for linear operators, and in addition it is more adequate for nonlinear problems because of its high algebraic order.

All optimal time advancing RK schemes given in [2, 3, 4, 5, 12] have in common that they are derived by minimizing some measures of the dispersion and dissipation errors introduced by the temporal discretization with some additional stability bounds. Clearly these schemes make sense when applied to very accurate space discretizations. However, the dispersive and dissipative behavior of a discretization scheme depends on the total dispersion and dissipation errors introduced by the spatial and temporal discretizations. This fact led to Ramboer *et al.* [19] to consider the errors of both discretizations and to

derive some six-stage RK time advancing schemes by selecting the free parameters of the time advancing scheme such that minimize the total dispersion and dissipation errors for two specific spatial discretizations: fourth-order FV (finite volume) compact central and third-order FV upwind discretizations.

In this paper, new six-stage RK time advancing schemes coupled with new symmetric FD spatial discretizations are derived taking into account the total dispersion and dissipation errors introduced by both discretizations. Hence, the spatial and temporal discretizations are optimized simultaneously in contrast with the optimization carried out by other authors [2, 3, 12]. The main difference with the optimization carried out in [19] is that we select also the free parameters of the spatial discretization so that they minimize the total dispersion and dissipation errors. The motivation is to provide explicit numerical schemes according to accuracy and stability requirements usually demanded in CAA. The paper is organized as follows: In section 2 we analyze the dispersion and dissipation errors for schemes constituted by finite differences for the spatial derivation and Runge–Kutta algorithms for the time integration (FD-RK schemes). In section 3 we present the optimization process and we derive optimized FD-RK schemes by minimizing their total dispersion and dissipation errors. These schemes are fourth-order central FD with a number of points greater or equal to nine and fourth-order six-stage RK algorithms. In section 4 we construct the fourth-order six-stage RK algorithms in low storage form. In section 5 some numerical experiments are presented comparing the accuracy and the efficiency of the new optimized FD-RK schemes with other low dispersive and low dissipative explicit schemes given in [2] and [3]. The final section is devoted to conclusions.

2 Dispersion and dissipation for FD-RK schemes

In this section we review briefly some results on the Fourier analysis of FD-RK schemes when applied to the linear scalar wave test equation for $u = u(t, x)$

$$\frac{\partial u}{\partial t} + c\frac{\partial u}{\partial x} = 0, \quad x \in \mathbf{R},\ t \geq 0, \tag{1}$$

with a given initial condition $u(0, x) = \Phi(x)$ where $c > 0$ is the velocity of the wave.

For the spatial discretization we will consider central finite difference schemes δ_x with a $(2N + 1)$-point stencil of type

$$\delta_x u(t, x_\ell) = \frac{1}{\Delta x} \sum_{j=-N}^{N} a_j\, u_{\ell+j}, \quad u_k = u(t, x_k), \tag{2}$$

where Δx is the mesh spacing and $x_j = j\,\Delta x$. Usually, the real coefficients a_j are taken such that the approximation (2) is of order p, i. e.

$$\partial_x u(t, x_\ell) - \delta_x u(t, x_\ell) = \mathcal{O}\left(\Delta x^p\right), \qquad p \geq 1, \tag{3}$$

and therefore the coefficients a_j must satisfy the following linear conditions:

$$\sum_{j=-N}^{N} j^s a_j = \delta_{1,s}, \quad s = 0, 1, \ldots, p, \tag{4}$$

where $\delta_{p,q}$ is the Kronecker delta defined by $\delta_{1,s} = 0$, $s \neq 1$ and 1 otherwise. It can be easily seen that the maximum attainable order by a symmetric $(2N+1)$-point stencil FD is $(N+1)$ for N even and N otherwise.

By using the spatial discretization (2), the semidiscretization of the convective equation (1) is

$$\partial_t u_j + \frac{c}{\Delta x} \sum_{\ell=-N}^{N} a_\ell \, u_{j+\ell} = 0, \qquad j = 0, \pm 1, \ldots \tag{5}$$

First, we present the results of some numerical experiments. So, we display in Figure 1 the numerical solution obtained by solving exactly the semidiscretization of the wave equation (1) given by

$$\begin{cases} \partial u_j + c\delta_x u_j = 0, \quad t \in [0, 400], \\ u_j(0) = \Phi(x_j), \end{cases} \tag{6}$$

for the maximum order $(2N+1)$-point symmetric schemes (2) for $N = 3, 4, 5$ with $c = 1$, and the Gaussian initial condition $\Phi(x) = \Phi_1(x) = 0.5\exp(-x^2/9)$, $\Delta x = 1$, $x_j = j$, $j = -50, \ldots, 450$ at the time instant $t = 400$ together with the exact solution of the wave equation. Note that the exact solution is a Gaussian type wave that moves from left to right with constant velocity $c = 1$ preserving its shape, so that $u(x,t) = \Phi_1(x - t)$.

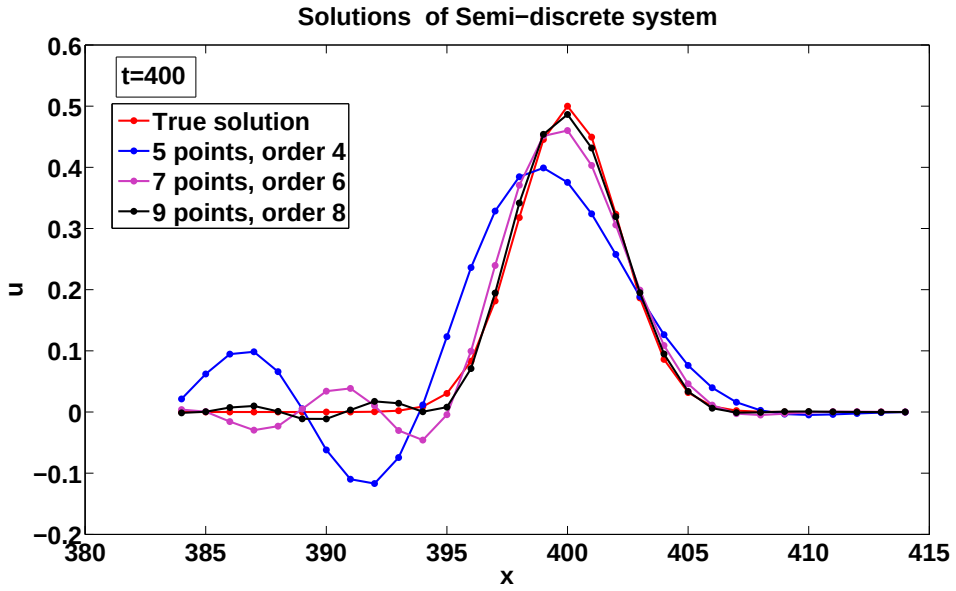

Figure 1: Numerical solution of the linear wave test equation semidiscretized with $(2N+1)$-point central symmetric schemes for $N = 2, 3, 4$.

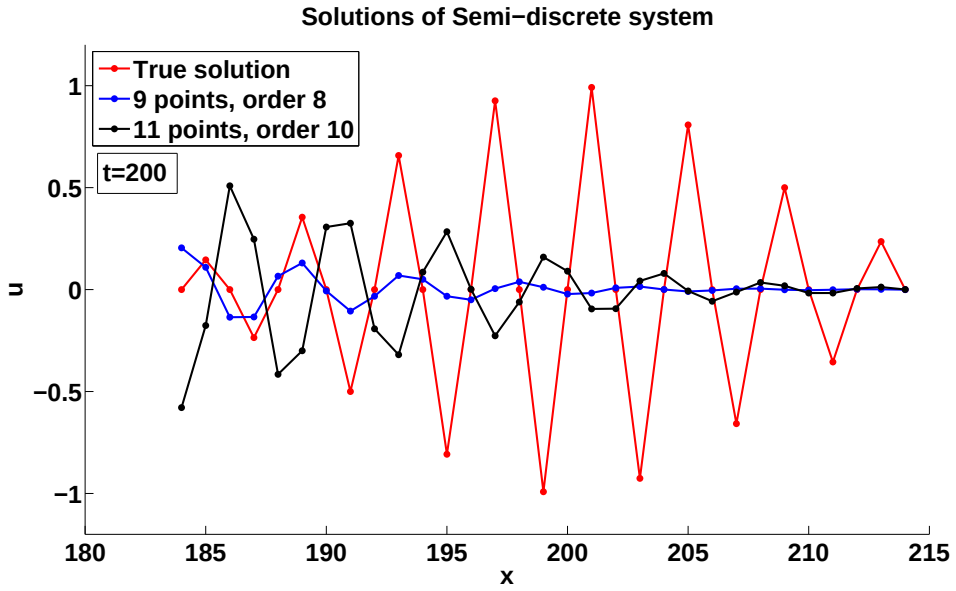

Figure 2: Numerical solution of the wave test equation, Sine-Gaussian initial condition, semidiscretized with $(2N+1)$-point schemes for $N = 4, 5$.

From Figure 1, it follows that for in the case of the fourth-order discretization, the spatial dispersion errors introduce strong changes in the shape of the wave and that these changes are smaller when the order increases, but in any case they are not negligible.

In Figure 2 we present the solutions obtained taking a Sine-Gaussian initial condition given by $\Phi(x) = \Phi_2(x) = \sin(\pi x/2)\ \exp(-x^2/9)$ for $\Delta x = 1$, $x_j = -50, \ldots, 250$, where the time interval is $[0, 200]$. Now, since the problem is more difficult due to the spectral contents of $\Phi_2(x)$, we have taken the higher order spatial symmetric discretizations of orders 8 and 10 corresponding to 9 and 11 points respectively. Now even with the high order spatial discretizations the profile of the wave is destroyed.

In order to explain the behavior of the spatial difference schemes, we apply to (1) and (5) the spatial Fourier transforms given in the continuous and discrete case respectively by

$$\widehat{u}(k,t) = \int_{-\infty}^{\infty} \mathrm{e}^{-ikx}\, u(x,t)\, \mathrm{d}x, \quad \widehat{u}(k,t) = \Delta x \sum_{j=-\infty}^{j=+\infty} \mathrm{e}^{-ikx_j}\, u(x_j,t),$$

obtaining

$$\partial_t \bar{u}(k,t) + ick\ \bar{u}(k,t) = 0, \qquad \partial_t \widehat{u}(k,t) + ick^*\ \widehat{u}(k,t) = 0,$$
$$k \in \mathbb{R}, \qquad k \in [-\pi/\Delta x, \pi/\Delta x],$$

where k^* represents the numerical (complex) wavenumber of the FD scheme (i.e., an approximation to the the exact wavenumber k) which is given by

$$k^* = -\frac{i}{\Delta x} \sum_{\ell=-N}^{N} a_\ell\, \mathrm{e}^{i(\ell\, k\Delta x)}. \tag{7}$$

For a given N, the quantity $k^*\Delta x$ is usually called the effective or numerical wavenumber and as follows from (7) is a function of the exact wavenumber $k\Delta x$. Further, for a discretization with order p, exact and effective wavenumbers agree up to order $(\Delta x)^{p+1}$ and $(k^*\Delta x)/(k\Delta x) \to 1$ as $\Delta x \to 0^+$. However when $k\Delta x \leq \pi$ separates from 0, the dispersion error may become very large. In Figure 3 we show the behavior of $(k^*\Delta x)$ as a function of $(k\Delta x)$ for $2N+1 = 5, 7, 9, 11$ when $k\Delta x \in [0, \pi]$. In all cases $(k^*\Delta x)$ has a unique maximum $k_{\max}\Delta x$ in this interval and this implies that clearly those waves with $k \geq k_{\max}$ will be badly represented by the spatial discretization. In other words, for the $(2N+1)$-point stencil finite difference scheme of maximum order, the spectral components of the initial condition $\Phi(x)$ with wavenumbers $k \geq k_{\max}$ are not suitably represented by the discretization (2).

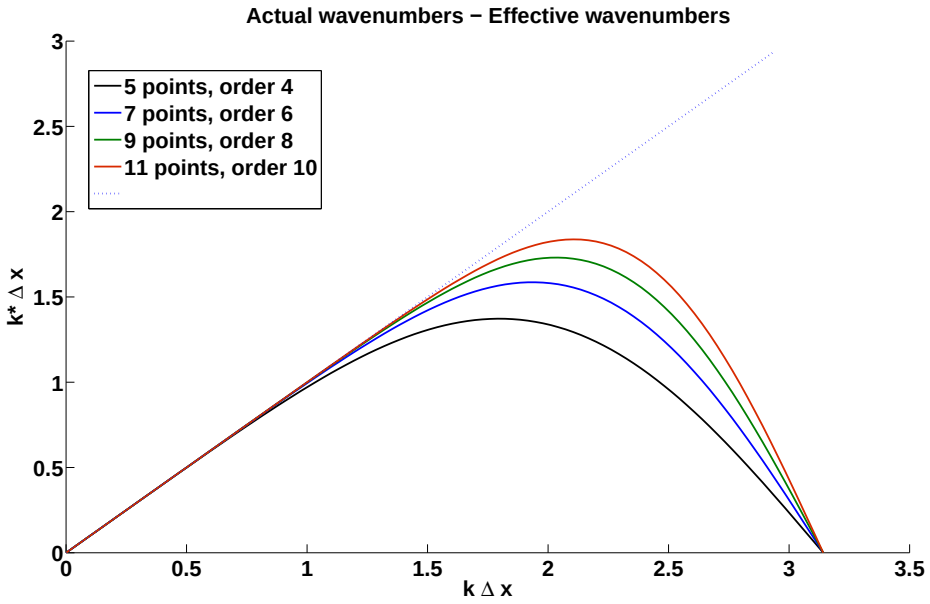

Figure 3: Numerical scaled wavenumbers versus actual scaled wavenumbers.

In addition to this, it has been remarked by several authors [22] that the requirement $k \leq k_{\max}$ is not enough to ensure a good dispersion behavior of the spatial discretization because even for $k \lesssim k_{\max}$ the error in the numerical wavenumber can be large. Then, Tam *et al.* [22] introduced the additional condition

$$k \leq k_c = \max\{k \geq 0, |k - k^*| \leq \varepsilon\}, \tag{8}$$

where ε is a small quantity that in some practical calculations has been taken empiricallly as $\varepsilon = 10^{-3}$ because it leads to a reasonable dispersion error. In Table 1 we present the values of $k_{\max}$ and k_c for the high order symmetric FD $(2N+1)$-points schemes with $N = 2, 3, 4, 5$.

Table 1: Dispersion values, $k_{\max}$ and k_c, for $(2N+1)$-points schemes with $N = 2, 3, 4, 5$

$2N+1$	order	$k_{\max}$	k_c
5	4	1.37	0.69
7	6	1.59	0.97
9	8	1.73	1.16
11	10	1.84	1.32

Taking into account the values in Table 1 it is possible to explain the numerical results of the above examples. In the first example, since the spectral contents of $\Phi_1(x)$ is the right half of a Gaussian type function centered at $k = 0$, the methods with 11 points are able to deal accurately most of the relevant spectral contents of $\Phi_1(x)$ (see Figure 4). Nevertheless in the second example, since the Fourier contents is a Gaussian type function centered around $\pi/2$ all the considered methods cannot include the relevant spectral contents of $\Phi_2(x)$ and then it is not a suitable discretization for this function. To cope with problems

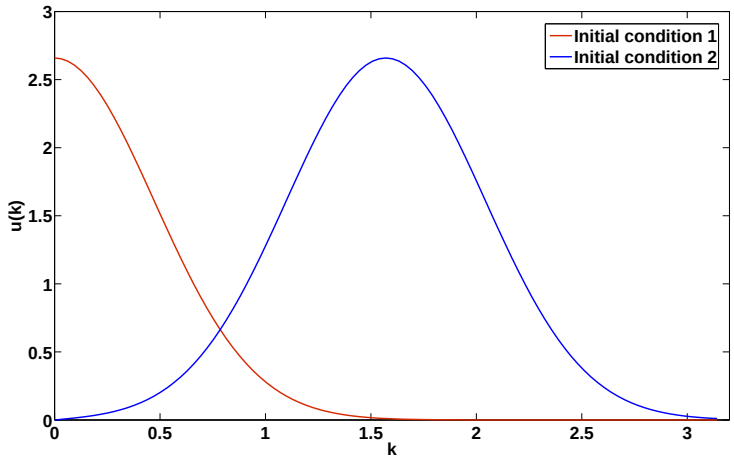

Figure 4: Spectral contents of $\Phi_i(x)$.

where the spectral contents of the solution is not close to the origin, several authors have proposed discretizations (2) with order smaller than the maximum order attainable and using the available parameters to get larger values of $k_{\max}$ and k_c. This idea was used by Tam and Webb [22] to derive two 7- and 9-point stencil discretizations called DRP (dispersion relation preserving methods) and more recently Bogey and Bailly [3] have constructed other 9-, 11- and 13-points discretizations. In Table 2 we collect the dispersion properties of these methods together with the standard symmetric finite difference ones.

Next, Figures 5 and 6 show the profiles of the semidiscrete and exact solutions at the final time in the above two examples for several optimized schemes. It must be noticed

Table 2: Dispersion values, $k_{\max}$ and k_c, for some standard and optimized difference schemes.

method	$2N+1$	**order**	$k_{\max}$	k_c
Symmetric FD	5	4	1.37	0.69
Symmetric FD	7	6	1.59	0.97
Symmetric FD	9	8	1.73	1.16
Symmetric FD	11	10	1.84	1.32
Tam-Webb	7	4	1.73	1.45
Tam-Webb	9	6	1.77	1.28
Bogey-Bailly	9	4	1.10	1.50
Bogey-Bailly	11	4	1.98	1.66
Bogey-Bailly	13	4	2.14	1.92

that in the second example, the 13-point discretization preserves quite accurately the shape of the wave.

2.1 Dispersion and dissipation of the spatial FD scheme

Comparing the exact solution of the linear wave equation (1) with the initial condition $u(x,0) = \mathrm{e}^{ikx}$ given by

$$u_{\mathrm{ex}}(x,t) = \mathrm{e}^{ik(x-ct)}, \tag{9}$$

and the corresponding to the semidiscretization (5)

$$u_{\mathrm{sd}}(x_j,t) = \mathrm{e}^{i(kx_j - k^* ct)}, \qquad j = 0, \pm 1, \ldots, \tag{10}$$

the dispersion and dissipation errors introduced by the spatial discretization are

$$\frac{u_{\mathrm{sd}}(x_j,t)}{u_{\mathrm{ex}}(x_j,t)} = \mathrm{e}^{i(k-k^*)ct} = \underbrace{\mathrm{e}^{\mathrm{Im}(k^*)ct}}_{\text{dissipation}} \underbrace{\mathrm{e}^{i(k-\mathrm{Re}(k^*))ct}}_{\text{dispersion}}. \tag{11}$$

If we denote

$$\phi_s(z) := k\Delta x - \mathrm{Re}(k^*\Delta x) = z - \sum_{j=1}^{N} (a_j - a_{-j}) \sin(jz), \tag{12}$$

$$d_s(z) := \mathrm{Im}(k^*\Delta x) = -a_0 - \sum_{j=1}^{N} (a_j + a_{-j}) \cos(jz), \tag{13}$$

equation (11) can be expressed as

$$\frac{u_{\mathrm{sd}}(x_j,t)}{u_{\mathrm{ex}}(x_j,t)} = \left[\mathrm{e}^{d_s(z)}\ \mathrm{e}^{i\phi_s(z))}\right]^{\frac{ct}{\Delta x}}. \tag{14}$$

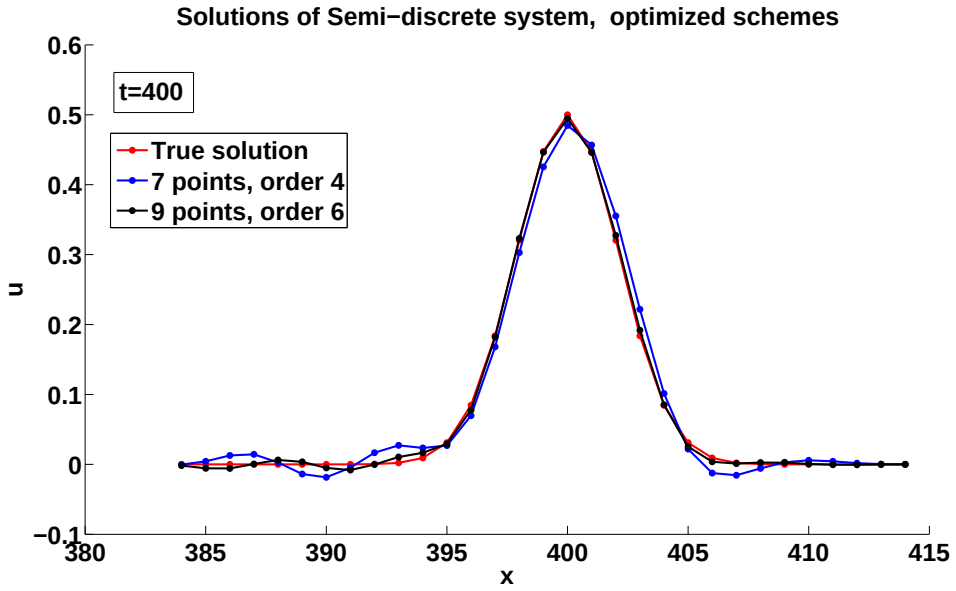

Figure 5: Numerical solution of the wave test equation, Gaussian initial condition, with optimized schemes with $N = 3, 4$.

Thus, the spatial dispersion error is: $\phi_s(z)$, the spatial dissipation error is: $1 - \mathrm{e}^{d_s(z)}$, and the central FD scheme is dispersive of order q and dissipative of order r if

$$\phi_s(z) = \mathcal{O}\left(z^{q+1}\right), \qquad d_s(z) = \mathcal{O}\left(z^{r+1}\right), \quad z \to 0. \tag{15}$$

If we consider symmetric FD schemes, then the coefficients satisfy

$$a_0 = 0, \qquad a_j = -a_{-j}, \quad j = 1, \ldots, N, \tag{16}$$

and in this case it follows from (7) that k^* is real and the schemes are zero-dissipative, i. e.

$$d_s(z) = 0, \qquad \phi_s(z) = z - 2\sum_{j=1}^{N} a_j \sin(jz). \tag{17}$$

2.2 Dispersion and dissipation of the time advancing RK scheme

To advance the solution $U(t) = (u_j(t))$ of a general differential system in ODE's

$$\partial_t U = F(t, U), \tag{18}$$

from the time level t^n to the next time level $t^{n+1} = t^n + \Delta t$ we will use explicit s-stage RK schemes [9] defined by the Butcher tableau

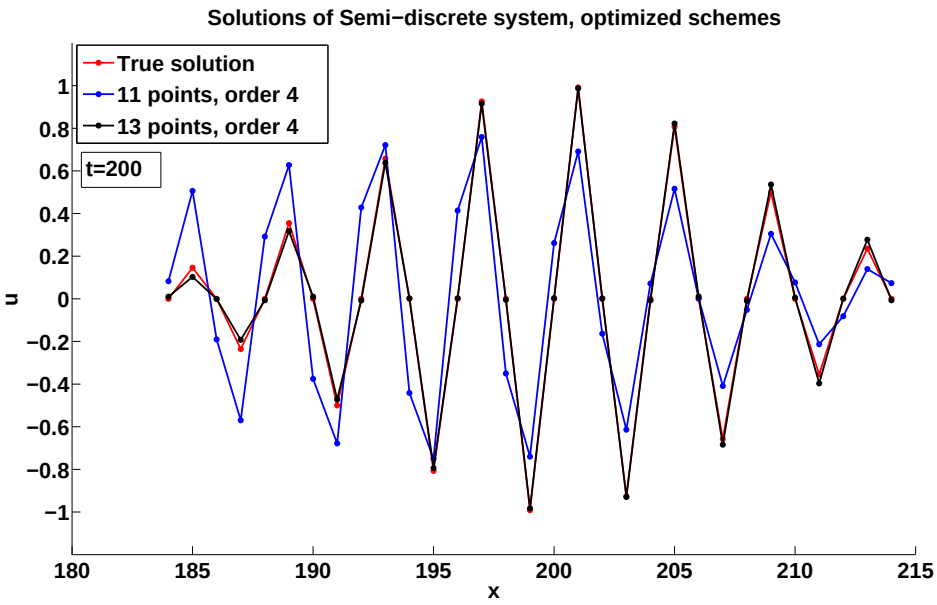

Figure 6: Numerical solution of the wave test equation, Sine-Gaussian initial condition, with optimized schemes with $N = 5, 6$.

$$\begin{array}{c|c} \mathbf{c} & \mathbf{A} \\ \hline & \mathbf{b}^T \end{array} \quad = \quad \begin{array}{c|ccccc} 0 & 0 & & & & \\ c_2 & a_{21} & 0 & & & \\ \vdots & \vdots & \ddots & \ddots & & \\ c_s & a_{s,1} & \cdots & a_{s,s-1} & 0 & \\ \hline & b_1 & \cdots & b_{s-1} & b_s \end{array} \tag{19}$$

with $\mathbf{c} = \mathbf{A}\mathbf{e}$, $\mathbf{e} = (1, \ldots, 1)^T, \mathbf{b} \in \mathbb{R}^s$. These coefficients b_j, c_j, and a_{jk} are real constants that define the method. The step from U^n at the time level t^n to U^{n+1} at the time level t^{n+1} can be written as

$$\begin{aligned} U^{n+1} &= U^n + \Delta t \sum_{i=1}^{s} b_i \, F_i, \\ F_i &= F(t^n + c_i \, \Delta t, \, U^n + \Delta t \sum_{j=1}^{i-1} a_{i\,j} \, F_j), \quad i = 1, \ldots, s. \end{aligned} \tag{20}$$

For autonomous equations $F(t, U) = \Lambda \, U$ with a linear operator Λ, the algorithm (20) becomes

$$U^{n+1} = R(\Delta t \, \Lambda) \, U^n, \tag{21}$$

where $R(\zeta)$ is the so called amplification function of (19) given by

$$R(\zeta) = 1 + \zeta \mathbf{b}^T (I - \zeta \mathbf{A})^{-1} \mathbf{e}, \qquad \zeta \in \mathbb{C}. \tag{22}$$

For explicit s-stage RK schemes the amplification function is a polynomial of degree $\leq s$ given by

$$R(\zeta) = 1 + \sum_{\ell=1}^{s} \gamma_\ell \, \zeta^\ell, \tag{23}$$

with $\gamma_\ell = \mathbf{b}^T \, \mathbf{A}^{\ell-1} \, \mathbf{e}$, and it satisfies

$$|R(-ix)| = |R(ix)|, \qquad \arg R(-ix) = -\arg R(ix), \quad \forall x \in \mathbb{R}. \tag{24}$$

Note that if the RK scheme (19) has linear order p then $\gamma_\ell = 1/\ell!$, $\ell = 1, \ldots, p$, and (23) is an approximation to the exponential function e^ζ at the origin at least of the same order.

In order to illustrate the behavior of standard RK time integrators, we start considering the application of the classical four-stage fourth-order RK4 method with a fixed step size to the semidiscretization (6) with initial condition $\Phi(x) = \Phi_1(x)$. Concerning the choice of the step size recall that when a scalar linear problem $y' = \lambda y$ is integrated by a one step method, the solution satisfies $y(t_n + \Delta t) = \mathrm{e}^{\lambda \Delta t} y(t_n)$ whereas the numerical solution satisfies $y_{n+1} = R(\lambda \Delta t) y_n$, where $R(z)$ is given by (23). Note that all eigenvalues of the semidiscretization (6) are pure imaginary simple $\pm iw$ and then to satisfy the stability requirement we should have $|R(iw\Delta t)| \leq 1$ for all $w \in [0, ck_{\max}]$. On the other hand it is well known that the (imaginary) stability interval of the fourth-order RK is $[-2\sqrt{2}, 2\sqrt{2}]$, thus if we take the DRP spatial discretization of Tam and Webb [22] with 9-points and order 6, according to Table 2, $1.77\Delta t \leq 2\sqrt{2}$ which implies $\Delta t \leq 1.597$. Figure 7 shows the profiles of the numerical and exact solution with $\Delta t = 1.597$ at the final time level. This example shows large phase and amplitude errors in the numerical solution. In addition, similar experiments with $\Delta t = 1$ show smaller but not negligible errors and to get accurate solutions, time steps of $\Delta t \simeq 0.5$ are necessary. These experiments imply that in the standard RK4 stepsizes much smaller than the stability limit are necessary to preserve the dissipation and dispersion properties of this wave type solutions.

Now observe that as remarked above for all wavenumber k the discrete function (e^{ikx_j}) is an eigenfunction of the linear operator Λ defined by (5) corresponding to the eigenvalue $-ick^*$. Hence the Fourier wave $u_j(t) = \beta_k(t) \, \mathrm{e}^{ikx_j}$, $j = 0, \pm 1, \ldots$ will be a solution of (5) iff

$$\partial_t \beta_k(t) = -ick^* \beta_k(t), \tag{25}$$

and the exact solution of (5) with $U^n = (\mathrm{e}^{ikx_j})$ is

$$U_{\mathrm{ex}}^{n+1} = \mathrm{e}^{-ick^* \Delta t} \, U^n. \tag{26}$$

By linearity, the corresponding solution (numerical solution) of the RK scheme will be

$$U_{\mathrm{RK}}^{n+1} = R(-ick^* \Delta t) \, U^n. \tag{27}$$

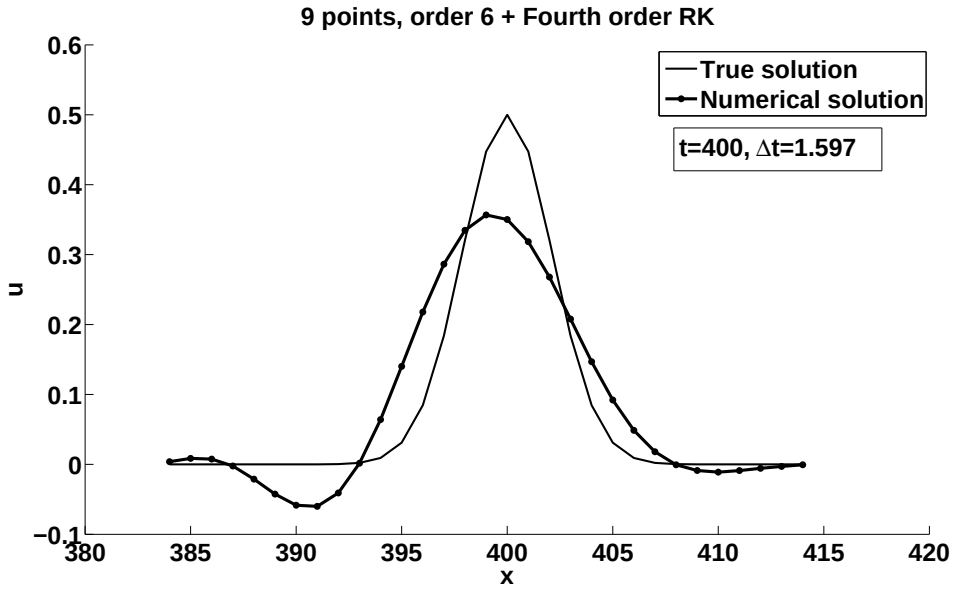

Figure 7: Numerical solution of the wave test equation, Gaussian initial condition, with DRP sixth-order spatial discretization and classical fourth-order RK for time discretization.

As a consequence of (26) and (27) the dispersion and dissipation errors introduced by the temporal discretization at the wavenumber k are defined by

$$\frac{U_{\mathrm{RK}}^{n+1}}{U_{\mathrm{ex}}^{n+1}} = \frac{R(-ick^*\Delta t)}{\mathrm{e}^{-ick^*\Delta t}} = \underbrace{|R(-i\theta)|\mathrm{e}^{-\,\mathrm{Im}(\theta)}}_{\text{dissipation}}\ \underbrace{\mathrm{e}^{i(\mathrm{Re}(\theta)+\arg R(-i\theta))}}_{\text{dispersion}}, \tag{28}$$

where $\theta = ck^*\Delta t$, and they are given, respectively, by

$$\phi_t(\theta) = \mathrm{Re}(\theta) + \arg R(-i\theta), \quad d_t(\theta) = 1 - |R(-i\theta)|\mathrm{e}^{-\,\mathrm{Im}(\theta)}. \tag{29}$$

For the case of symmetric FD schemes, θ is real ($\mathrm{Im}(k^*) = 0$) and equations (28)–(29) reduce to

$$\frac{U_{\mathrm{RK}}^{n+1}}{U_{\mathrm{ex}}^{n+1}} = \frac{R(-ick^*\Delta t)}{\mathrm{e}^{-ick^*\Delta t}} = \underbrace{|R(i\theta)|}_{\text{dissipation}}\ \underbrace{\mathrm{e}^{i(\theta-\arg R(i\theta))}}_{\text{dispersion}}, \tag{30}$$

$$\phi_t(\theta) = \theta - \arg R(i\theta), \quad d_t(\theta) = 1 - |R(i\theta)|. \tag{31}$$

This analysis has led in the last decade to the construction of special RK time advancing schemes taking into account instead of the usual order-stability properties the following ones:

C1) Stability: $|R(iw\Delta t)| \leq 1$ for all $w \in [0, ck_{\max}]$.

C2) Dissipation error: $|1 - R(iw\Delta t)|$ small for all $w \in [0, ck_c]$.

C3) Dispersion error: $|\arg R(iw\Delta t) - w\Delta t|$ small for all $w \in [0, ck_c]$.

C4) Maximum linear and non linear order. In the linear case defined by the maximum p such that $R(z) - \mathrm{e}^z = \mathcal{O}(z^{p+1})$, and in the non linear case by Butcher's conditions.

C5) Low storage implementation.

The last requirement C5) has been introduced because in practical calculations (typically 2D and 3D-dimensional problems of CAA) the number of spatial grid points and consequently the dimensionality of the system can be very high.

Therefore, as remarked by several authors (see e.g. [5], [7], [8], [20], [23], [14], [15]), effective integrators for practical problems must use the minimum number of registers.

Advancing a step $U^n \to U^{n+1}$ with a s-stage RK method in a problem of dimension m requires, in general, the storage of $s + 1$ vectors of dimension m and there are problems which arise in the semi discretization of some PDEs in which m is very large. This fact implies that the efficiency of the Runge–Kutta method depends strongly on the number of registers used in the computation and therefore methods with minimum storage requirements are preferred. Thus, for a given number of stages s, we want to consider minimum storage methods, i.e. that can be implemented with two m-registers, having the best stability and accuracy properties.

The simplest minimum storage one-step method is Euler's method ($U^{n+1} = U^n + \Delta t f(t_n, U^n)$, $n = 0, 1, \ldots$) that requires only two m-registers and consequently the simplest s-stage minimum storage method results of a repeated application of Euler's method with step sizes $c_j \Delta t$, $j = 1, \ldots, s$ with $\sum_{j=1}^{s} c_j = 1$, however their accuracy is not enough in many applications. Within the minimum storage schemes (two registers of size m), the (W)-schemes of Williamson [23] have been very popular in Computational Aero Acoustics (CAA) problems in the last years. These (W)-schemes can be defined by the algorithm:

Data: $V^1 = 0, \quad U^1 = y_n$
Result: $y_{n+1} = U^{s+1}$
for $j = 1$ **to** s **do**
  $V^{j+1} = \alpha_j \, V^j + f(t_n + c_j \Delta t, U^j)$
  $U^{j+1} = U^j + \Delta t \, \beta_{j+1} \, V^{j+1}$
end

Algorithm 1: Williamson scheme

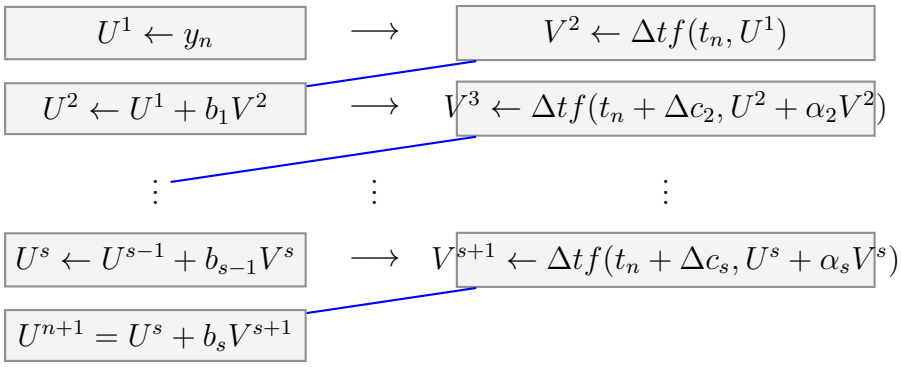

Here, $\alpha_j, \beta_{j+1}, j = 1, \ldots, s$ are the $2s$ free parameters, but noting that $V^1 = 0$, then α_1 is redundant and it is usual to choose $\alpha_1 = 0$.

Thus Stanescu and Habashi [20] have derived several (W)-schemes with amplification functions obtained by Hu *et al.* [12] that minimize the dissipation and dispersion errors for the linear wave test equation (1). Other fourth-order (non linear) (W)-schemes with minimum local error were derived by Carpenter and Kennedy [8]. More recently, (W)-storage schemes addressed to problems in the field of CAA have been proposed in [1], [2]. The advantage of Williamson schemes over Euler's compositions is that s-stage Williamson methods have $2s - 1$ free parameters and then allow us to obtain better accuracy and stability properties than in s-stage Euler's compositions.

Alternative families of minimum storage schemes, proposed by van der Houwen ([11], Eq. 2.2.4') and referred to as (vdH)-schemes, have been considered also to derive different low storage methods. They have been extensively studied by Kennedy, Carpenter and Lewis [13] to obtain optimal schemes of several orders having in mind the semidiscretization of Navier-Stokes equations including also local error control by embedded pairs (of course with additional storage requirements). Also Calvo *et al.* [4], [5] have obtained some optimal (vdH)-methods for acoustic problems. The next algorithm shows this class of schemes:

Data: $V^1 = 0, \quad U^1 = y_n$
Result: $y_{n+1} = U^{s+1}$
for $j = 1$ **to** s **do**
  $V^{j+1} = f(t_n + c_j \Delta t, U^j + \Delta t\, \gamma_j\, V^j)$
  $U^{j+1} = U^j + \Delta t\; b_j\; V^{j+1}$
end

Algorithm 2: van der Houwen scheme

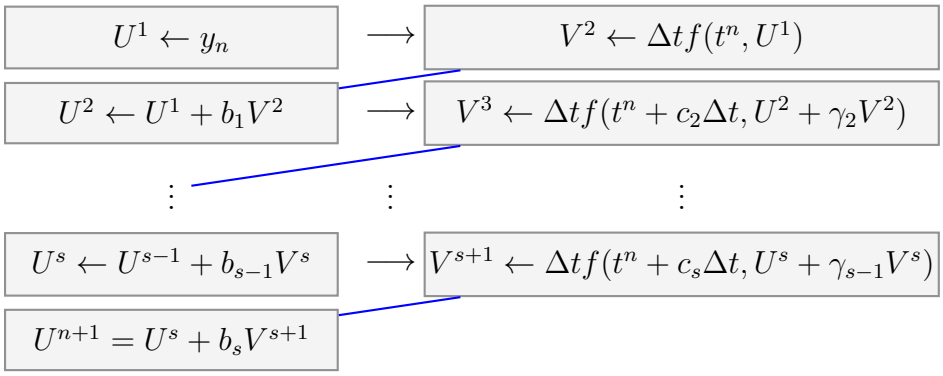

It must be noticed that the s-stage (vdH)-schemes have also $2s-1$ free parameters ($\gamma_1 = 0$) and therefore have the same flexibility than the Williamson methods, although it can be seen that the (vdH)- and (W)-families do not contain the same RK methods. Recently, by using the Shu-Osher form, two new general families of low storage explicit Runge–Kutta methods have been given by Ketcheson [14], [15], and Calvo *et al.* [7].

Algorithm 2 expressed in Butcher's notation is defined by the tableau of coefficients (19) with

$$\begin{aligned} &a_{j,j-1} = b_{j-1} + \gamma_{j-1}, \quad j = 2, \ldots, s, \\ &a_{j\ell} = b_\ell, \quad j-1 \le \ell \le s-2. \end{aligned} \tag{32}$$

Since the requirements C1)–C3) depend only on the amplification function $R(z) = 1 + \sum_{j=1}^{s} \gamma_j z^j$, of the considered RK method, many authors have derived "optimal" methods for several values of the number of stages s. Thus Hu *et al.* [12] obtained optimal methods for $s = 4, 5, 6$. Also Bogey and Bailly [3] have derived optimal methods combined with spatial stencils with 9-, 10- and 11-points. In the same line Calvo *et al.* [4], [5] have derived optimal methods for $s = 5, 6$.

To measure the quality of a method defined by $R(z) = 1 + \sum_{j=1}^{s} \gamma_j z^j$, it has been usual to compare the following quantities

$$\begin{aligned} &S = \max\{z > 0, |R(iz)| \le 1\}, \\ &L_d = \max\{z > 0, ||R(iz)| - 1| \le 10^{-3}\}, \\ &L_\varphi = \max\{z > 0, |\arg(R(iz)) - z| \le 10^{-3}\}. \end{aligned} \tag{33}$$

In Table 3 the values of these parameters corresponding to several methods are presented.

In Figure 8 we display the profiles of the exact and numerical solutions of example 1 for the six-stages fourth-order RK method of Calvo *et al.* given in [4] at the final time level. As can be seen, the shape of the wave is reproduced properly even with a large time stepsize $\Delta t = 1.0$

To end this section let us note that in the frame of implicit RK schemes there are methods such as Gauss ones that possess the best properties of stability and dissipation

Table 3: Values of S, L_d and L_φ parameters for several RK methods

method	**order**	**order (lin.)**	**stages**	S	L_d	L_φ
Classic	3	3	3	1.73	0.40	0.49
Classic	4	4	4	2.83	0.73	0.68
Hu *et al.*	2	2	4	2.85	0.85	0.86
Hu *et al.*	2	2	5	3.54	1.72	1.35
Hu *et al.*	3	4	6	1.75	1.41	1.27
Calvo *et al.*	3	3	5	3.48	0.91	1.09
Calvo *et al.*	4	4	5	3.48	1.25	0.91
Calvo *et al.*	4	4	6	3.82	2.00	1.14
Allampalli	3	4	7	5.67	1.28	1.07
Gauss	2	2	1	∞	∞	0.23
Gauss	4	4	2	∞	∞	0.95

($S = L_d = \infty$) although they have a non zero dispersion error that depends on s. For example, the fourth-order Gauss method has $L_\varphi = 0.95$.

In Figure 9 we display the profiles of the exact and numerical solutions of example 1 for the two-stage Gauss method with order four at the final time level. Now, if the spatial discretization has good dissipation and dispersion properties, the time integrator reproduces quite accurately the shape of the solution with the step size $\Delta t = 1$. However the main drawback of Gauss methods for CAA problems is its implicitness that entails a very high computational cost.

2.3 Dispersion and dissipation of the FD-RK scheme

The total dispersion and dissipation errors introduced by the FD-RK scheme are obtained by comparing the numerical solution of the semidiscretization (5) at the time level t^{n+1} and $u_j^n = \mathrm{e}^{ik(x_j - c\,t^n)}$

$$u_j^{n+1} = R(-ick^*\Delta t)\,\mathrm{e}^{ik(x_j - c\,t^n)}, \quad j = 0, \pm 1, \ldots, \tag{34}$$

with the exact solution of (1) with $u(x,0) = \mathrm{e}^{ikx}$

$$u_{\mathrm{ex}}(x_j, t^{n+1}) = \mathrm{e}^{-ick\Delta t}\,\mathrm{e}^{ik(x_j - c\,t^n)}, \quad j = 0, \pm 1, \ldots, \tag{35}$$

and writing the total errors as the product of the spatial errors with the temporal errors

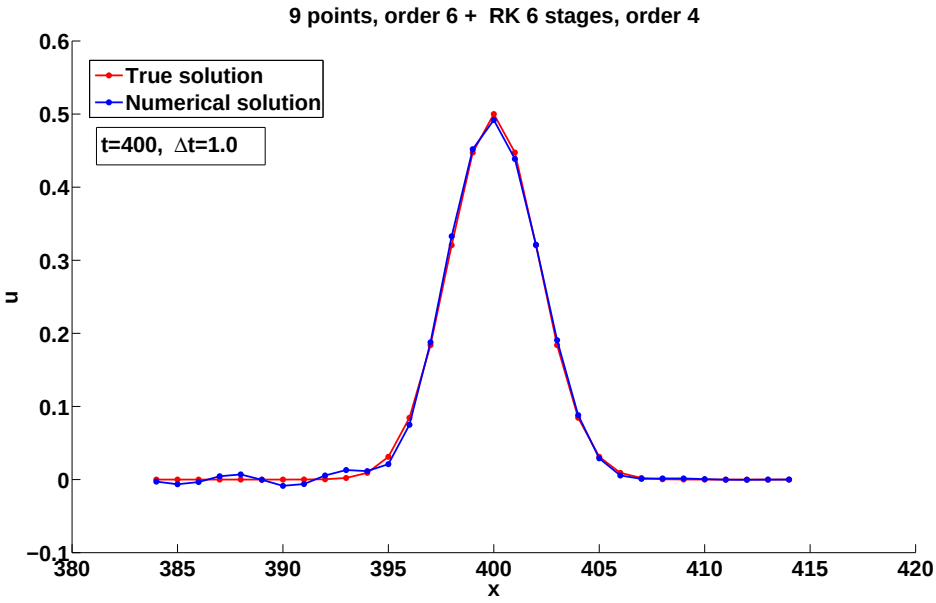

Figure 8: Numerical solution of the wave test equation, Gaussian initial condition, with DRP sixth order spatial discretization and Calvo *et al.* [4] optimized six stages, fourth-order RK for time discretization.

$$\frac{u_j^{n+1}}{u_{\rm ex}(x_j,t^{n+1})} = \frac{R(-ick^*\Delta t)}{{\rm e}^{-ick\Delta t}} = \underbrace{\frac{R(-ick^*\Delta t)}{{\rm e}^{-ick^*\Delta t}}}_{\text{temporal errors}} \quad \underbrace{\frac{{\rm e}^{-ick^*\Delta t}}{{\rm e}^{-ick\Delta t}}}_{\text{spatial errors}} . \tag{36}$$

Using the notation: $\alpha = \dfrac{c\Delta t}{\Delta x}$ for the CFL number and $z^* = k^*\Delta x$, (36) can be written as

$$\frac{u_j^{n+1}}{u_{\rm ex}(x_j,t^{n+1})} = \underbrace{|R(-i\alpha z^*)|}_{\text{total dissipation}} \underbrace{{\rm e}^{i[\alpha z + \arg R(-i\alpha z^*)]}}_{\text{total dispersion}}, \tag{37}$$

where

$$z^* = \sum_{j=1}^{N}(a_j - a_{-j})\sin(jz) - i\left(a_0 + \sum_{j=1}^{N}(a_j + a_{-j})\cos(jz)\right), \tag{38}$$

and the total dispersion and dissipation errors are given, respectively, by

$$\phi_{\rm Tot}(\alpha,z) = \alpha z + \arg R(-i\alpha z^*), \qquad d_{\rm Tot}(\alpha,z) = 1 - |R(-i\alpha z^*)|. \tag{39}$$

Again, for symmetric FD schemes $z^* = z - \phi_s(z)$ is real and equations (37) and (39) reduce to

$$\frac{u_j^{n+1}}{u_{\rm ex}(x_j,t^{n+1})} = \underbrace{|R(i\alpha z^*)|}_{\text{total dissipation}} \underbrace{{\rm e}^{i[\phi_t(\alpha z^*) + \alpha\phi_s(z)]}}_{\text{total dispersion}} , \tag{40}$$

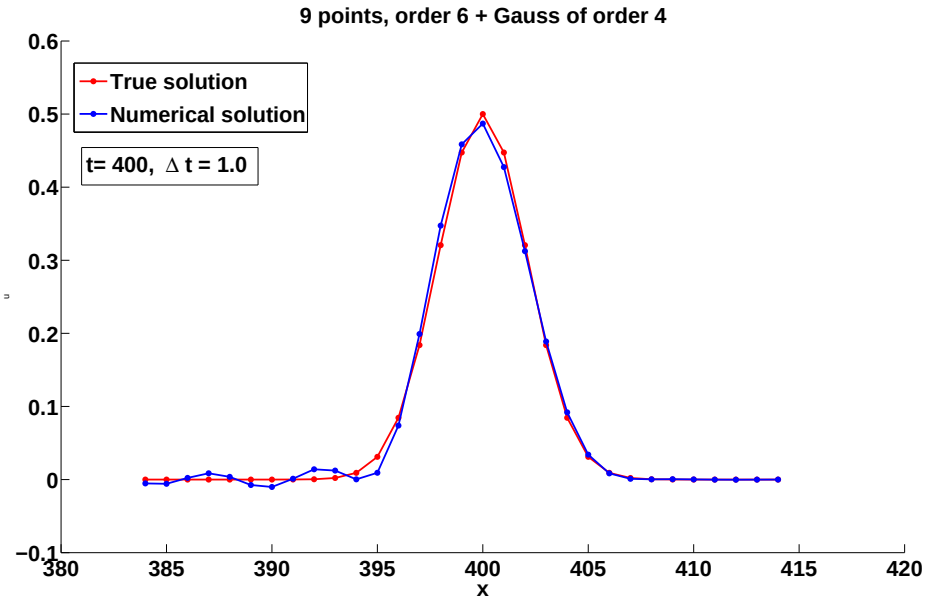

Figure 9: Numerical solution of the wave test equation, Gaussian initial condition, with DRP sixth-order spatial discretization and fourth-order Gauss RK for time discretization.

and we define

$$\phi_{\rm Tot}(\alpha, z) = \phi_t(\alpha z^*) + \alpha\, \phi_s(z), \qquad d_{\rm Tot}(\alpha, z) = 1 - |R(i\alpha z^*)|. \tag{41}$$

Next we illustrate the spatial, temporal and total errors for two FD-RK schemes. First of all we combine the standard eigth-order nine-points symmetric FD scheme (SFD9) with the classical four-stage fourth-order RK time advancing algorithm (RK4). In this case there is no dissipation error in the spatial discretization and the total dissipation error is due to the time advancing algorithm. For the dispersion error, we display in Figure 10 the (scaled) spatial, temporal and total errors for $z = k\Delta x \in [0,\, \pi/2]$ and $\alpha = 1$. It can be seen that for $z = k\Delta x \leq 0.75$ the effect of the spatial error $\phi_s(z)$ on the total error $\phi_{\rm Tot}(1, z)$ is negligible but for $z = k\Delta x > 0.75$ the spatial error is comparable or even greater than the temporal error and taking into account that both have the same sign both errors have a cumulative effect on the total error.

As a second scheme we combine the same spatial discretization with the six-stage low-dissipation and low-dispersion RK scheme (RKHu6) given by Hu *et al.* [12]. By the symmetry of the spatial scheme only the temporal dissipation is responsible for the total dissipation error and we focus on the dispersion errors. In Figure 11 we display the spatial, temporal and total errors for $z = k\Delta x \in [0,\, \pi/2]$ and $\alpha = 1$. In this case a smaller total error $\phi_{\rm Tot}$ than in the previous case is obtained but the small temporal error ϕ_t achieved in the optimization of the time advancing scheme RKHu6 is compensated by the large spatial error ϕ_s. However, the computational cost of the scheme RK4 is reduced by a

factor of 2/3 with respect to computational cost of the scheme RKHu6. In Figure 12 we show the spatial, temporal and total errors for the scheme SFD9-RK4 at a CFL number $\alpha = 2/3$ so that both schemes have the same computational cost, and it can be seen that both schemes have a comparable total error ϕ_{Tot}.

These examples show that in the linear error analysis it is crucial to consider the total errors to achieve optimal schemes.

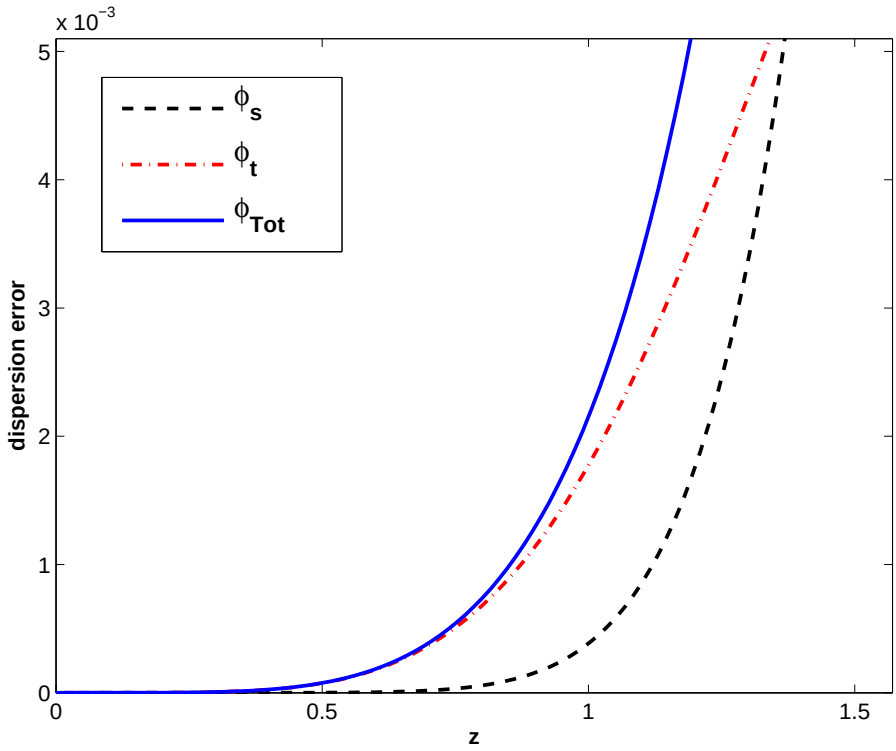

Figure 10: Dispersion errors (scaled by $1/\pi$) for $SFD9$-$RK4$ at $\alpha = 1$.

3 Optimization of the FD-RK schemes

In this section new FD-RK schemes are derived by minimizing the total dispersion and dissipation errors.

For the spatial discretization we will consider symmetric FD schemes (16) using $2N+1$ grid points with $N = 4$, 5, 6, and accuracy order four. In view of (4), the available coefficients a_j satisfy the conditions

$$a_0 = 0, \qquad \sum_{j=1}^{N} j a_j = \frac{1}{2}, \qquad \sum_{j=1}^{N} j^3 a_j = 0. \tag{42}$$

and the coefficients a_1 and a_2 can be expressed in terms of a_j, $j = 3, \ldots, N$ which will be used as free parameters in the optimization process.

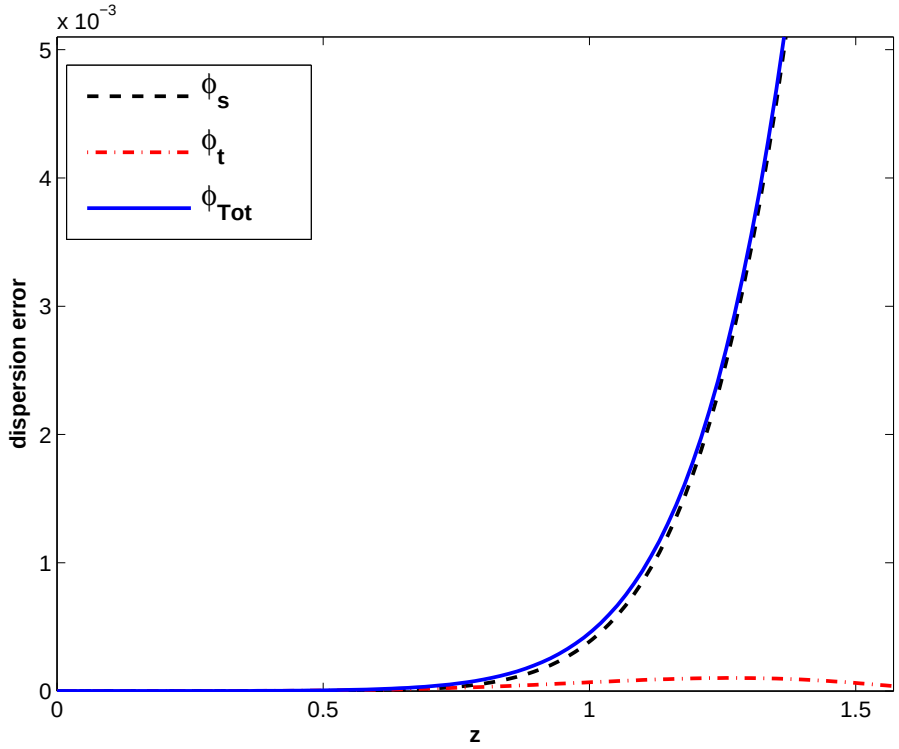

Figure 11: Dispersion errors (scaled by $1/\pi$) for $SFD9$-$RKHu6$ at $\alpha = 1$.

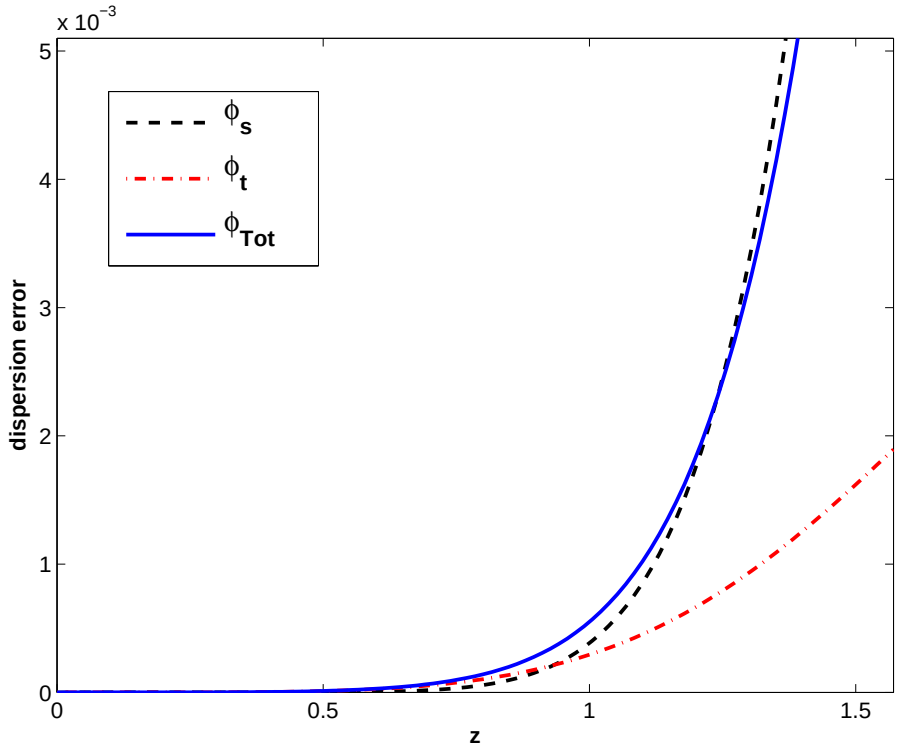

Figure 12: Dispersion errors (scaled by $1/\pi$) for $SFD9$-$RK4$ at $\alpha = 2/3$.

For time advancing we will use low storage six-stage explicit RK methods with order four. In the application to linear differential equations they are characterized by the amplification function

$$R(\zeta) = 1 + \zeta + \frac{1}{2!}\,\zeta^2 + \frac{1}{3!}\,\zeta^3 + \frac{1}{4!}\,\zeta^4 + \beta_5\,\zeta^5 + \beta_6\,\zeta^6, \tag{43}$$

with the free parameters β_5 and β_6.

Now the resulting schemes, denoted by SFD_{2N+1}-RK_6 with $N = 4,\ 5,\ 6$, depend on the free parameters $a_3, \ldots, a_N$, β_5 and β_6 which will be determined by minimizing the following error measure

$$\iint_D \left[\left(\frac{\phi_{\mathrm{Tot}}(\alpha, z)}{\pi} \right)^2 + d^2_{\mathrm{Tot}}(\alpha, z) \right] \mathrm{d}\alpha\, \mathrm{d}z, \tag{44}$$

where the integration region is defined by $D = \{(\alpha, z) \mid \alpha \in (0, 1], z \in [z_{\min}, z_{\max}]\}$ for some given $z_{\min}$ and $z_{\max}$. Further we impose the stability condition

$$|R(i\alpha z^*)| < 1, \quad \alpha \in (0, 1], \quad z \in (0, z_{\max}], \tag{45}$$

with z^* given by (38).

We notice that the main difference of (44) with error measures considered by other authors (for example [2, 3, 12, 19]) is the use of the total dispersion and dissipation errors on a two-dimensional region associated to spatial and temporal discretizations. The constraint (45) was imposed in order to obtain optimized schemes which are stable on the range of wavenumbers in which the dispersion and dissipation behavior is acceptable in terms of accuracy.

Here we chose the wavenumbers limits $z_{\min} = \pi/16$ and $z_{\max} = \pi/2$ which amounts to consider waves between 32 points per wavelength and 4 points per wavelength, respectively, and for the scheme with $N = 6$ we also use $z_{\max} = 3\pi/5$ as in [3]. The coefficients β_5, β_6 and a_j obtained for the optimized FD-RK schemes are given in Tables 4 and 5.

To compare the dispersive and dissipative behavior of the new optimized schemes we consider some FD-RK schemes recently published in the scientific literature [2, 3] which have been optimized independently in space and in time. The optimized spatial FD schemes derived in [3] together with the fourth-order six-stage RK algorithm derived in [2], and they will be referred as $FDo9p$-RKB_6, $FDo11p$-RKB_6 and $FDo13p$-RKB_6. Figures 13–18 show the total dispersion and dissipation errors: $\phi_{\mathrm{Tot}}(\alpha, z)/\pi$ and $d_{\mathrm{Tot}}(\alpha, z)$ depicted as a function of $z = k\Delta x$ ($0 \le z \le z_{\max}$) at a CFL number $\alpha = 1$. These figures show that the new optimized schemes have generally a better dispersive and dissipative behavior than those optimized independently in space and in time, in particular for wavenumbers near to $z = \pi/2$.

Next a quantitative comparison of schemes by taking dispersion and dissipation error bounds: $|\phi_{\mathrm{Tot}}(\alpha,z)/\pi| \leq 10^{-3}$ and $|d_{\mathrm{Tot}}(\alpha,z)| \leq 10^{-4}$ is given. These limits indicate the maximum wavenumbers $z = k\Delta x$ properly calculated which can also be expressed in terms of the number of points per wavelength $N_p = 2\pi/k\Delta x$ with respect to the grid-size Δx. They are reported in Table 6 for the schemes considered in the comparison at a CFL number $\alpha = 1$. For the same $(2N+1)$-points stencil, the new optimized schemes have generally better accuracy limits in phase than the schemes optimized independently in space and in time. In addition, waves with four points per wavelength at $\alpha = 1$ are taken into account only by the schemes SFD_{11}-$RK_6(a)$ and SFD_{13}-$RK_6(a)$.

Table 4: Coefficients of the optimized SFD_{2N+1}-$RK_6(a)$ schemes with $z_{\max} = \pi/2$

$N = 4$	$N = 5$	$N = 6$
$\beta_5 = 0.00785313645903$	$\beta_5 = 0.00785780000000$	$\beta_5 = 0.00785812800000$
$\beta_6 = 0.00092656241553$	$\beta_6 = 0.00094507900000$	$\beta_6 = 0.00094851200000$
$a_1 = 0.84332103556666$	$a_1 = 0.88131666666666$	$a_1 = 0.90280686066667$
$a_2 = -0.24646064685333$	$a_2 = -0.29651333333333$	$a_2 = -0.32759725333333$
$a_3 = 0.06024952338000$	$a_3 = 0.09657000000000$	$a_3 = 0.12294034000000$
$a_4 = -0.00778707800000$	$a_4 = -0.02315000000000$	$a_4 = -0.03812260000000$
	$a_5 = 0.00292000000000$	$a_5 = 0.00835681000000$
		$a_6 = -0.00095450400000$

Table 5: Coefficients of the optimized SFD_{13}-$RK_6(b)$ scheme with $z_{\max} = 3\pi/5$

$\beta_5 = 0.00784952503800$
$\beta_6 = 0.00099024688453$
$a_1 = 0.91934276215510$
$a_2 = -0.35241708459276$
$a_3 = 0.14520000000000$
$a_4 = -0.05177590000000$
$a_5 = 0.01379215888197$
$a_6 = -0.00199429789657$

Table 6: Dispersion and dissipation limits in wavenumbers $z = k\Delta x$ and in points per wavelength $N_p = 2\pi/k\Delta x$ with respect to the grid-size Δx at $\alpha = 1$.

	Dispersion	$\lvert\phi_{\rm Tot}/\pi\rvert \leq 10^{-3}$	Dissipation	$\lvert d_{\rm Tot}\rvert \leq 10^{-4}$
	$k\Delta x$	$2\pi/k\Delta x$	$k\Delta x$	$2\pi/k\Delta x$
$FDo9p\text{-}RKB_6$	1.43	4.39	1.88	3.34
$FDo11p\text{-}RKB_6$	1.44	4.38	1.82	3.45
$FDo13p\text{-}RKB_6$	1.40	4.49	1.80	3.49
$SFD_9\text{-}RK_6(a)$	1.46	4.31	1.65	3.81
$SFD_{11}\text{-}RK_6(a)$	1.63	3.85	1.74	3.61
$SFD_{13}\text{-}RK_6(a)$	1.74	3.61	1.75	3.56
$SFD_{13}\text{-}RK_6(b)$	1.89	3.32	1.51	4.16

4 Construction of the low storage RK methods

In this section we analyze the low-storage explicit RK methods with $s = 6$ stages and non linear algebraic order 4 given in the previous section. These schemes satisfy the order conditions

$$\begin{array}{llll} \mathbf{b}^T\mathbf{e} = 1, & \mathbf{b}^T\mathbf{c} = 1/2, & \mathbf{b}^T\mathbf{c}^2 = 1/3, & \mathbf{b}^T\mathbf{A}\mathbf{c} = 1/6, \\ \mathbf{b}^T\mathbf{c}^3 = 1/4, & \mathbf{b}^T(\mathbf{c}\cdot\mathbf{A}\mathbf{c}) = 1/8, & \mathbf{b}^T\mathbf{A}\mathbf{c}^2 = 1/12, & \mathbf{b}^T\mathbf{A}^2\mathbf{c} = 1/24. \end{array} \tag{46}$$

In addition to the equations given by (46), the coefficients of (32) also satisfy the two additional conditions

$$\mathbf{b}^T\mathbf{A}^3\mathbf{c} = \beta_5, \quad \mathbf{b}^T\mathbf{A}^4\mathbf{c} = \beta_6, \tag{47}$$

obtained in the optimization process of the previous section.

Since we have a set of ten nonlinear equations (46)–(47) for the eleven coefficients $(b_1, \ldots, b_6, \gamma_1, \ldots, \gamma_5)$, one parameter is free, and therefore some additional requirements can be imposed for its determination. Here, we use this degree of freedom to solve numerically the nonlinear system (46)–(47) by taking into account standard requirements in the derivation of practical RK methods:

- The weights satisfy $|b_i| \leq 2$, $i = 1, \ldots, 6$.
- The nodes satisfy $c_i \neq c_j$, $\forall\, i \neq j$ and $0 \leq c_i \leq 1$, $i = 1, \ldots, 6$.
- Minimize the Euclidean norm of the leading term of the local error of the advancing approximation, i.e. $\|\tau^{(5)}\|_2 = \sum \left| C_j^{(5)} \right|^2$, where $C_j^{(5)}$ are the coefficients of the

elementary differentials of order five in the local error expansion in powers of the step size Δt.

We have taken a fine grid in the free parameter and we have tested the first two requirements at each point. From the avalilable points, we have started a minimization process of the third condition and finally the coefficients obtained for the low-storage RK algorithms associated to the optimized schemes of the previous section are given in Tables 7–10.

Table 7: Coefficients of the low-storage RK algorithm for the SFD_9-$RK_6(a)$ scheme

$c_1 = 0$	$b_1 = 0.11542410418395$	$\gamma_1 = 0.18457589581605$
$c_2 = 0.30000000000000$	$b_2 = 0.14337328928437$	$\gamma_2 = 0.12830567193128$
$c_3 = 0.38710306539960$	$b_3 = 0.34923156739002$	$\gamma_3 = 0.10871574089416$
$c_4 = 0.71674470175250$	$b_4 = -0.52556842961887$	$\gamma_4 = 0.60238704717262$
$c_5 = 0.68484757841209$	$b_5 = 0.49748516677020$	$\gamma_5 = 0.27184007546667$
$c_6 = 0.85178577347634$	$b_6 = 0.42005430199034$	

Table 8: Coefficients of the low-storage RK algorithm for the SFD_{11}-$RK_6(a)$ scheme

$c_1 = 0$	$b_1 = 0.10974285720869$	$\gamma_1 = 0.18025714279131$
$c_2 = 0.29000000000000$	$b_2 = 0.13448959704914$	$\gamma_2 = 0.13857764418235$
$c_3 = 0.38281009844018$	$b_3 = 0.38294944978031$	$\gamma_3 = 0.08426505141729$
$c_4 = 0.71144695545543$	$b_4 = -0.60216813067103$	$\gamma_4 = 0.66860432485845$
$c_5 = 0.69361809822556$	$b_5 = 0.49945631650501$	$\gamma_5 = 0.30908387736075$
$c_6 = 0.83355396723287$	$b_6 = 0.47552991012788$	

Table 9: Coefficients of the low-storage RK algorithm for the SFD_{13}-$RK_6(a)$ scheme

$c_1 = 0$	$b_1 = 0.11287033711698$	$\gamma_1 = 0.19025714279131$
$c_2 = 0.30000000000000$	$b_2 = 0.14141097168321$	$\gamma_2 = 0.13989004259688$
$c_3 = 0.38412249685471$	$b_3 = 0.36534072934351$	$\gamma_3 = 0.08964556109275$
$c_4 = 0.71682746513089$	$b_4 = -0.54871438354286$	$\gamma_4 = 0.66668799693474$
$c_5 = 0.69170177030185$	$b_5 = 0.47533937806862$	$\gamma_5 = 0.31691629028663$
$c_6 = 0.84138638015875$	$b_6 = 0.45375296733053$	

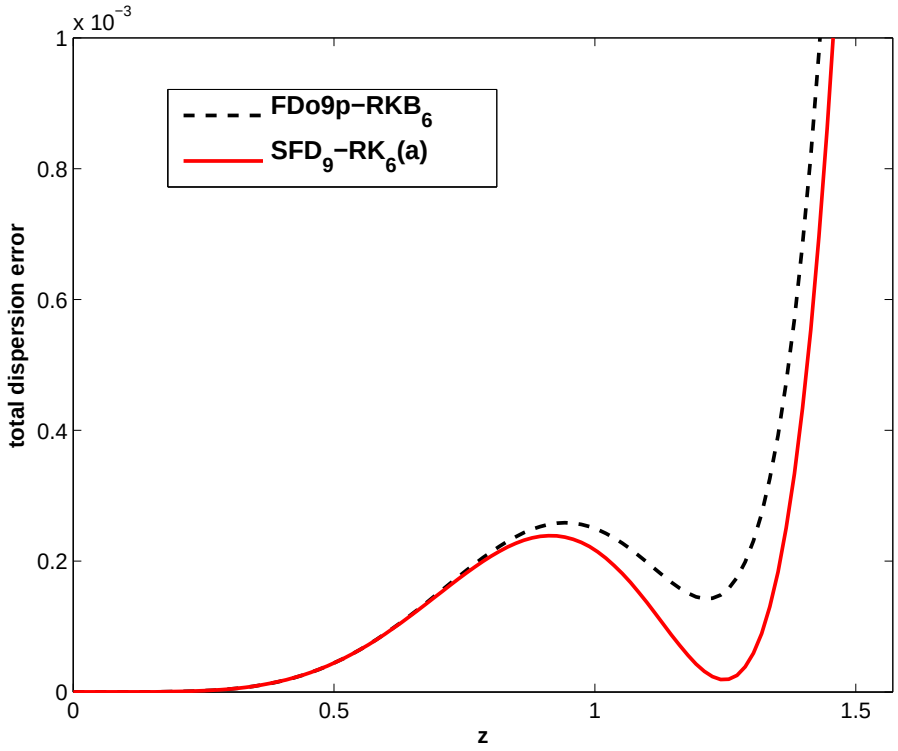

Figure 13: Total dispersion errors at $\alpha = 1$.

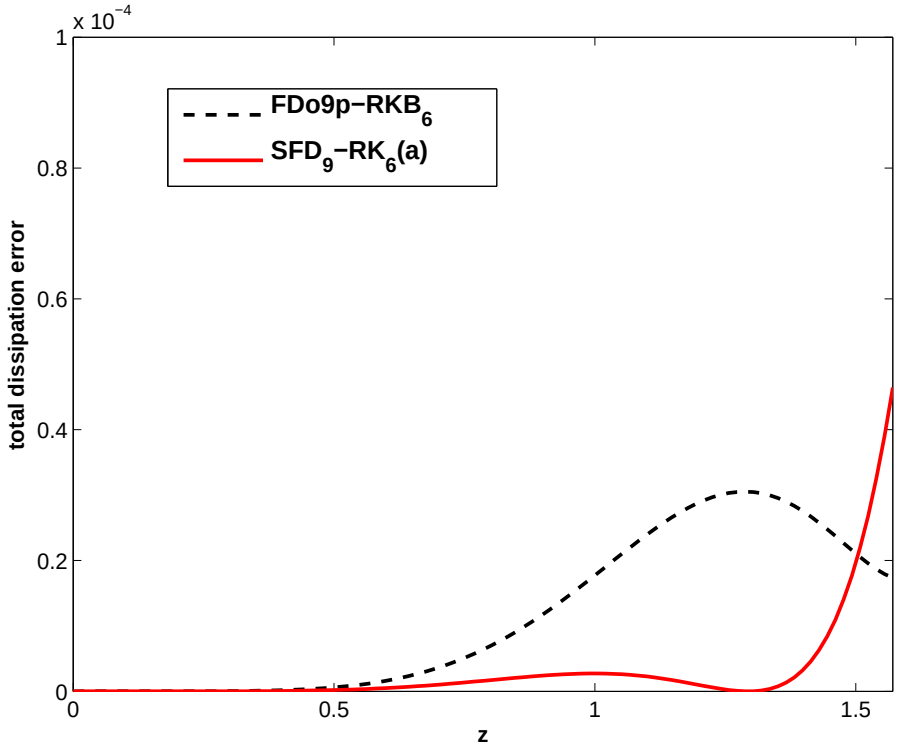

Figure 14: Total dissipation errors at $\alpha = 1$.

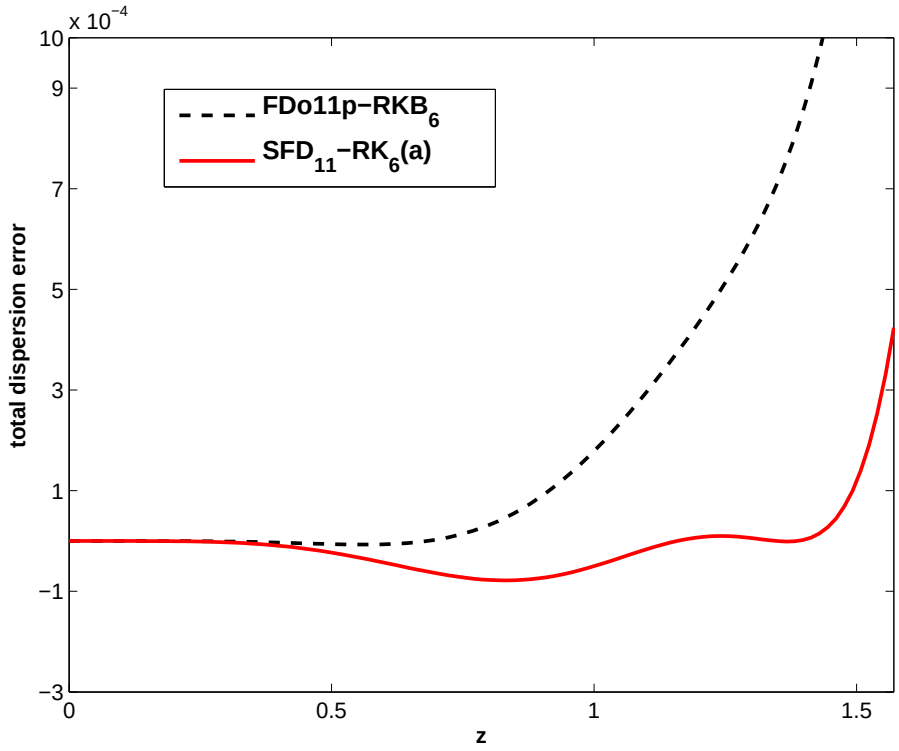

Figure 15: Total dispersion errors at $\alpha = 1$.

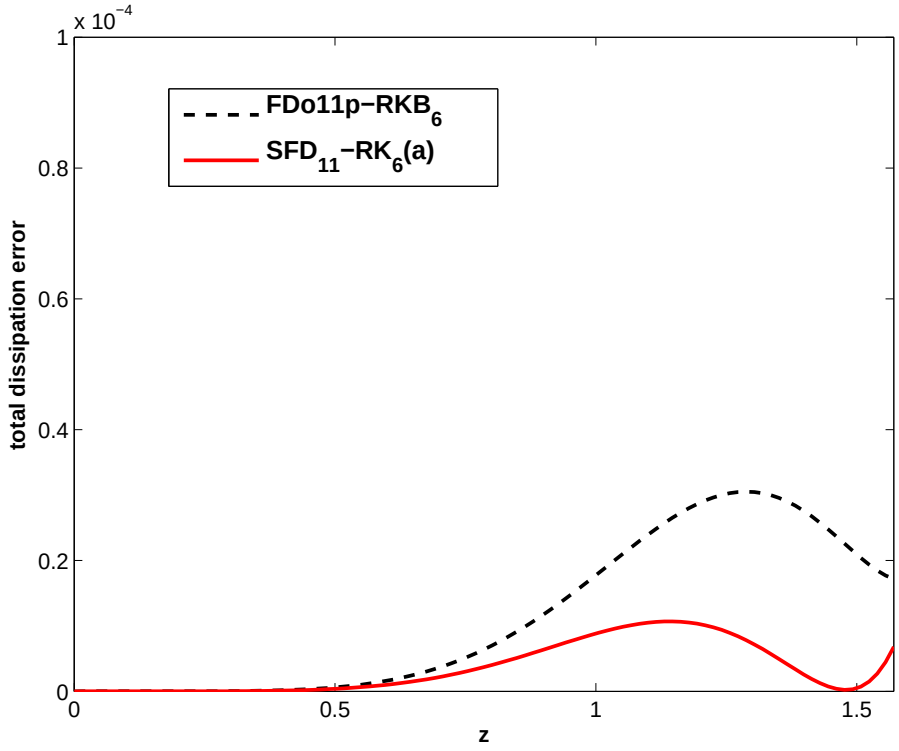

Figure 16: Total dissipation errors at $\alpha = 1$.

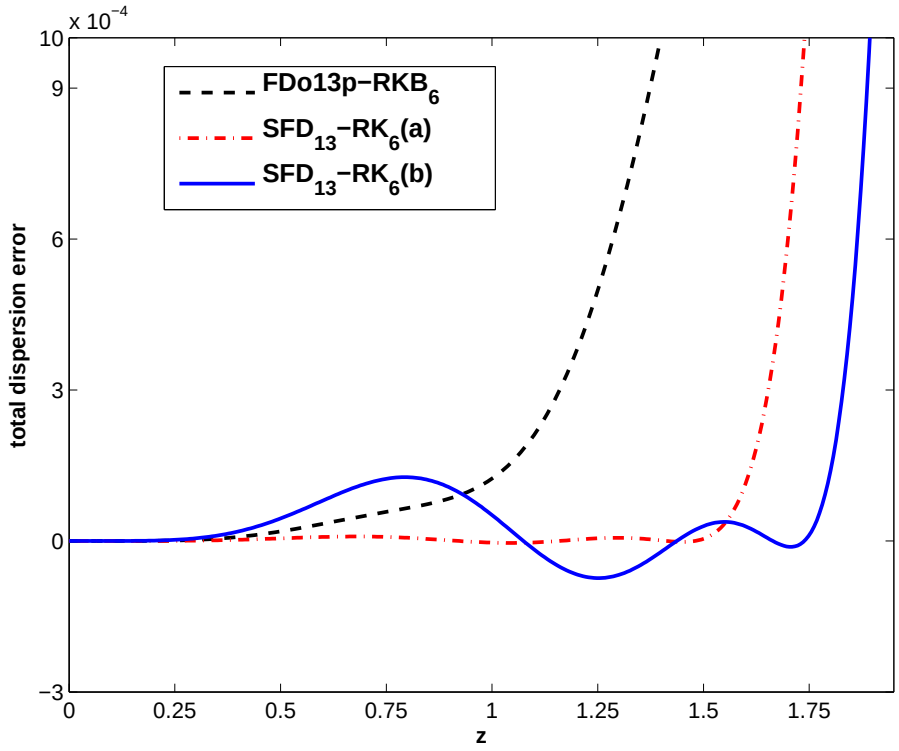

Figure 17: Total dispersion errors at $\alpha = 1$.

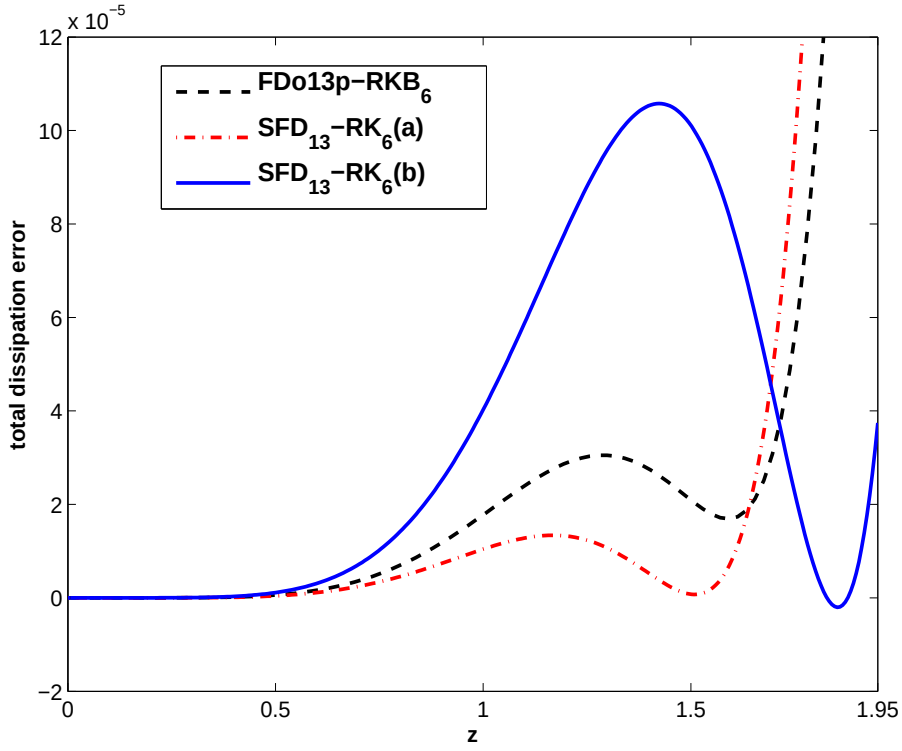

Figure 18: Total dissipation errors at $\alpha = 1$.

Table 10: Coefficients of the low-storage RK algorithm for the SFD_{13}-$RK_6(b)$ scheme

$c_1 = 0$	$b_1 = 0.11542109063167$	$\gamma_1 = 0.20457890936833$
$c_2 = 0.32000000000000$	$b_2 = 0.14461329419966$	$\gamma_2 = 0.12109473781601$
$c_3 = 0.38112912264734$	$b_3 = 0.36393100640076$	$\gamma_3 = 0.11419683938110$
$c_4 = 0.73816223061319$	$b_4 = -0.43062100269419$	$\gamma_4 = 0.50989197038198$
$c_5 = 0.70323635891988$	$b_5 = 0.33271255388848$	$\gamma_5 = 0.31562989999482$
$c_6 = 0.84168684242120$	$b_6 = 0.47394305757361$	

5 Numerical experiments

In order to test the effectiveness of the optimized low storage RK schemes derived in the above section, we use several model problems with linear and nonlinear wave propagation. In particular, we have considered a one dimensional convection equation involving long-range sound propagation, and two Euler model problems. The new optimized schemes have been compared with the schemes $FDo9p$-RKB_6, $FDo11p$-RKB_6 and $FDo13p$-RKB_6 developed in [2, 3].

5.1 One dimensional convection equation

In our first numerical experiments we have considered the two basic problems studied by Bogey and Bailly in [3]. The aim is to check the long-range propagation of two initial disturbances by the one-dimensional convective wave equation (1) with $c = 1$ given by

$$u(x,0) = \sin\left(\frac{2\pi x}{a\Delta x}\right)\exp\left(-\log(2)\left(\frac{x}{b\Delta x}\right)^2\right),$$

where the parameters a and b are $a = 8$ and $b = 3$ for the case I and $a = 4$ and $b = 9$ for the case II.

As remarked in [3] these choices of a and b have been made for the spectral contents of $u(x,0)$. Thus in case I the spectral content of $u(x,0)$ is a Gaussian function centered around $k\Delta x = \pi/4$ with wavenumbers $k\Delta x \in (0, \pi/2)$ whereas in case II the Gaussian function is centered around $k\Delta x = \pi/2$.

For the case I the initial disturbance is propagated over $800\Delta x$ which corresponds to 100 times the dominant wavelength. Figures 19–24 show the results obtained with the schemes of 9, 11 and 13 points, respectively, for a CFL number $\alpha = 1$. Figures 19, 21 and 23 show the solution computed with the numerical schemes whereas Figures 20, 22 and 24 show the total errors given by $|u_{\text{ex}} - u_{\text{num}}|$. The solution obtained with the schemes of 9 points (Figure 19) shows dispersion of the initial disturbance for both schemes. In this case the total errors (Figure 20) of the scheme $FDo9p$-RKB_6 are slightly smaller than the

total errors of the scheme SFD_9-$RK_6(a)$. On the other hand, the results obtained with the 11 and 13-points schemes are different (Figures 21–24). Now the solutions obtained by using the schemes developed in [2, 3] are clearly distorted, whereas the solutions obtained by using the new optimized schemes superpose fairly on the exact solution. It is worth to remark that the total errors presented by the new optimized schemes are at least 2.5 times smaller than the total errors presented by the schemes developed in [2, 3]. These results are in agreement with the better dispersive properties of the new optimized schemes as analyzed in section 3. It should also be noted that the scheme SFD_{13}-$RK_6(a)$ is more accurate than the scheme SFD_{13}-$RK_6(b)$ for this problem.

Case II is a test model to investigate if wavenumbers $z = k\Delta x \simeq \pi/2$ are properly calculated with about four points per wavelength. As remarked in [3] these waves often appear in Large Eddy Simulation (LES) procedures. Now the initial disturbance is propagated over a distance of $200\Delta x$ which corresponds to 50 times the wavelength. Figures 25–28 show the results obtained with the schemes of 11 and 13 points for a CFL number $\alpha = 1$. The schemes of 9 points do not result accurate enough to solve this problem. The Figures 25 and 27 show the solution computed with the numerical schemes and the Figures 26 and 28 show the total errors ($|u_{\text{ex}} - u_{\text{num}}|$), as in the case I. The solutions obtained with the schemes developed in [2, 3] are clearly dispersed and dissipated. The solution obtained with the SFD_{11}-$RK_6(a)$ scheme is also dispersed and dissipated though its total errors are approximately two times lower than the total errors presented by the $FDo11p$-RKB_6 scheme. In this problem, the solution is only properly calculated by using the new SFD_{13}-$RK_6(a, b)$ schemes. The solution computed by the SFD_{13}-$RK_6(a)$ scheme is in phase with the exact one and it results slightly dissipated, whereas the solution computed by the SFD_{13}-$RK_6(b)$ scheme is the most accurate for this problem.

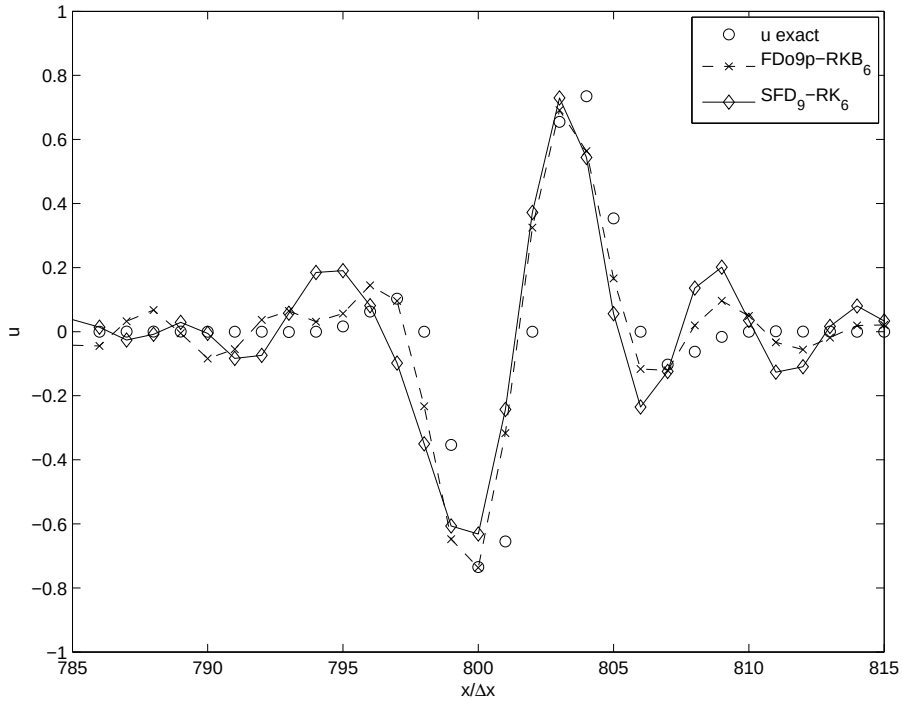

Figure 19: Solution at $\alpha = 1$ for the schemes SFD_9-$RK_6(a)$ and $FDo9p$-RKB_6.

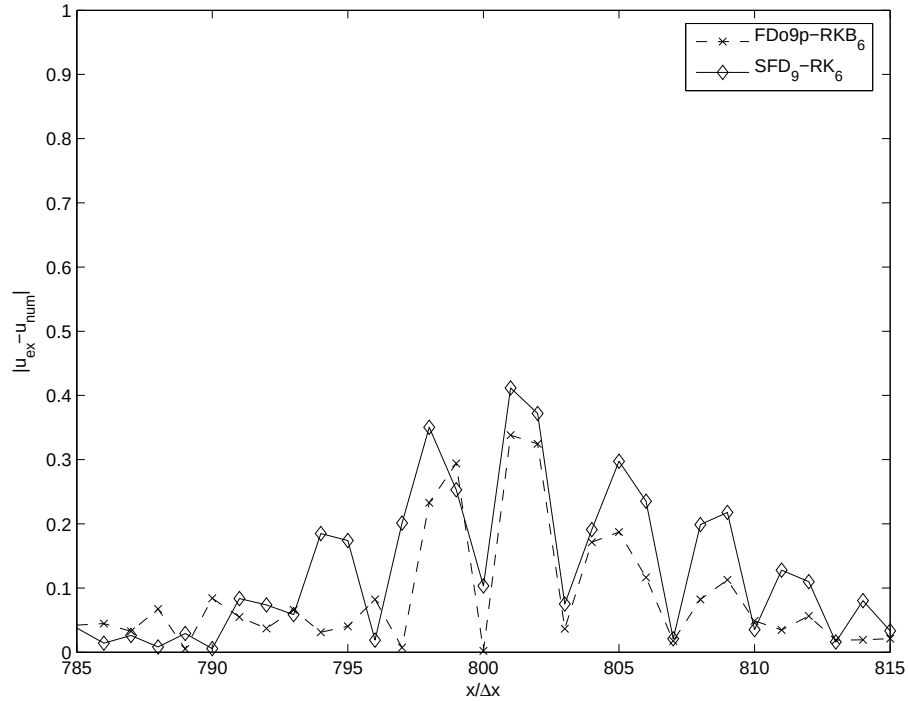

Figure 20: Errors at $\alpha = 1$ for the schemes SFD_9-$RK_6(a)$ and $FDo9p$-RKB_6.

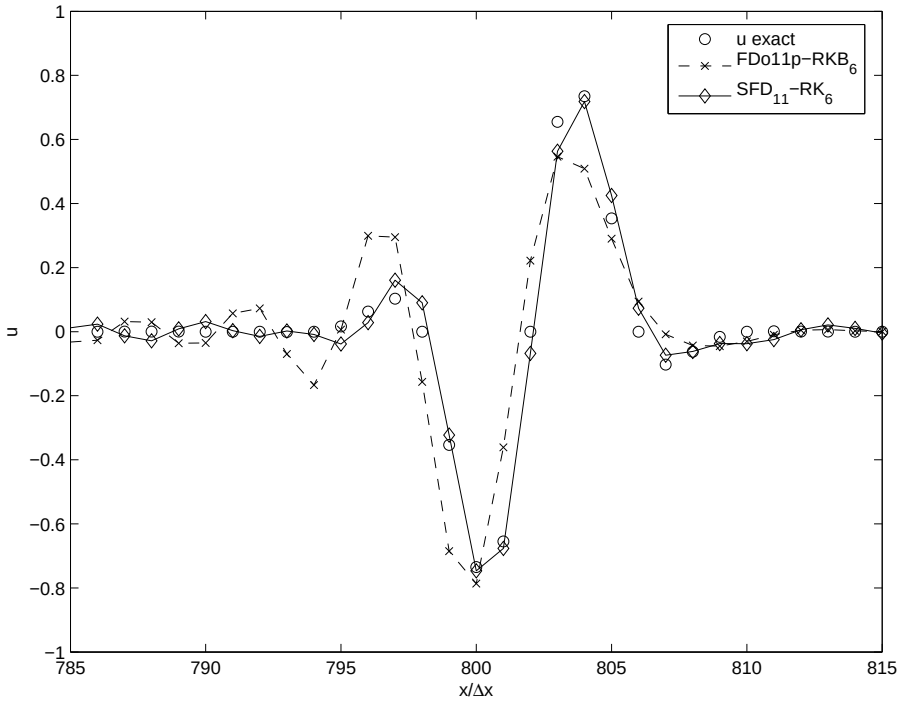

Figure 21: Solution at $\alpha = 1$ for the schemes SFD_{11}-$RK_6(a)$ and $FDo11p$-RKB_6.

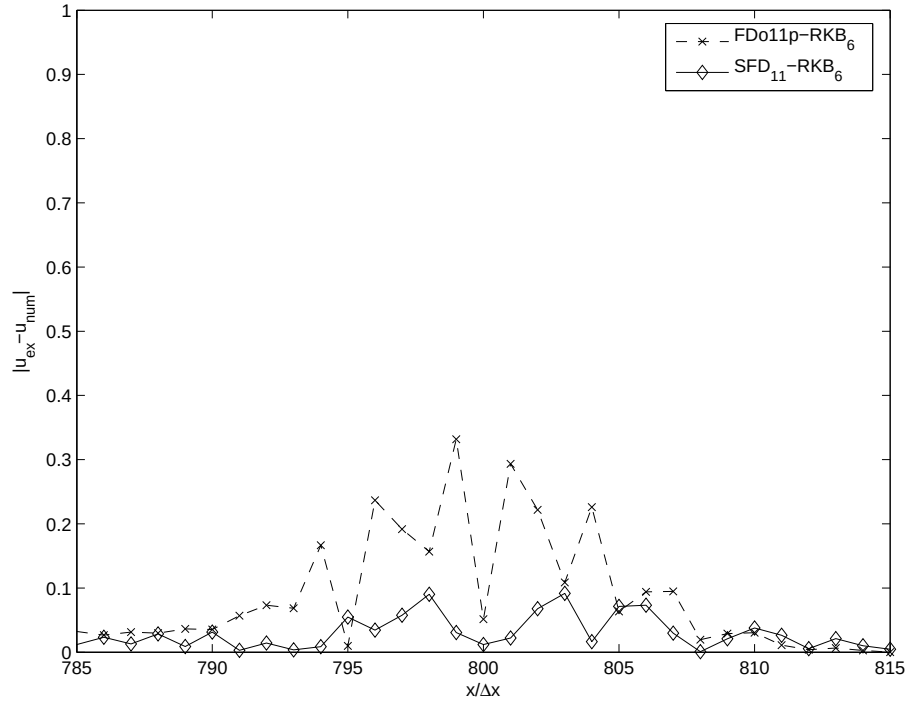

Figure 22: Errors at $\alpha = 1$ for the schemes SFD_{11}-$RK_6(a)$ and $FDo11p$-RKB_6.

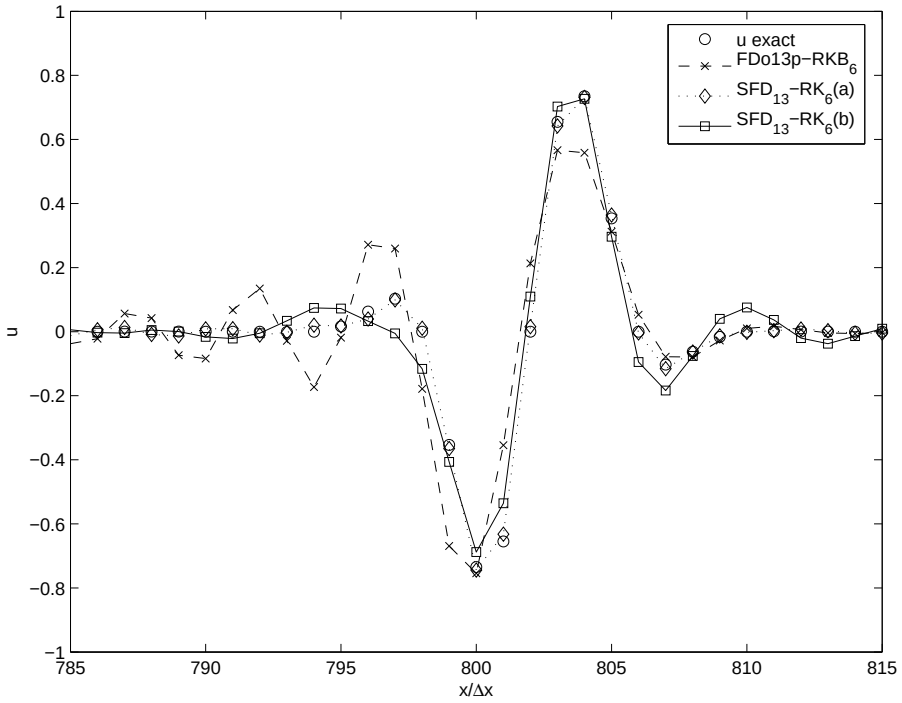

Figure 23: Solution at $\alpha = 1$ for the schemes SFD_{13}-$RK_6(a,b)$ and $FDo13p$-RKB_6.

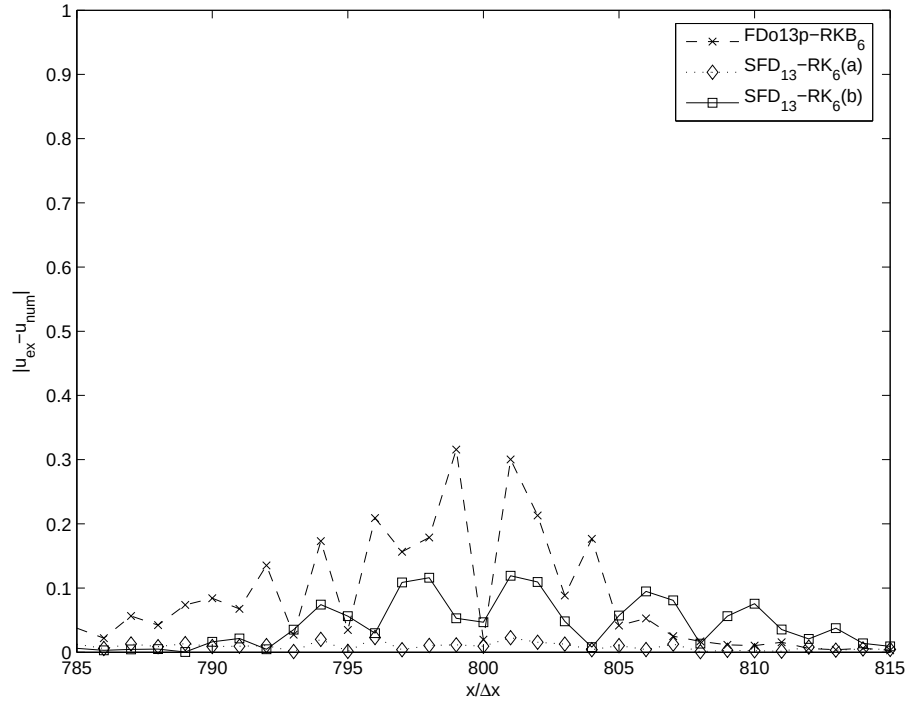

Figure 24: Errors at $\alpha = 1$ for the schemes SFD_{13}-$RK_6(a,b)$ and $FDo13p$-RKB_6.

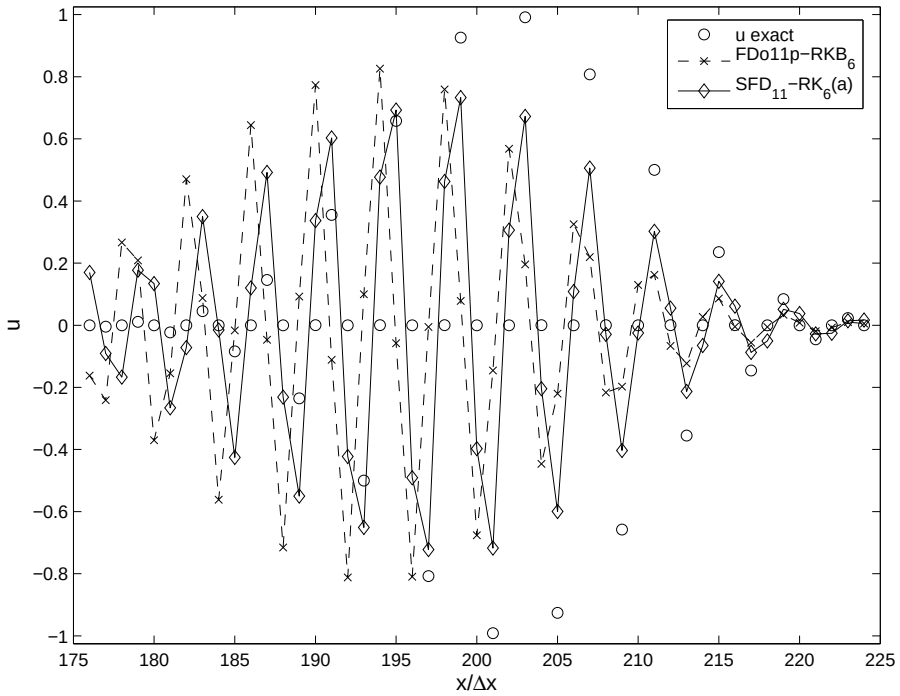

Figure 25: Solution at $\alpha = 1$ for the schemes SFD_{11}-$RK_6(a)$ and $FDo11p$-RKB_6.

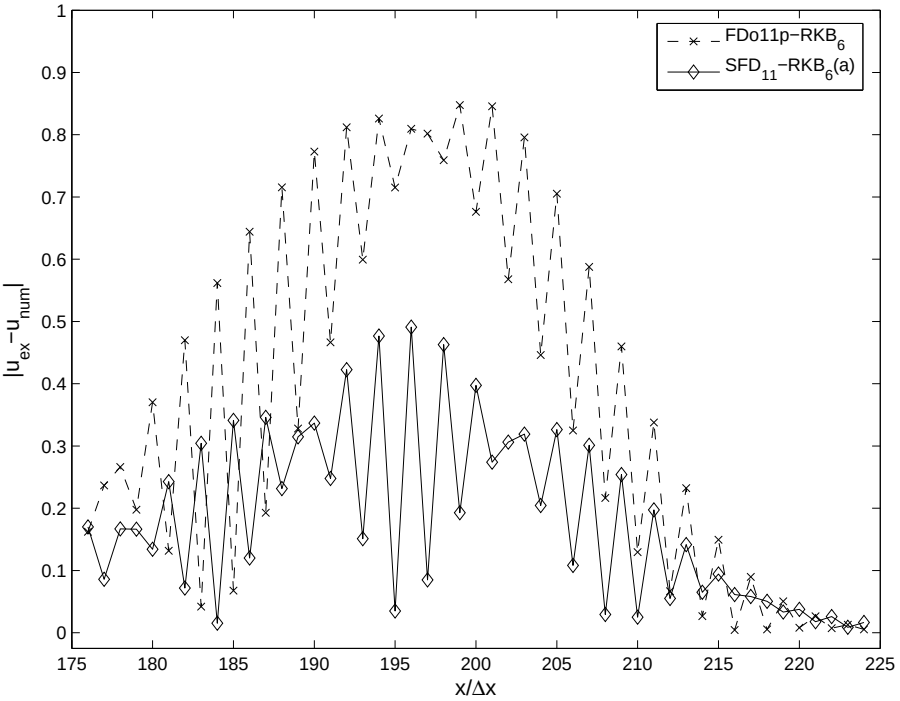

Figure 26: Errors at $\alpha = 1$ for the schemes SFD_{11}-$RK_6(a)$ and $FDo11p$-RKB_6.

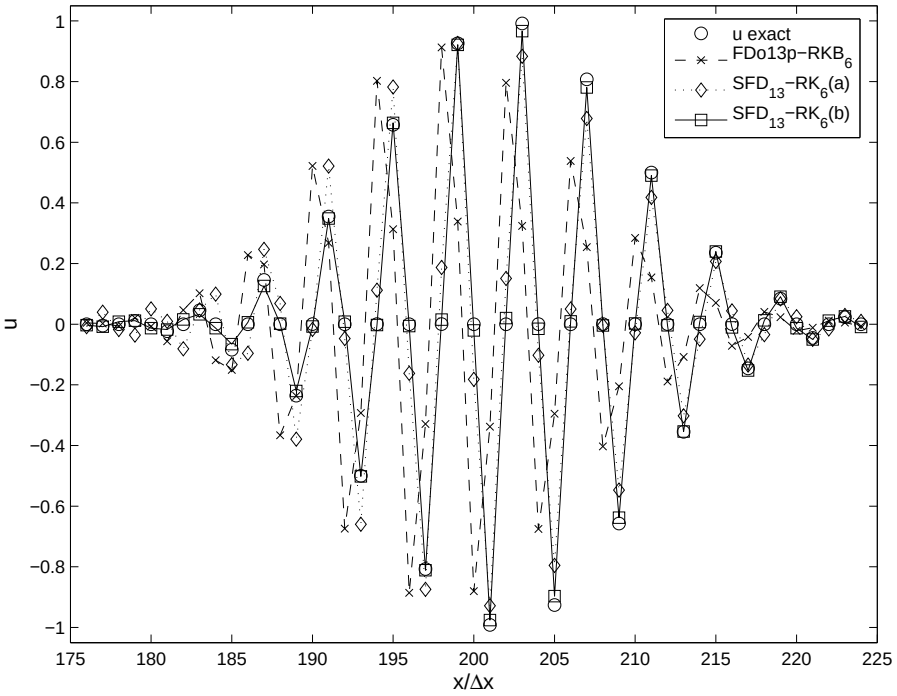

Figure 27: Solution at $\alpha = 1$ for the schemes SFD_{13}-$RK_6(a,b)$ and $FDo13p$-RKB_6.

5.2 One dimensional Euler model problems

In our second test problem we consider the one-dimensional linearized Euler equations (around u_0, ρ_0, p_0)

$$\begin{pmatrix} \rho_t \\ u_t \\ p_t \end{pmatrix} + \begin{pmatrix} u_0 & \rho_0 & 0 \\ 0 & u_0 & \dfrac{1}{\rho_0} \\ 0 & \gamma p_0 & u_0 \end{pmatrix} \begin{pmatrix} \rho_x \\ u_x \\ p_x \end{pmatrix} = 0. \tag{48}$$

Here ρ is the density, u the velocity and p the pressure. Using the transformation $(\rho, u, p) \to (r, v, w)$ given by

$$\rho = \frac{r+w}{c^2} + v, \qquad u = \frac{w-r}{c\,\rho_0}, \qquad p = r + w, \tag{49}$$

the PDE system (48) can be written in the diagonal form

$$\begin{pmatrix} r_t \\ v_t \\ w_t \end{pmatrix} + \begin{pmatrix} u_0 - c & 0 & 0 \\ 0 & u_0 & 0 \\ 0 & 0 & u_0 + c \end{pmatrix} \begin{pmatrix} r_x \\ v_x \\ w_x \end{pmatrix} = 0, \tag{50}$$

where $c = \sqrt{\frac{\gamma p_0}{\rho_0}}$ is the speed of sound, and therefore exact solutions can easily be computed for numerical comparison. We consider the case of subsonic regime, $0 < u_0 < c$, for the computations carried out with the FD-RK schemes. The computation domain is

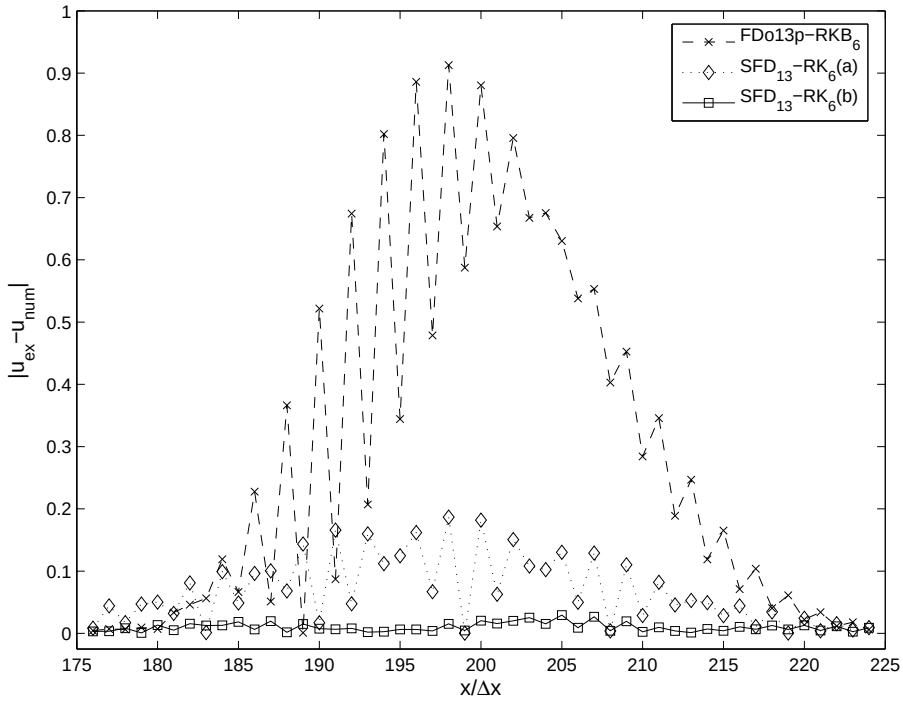

Figure 28: Errors at $\alpha = 1$ for the schemes SFD_{13}-$RK_6(a,b)$ and $FDo13p$-RKB_6.

taken large enough, $-250 \leq x \leq 250$, so that boundary conditions do not need to be implemented. The system (48) is solved with $\Delta x = 1$, $\alpha = 1$, and the time step size is determined from the CFL number as $\Delta t = \alpha\,\Delta x/(u_0 + c)$. The values of the coefficients are given by $u_0 = c/10$, $\gamma = 1.4$, $p_0 = 1$, $\rho_0 = 1$, and the initial perturbation used is

$$\begin{cases} \rho(x,0) = 1 \\ u(x,0) = 0 \\ p(x,0) = \mathrm{e}^{-(x/4)^2} \sin(2\pi x/5) \end{cases} \tag{51}$$

The results shown below are obtained after 200 time steps so that $t_{\text{end}} = 200\Delta t = 153.66$. Figures 29 and 31 show the density and Figures 30 and 32 show the errors on the density corresponding to the right travelling acoustic wave (it travels at a speed of $u_0 + c$) for the schemes of 11 and 13 points. Here the 9-points schemes do not give accurate solutions in this time interval. As it can be observed in these figures, the $FDo11p$-RKB_6 and $FDo13p$-RKB_6 schemes present important oscillations behind the acoustic wave. This is due to their total dispersion errors (see Figures 15 and 17). In general, the new optimized schemes show a better dispersive and dissipative behavior than the schemes proposed in [2, 3]. In addition, the errors of the acoustic wave for the new optimizations are smaller in amplitude than those of the schemes proposed in [2, 3]. In particular, the schemes of 13 points present lower trailing oscillations behind the acoustic wave than the schemes of 11 points. In addition, the most accurate results for this problem are given by

the SFD_{13}-$RK_6(b)$ scheme.

Finally we consider a nonlinear test problem, the one-dimensional Euler equations

$$\begin{pmatrix} \rho_t \\ u_t \\ p_t \end{pmatrix} + \begin{pmatrix} u & \rho & 0 \\ 0 & u & \dfrac{1}{\rho} \\ 0 & \gamma p & u \end{pmatrix} \begin{pmatrix} \rho_x \\ u_x \\ p_x \end{pmatrix} = 0. \tag{52}$$

The initial perturbation used is a Gaussian pressure pulse at the center of the domain given by

$$\begin{cases} \rho(x,0) = 1 \\ u(x,0) = 0 \\ p(x,0) = \dfrac{1}{\gamma} + \Delta p\, \mathrm{e}^{-\beta x^2} \end{cases} \tag{53}$$

where $\gamma = 1.4$, $\beta = 0.05$ and $\Delta p = 0.035$. The computation domain is taken large enough, $-400 \leq x \leq 400$, so that boundary conditions do not need to be implemented. The system (52) is solved in dimensionless form with $\alpha = 1$, $c = 1$, and the time step is determined from the CFL number as $c\,\Delta t = \alpha\,\Delta x$. The time integration is propagated up to $t_{\text{end}} = 150$ for several values of the grid-size Δx. For numerical comparison we have computed a reference solution by using thirtieth-order thirty-one-point standard finite differences for spatial derivation and the six-stage RK algorithm RKB_6 with the CFL number $\alpha = 0.01$ for time integration as in [2]. The initial perturbation and the computed reference solution for the pressure are shown in Figures 33 and 34, respectively. The error is evaluated as

$$\text{error} = \sum_{i=1}^{N} |p_{\text{ref}}(x_i) - p_{\text{num}}(x_i)|, \tag{54}$$

where N is the number of mesh points and p_{ref} the reference solution.

Figures 35 and 36 show the errors as a function of the grid-size Δx (in logarithmic scale) for the schemes of 9, 11 and 13 points. As it can be observed, for a grid-size Δx lower than 0.5, the order of accuracy defines the slope of the error curve. In this case all the schemes considered here present accuracy of fourth-order. On the other hand, when Δx is greater than 0.5, the slope of the error curve appears influenced by the dispersion and dissipation errors. Finally, we have observed that for this problem the most accurate results are given by the schemes SFD_{13}-$RK_6(a)$ and $FDo11p$-RKB_6.

6 Conclusions

A class of optimized explicit methods constituted by symmetric FD schemes for spatial derivation and low storage RK algorithms for time integration is proposed. The methods

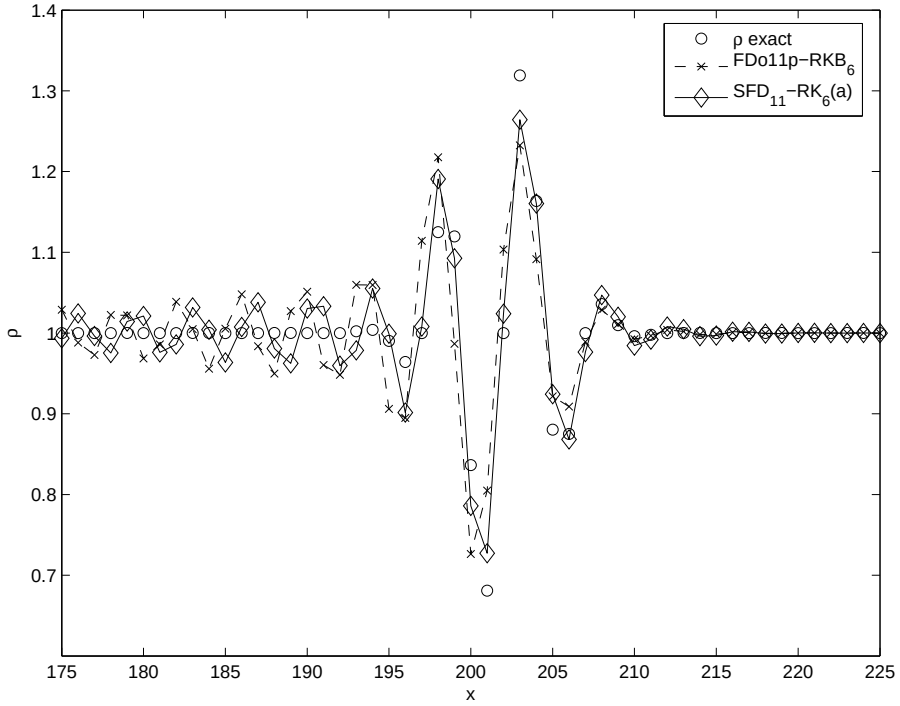

Figure 29: Density for the schemes SFD_{11}-$RK_6(a)$ and $FDo11p$-RKB_6.

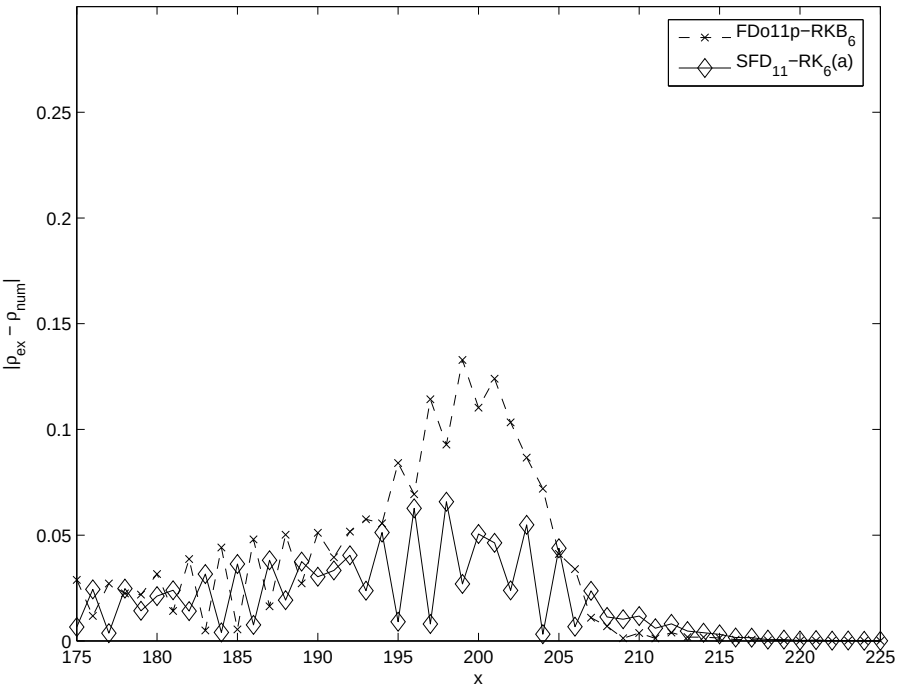

Figure 30: Errors on the density for the schemes SFD_{11}-$RK_6(a)$ and $FDo11p$-RKB_6.

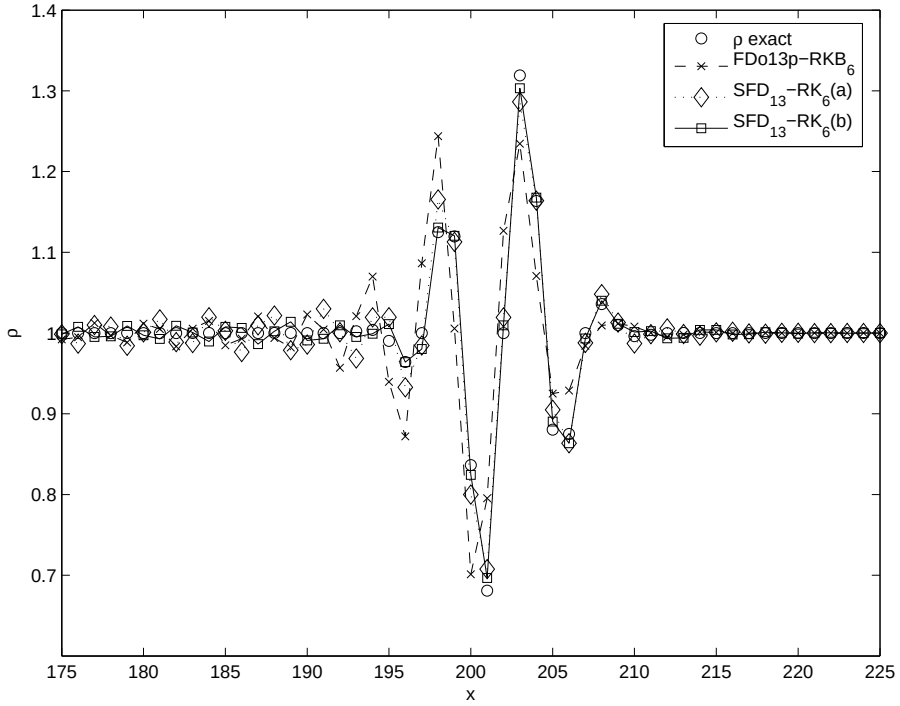

Figure 31: Density for the schemes SFD_{13}-$RK_6(a,b)$ and $FDo13p$-RKB_6.

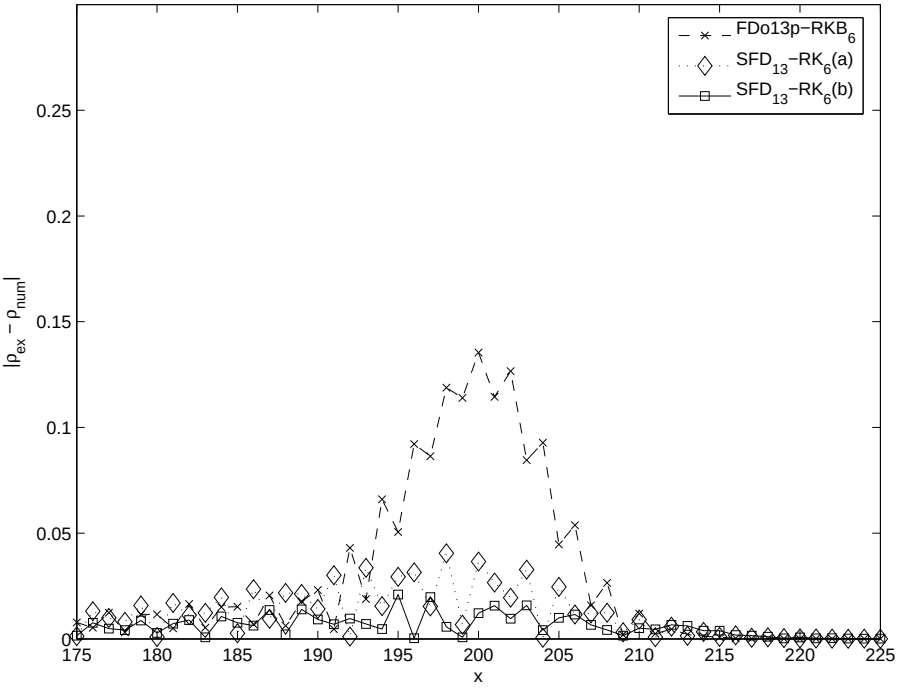

Figure 32: Errors on the density for the schemes SFD_{13}-$RK_6(a,b)$ and $FDo13p$-RKB_6.

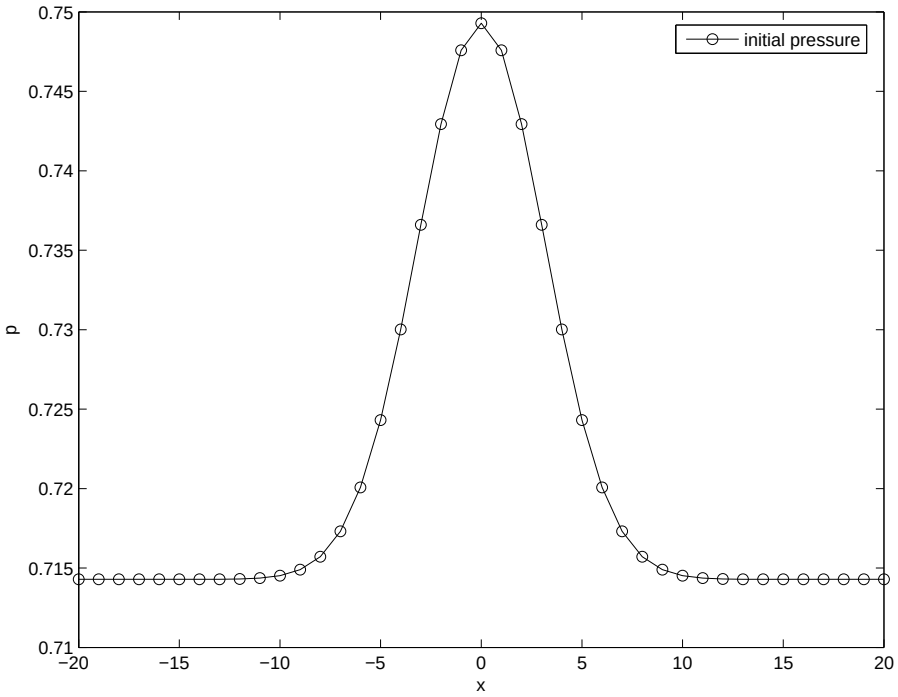

Figure 33: Initial pressure for the 1D Euler equations.

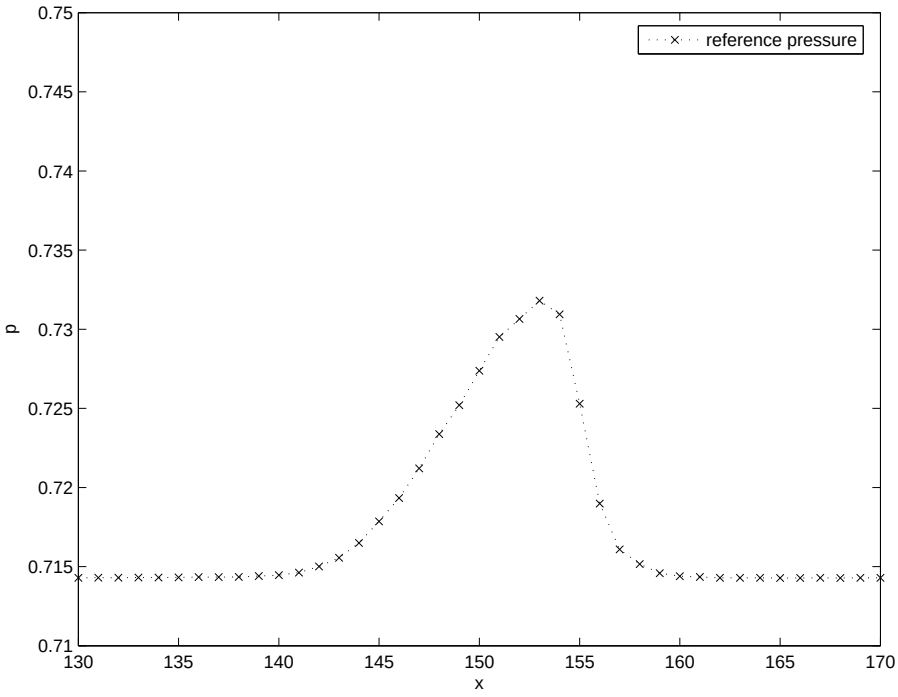

Figure 34: Reference pressure computed at $t = 150$ for the 1D Euler equations.

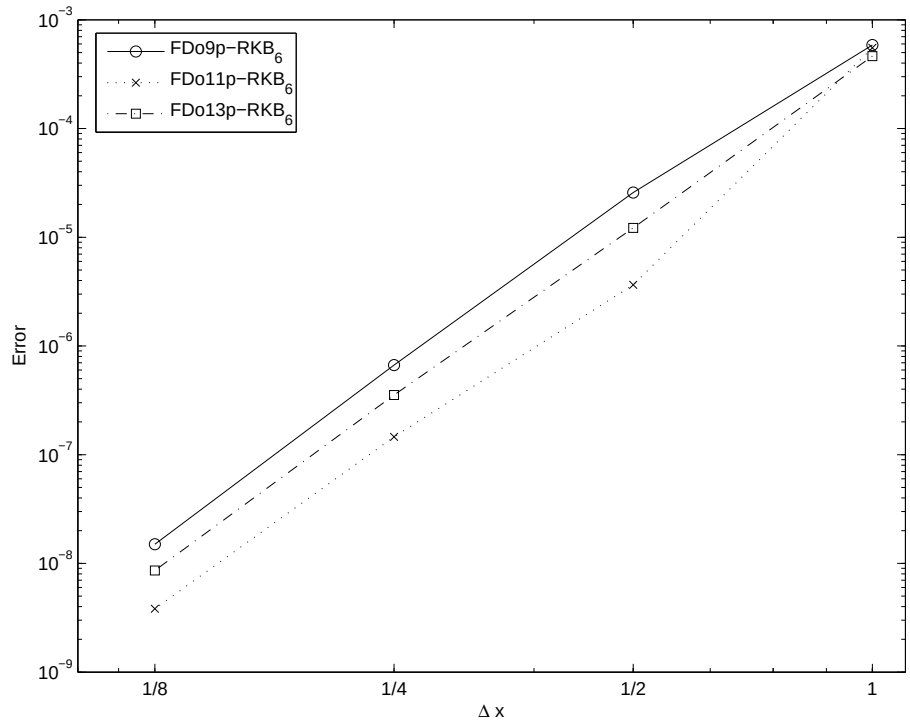

Figure 35: Propagation error as a function of Δx for the schemes of [2, 3].

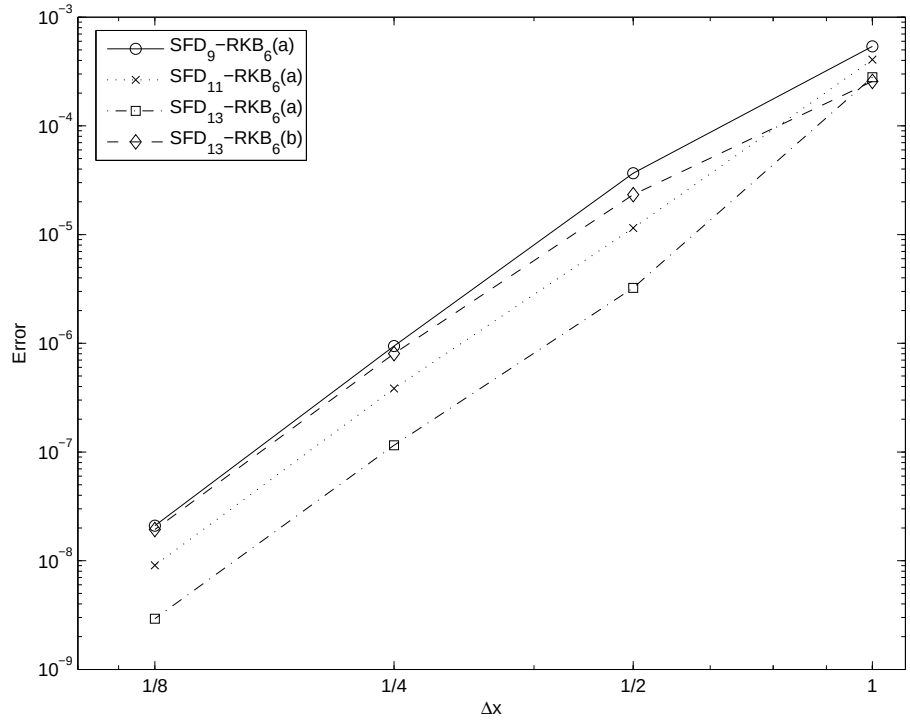

Figure 36: Propagation error as a function of Δx for the new schemes.

are characterized by the minimization of an error measure which takes into account the total dispersion and dissipation errors associated to spatial and temporal discretizations. This new approach allows to optimize the spatial scheme and the time advancement method simultaneously, in opposition to approaches followed by other authors. Optimizations were done on fourth-order symmetric FD schemes with 9, 11 and 13 points in combination with six-stage fourth-order explicit RK algorithms. Analysis of total dispersion and dissipation errors and evaluation of accuracy limits demonstrate the better dispersive properties of the new optimized methods when they are compared with the optimized schemes of [2, 3]. The numerical experiments carried out with 1D convection equations and 1D Euler model problems confirm the improvements in accuracy and efficiency of the new optimizations.

7 Future work

In the case of explicit RK methods we will investigate low-storage schemes when they are applied to solve differential problems related with the property of Total Variation Diminishing (TVD). When a RK method is used to solve an IVP:

$$U'(t) = F(U(t)), \quad U(t_0) = U_0 \tag{55}$$

resulting from an application of the method of lines to a Cauchy problem for a PDE, it yields approximations $U_n = (U_{n,1}, \ldots, U_{n,N})^T$ to the exact solution $U(n\Delta t)$ at $t_n = n\Delta t$, where $\Delta t > 0$ denotes the temporal step-size.

The property of TVD is

$$\|U_{n+1}\|_{TV} \leq \|U_n\|_{TV} \tag{56}$$

where $\|\cdot\|_{TV}$ is the seminorm defined by

$$\|U_n\|_{TV} = \sum_j |U_{n,j+1} - U_{n,j}|. \tag{57}$$

The main goal is the construction of high-order TVD Runge–Kutta schemes with the property of low-storage while preserving the TVD property.

Other research related with low-storage Runge–Kutta schemes is the analysis and study of new embedded pairs. It is well known that using a fixed step size policy is usually less efficient than allowing the step size to vary each step. Modern explicit Runge–Kutta methods have an error estimator that makes it possible to determine suitable step sizes to adjust dynamically the length of the step size in terms of the behavior of the local solution.

References

[1] V. Allampalli, R. Hixon, M. Nallasamy and S.D. Sawyer. High-accuracy large-step explicit Runge–Kutta (HALE-RK) schemes for computational aeroacoustics, J. Comput. Phys. **228**, 3837–3850 (2009).

[2] J. Berland, C. Bogey, C. Bailly: Optimized explicit schemes: matching and boundary schemes and 4th-order Runge–Kutta algorithm, 10th AIAA/CEAS Aeroacoustics Conference, Paper AIAA 2004-2814.

[3] C. Bogey, C. Bailly: A family of low dispersive and low dissipative explicit schemes for flow and noise computations, *J. Comput. Phys.*, **194** (2004) 194–214.

[4] M. Calvo, J.M. Franco, L. Rández: Minimum storage Runge–Kutta schemes for computational acoustics, *Comp. Math. Appl.*, **45** (2003) 535–545.

[5] M. Calvo, J.M. Franco, L. Rández: A new minimum storage Runge–Kutta scheme for computational acoustics, *J. Comput. Phys.*, **201** (2004) 1–12.

[6] M. Calvo, J.M. Franco, L. Rández: Highly stable RK time advancing schemes for Computational Aero Acoustics, Bol. Soc. Esp. Mat. Apl. **50**, (2010), 83–99.

[7] M. Calvo, J.M. Franco, L. Rández: On some new low storage implementations of time advancing Runge-Kutta methods, J. Computational Applied Mathematics, Vol. 236, **15** (2012), 3665–3675.

[8] M.H. Carpenter, C.A. Kennedy: A fourth-order $2N$-storage Runge–Kutta scheme, NASA TR TM109112, June 1994.

[9] E. Hairer, S.P. Norsett, G. Wanner: *Solving Ordinary Differential Equations I: Non-stiff Problems*, Springer–Verlag, Berlin, 1993.

[10] Z. Haras, S. Ta'asan: Finite difference schemes for long-time integration, *J. Comput. Phys.*, **114** (1994) 265–279.

[11] P. J. van der Houwen: Construction of Integration Formulas for Initial Value Problems, North-Holland, Amsterdam (1977).

[12] F.Q. Hu, M.Y Hussaini, J. Manthey: Low-dissipation and low-dispersion Runge–Kutta schemes for computational acoustics, *J. Comput. Phys.*, **124** (1996) 177–191.

[13] C.A. Kennedy, M.H. Carpenter, R.M. Lewis: Low-storage, explicit Runge–Kutta schemes for the compressible Navier–Stokes equations, NASA/CR-1999-209349, ICASE Report No. 99-22, 1999.

[14] D. I. Ketcheson, Highly efficient strong stability preserving Runge–Kutta methods with low storage implementations, SIAM Journal on Scientific Computing, **30**, 2113–2136 (2008).

[15] D. I. Ketcheson, Runge–Kutta Methods with Minimum-Storage Implementations, Journal of Computational Physics **229**, 1763–1773 (2010).

[16] J.W. Kim, D.J. Lee: Optimized compact finite difference schemes with maximum resolution, *AIAA Journal*, **34** (1996) 5.

[17] S.K. Lele: Compact finite difference schemes with spectral-like resolution, *J. Comput. Phys.*, **103** (1992) 16–42.

[18] K. Mahesh: A family of high order finite difference schemes with good spectral resolution, *J. Comput. Phys.*, **145** (1998) 332–358.

[19] J. Ramboer, T. Broeckhoven, S. Smirnov, C. Lacor: Optimization of time integration schemes coupled to spatial discretization for use in CAA applications, *J. Comput. Phys.*, **213** (2006) 777–802.

[20] D. Stanescu, W.G. Habashi: $2N$-storage low dissipation and dispersion Runge–Kutta schemes for computational acoustics, *J. Comput. Phys.*, **143** (1998) 674–681.

[21] C.K.W. Tam: Computational aeroacoustics: issues and methods, *AIAA Journal*, **33**(10) (1995) 1788–1797.

[22] C.K.W. Tam, J.C. Webb: Dispersion-relation-preserving finite difference schemes for computational acoustics, *J. Comput. Phys.*, **107** (1993) 262–281.

[23] J.H. Williamson: Low-storage Runge–Kutta schemes, *J. Comput. Phys.*, **35** (1980) 48–56.

Rev. Real Academia de Ciencias. Zaragoza. **67:** 51–103, (2012).
ISSN: 0370-3207

The Geometrical Formulation of Quantum Mechanics

J. Clemente-Gallardo

BIFI-Depto. de Física Teórica and Unidad Asociada IQFR-BIFI

Universidad de Zaragoza, Edificio I+D–Campus Río Ebro, 50018 Zaragoza (SPAIN)

Premio a la Investigación de la Academia 2012. Sección de Físicas

Abstract

The approaches to Classical and Quantum Mechanics are quite different in many aspects, the most striking one being the linear structure which is present in the Hilbert space $\mathcal{H}$ and which is considered usually as one of the most relevant aspects of the formalism. There are also suggestive similarities, as has been noted often (see [31, 32, 41, 49]) but they have been approached mainly from the algebraic point of view. Our goal in this paper is to describe an alternative description of Quantum Mechanics which is formally analogue to the description of nonrelativistic Classical Mechanics from a geometrical perspective. We will also discuss the main advantages of this new approach, and the most significative differences. We also present two applications to physically relevant examples: the ability to discuss independence of quantum observables (in the context of entanglement witnesses) and a Hamiltonian description of Ehrenfest equations for molecular systems.

1 Introduction

The aim of this paper is to summarize the most relevant aspects of a geometrical formulation of Quantum Mechanics, which is being developed since the last seventies and has been the main line of research of the author in the last five years. For the sake of simplicity, we will consider only the case of finite dimensional systems, although from a formal point of view, most of the results presented here can be extended to the infinite dimensional case. The original references to the results presented in this work can be found in [2, 3, 4, 7, 8, 24, 28, 29, 30] and are due to several people, who were kind enough

to share part of their knowledge and time with the author along these years. He would like that this work serve also as a small tribute for all of them.

The origins of the construction, though, go back to the end of the seventies, and has been developed by many different researchers. Just to mention the most relevant references ordered chronologically, let us refer to former interesting approaches as [48], the seminal work by Kibble [39], the works by Cantoni ([19, 20, 21, 22, 23]), by Cirelly and co-workers ([25, 26, 27]), the more physically oriented approach by Heslot [37], Bloch's paper ([11]), the work by Anandan[5, 6], and then Ashtekar and Schilling [9]. There are several interesting works by Brody and coworkers ([14] is the one closer to the work presented here, although other results, more oriented to Statistical Mechanics such as [13, 15, 16, 17, 18] are also relevant) and also from Spera and coworkers ([10, 47]) .

Abstracting from all these works, let us begin our study in a very general framework. If we want to describe a physical system, what would the minimal mathematical apparatus we need? From a fairly general point of view, the minimal mathematical structure we can think of contains:

- a space of states, which we denote as $\mathcal{S}$ and which encodes the information that we consider relevant to describe the physical system in an unambiguous way,
- a space of observables, that we denote as $\mathcal{O}$, and which encodes the set of possible representations of physical magnitudes,
- and finally, a way of representing the measurement process, i.e., a pairing $\mathcal{O}\times\mathcal{S} \to \mathbb{R}$ which assigns a real number to any magnitude and a given state.
- If we want to describe some sort of evolution, we must define also a differential (or difference, if the system is discrete) equation whose solutions define the trajectories of the physical system.

For instance, in the case of the the Hamiltonian (or Lagrangian) nonrelativistic Classical Mechanics, the situation is very well known:

- The states of the physical system are described by a phase space which contains the set of positions and momenta of the system (or the set of positions and the set of velocities if we are considering a Lagrangian description). Depending on the situation, $\mathcal{S}$ takes some extra structure, which is used to provide a tensorial description of the dynamics and the rest of the tools we use. Thus, we can find the form of a vector space, a cotangent bundle, a symplectic, a Poisson (or even, in a more general framework, a Dirac) manifold. Also, Riemannian metrics may be introduced in order to describe special systems.

- The set of observables corresponds to the set of functions defined on the phase space, the corresponding pairing being the evaluation of the functions on the corresponding point.

- The dynamics can be introduced in several equivalent ways, which encode within the different structures introduced, the content of Newton equations. In the case of Hamiltonian Mechanics, dynamics arises as the integral curves of the Hamiltonian vector field associated to a special function, called the Hamiltonian and denoted as h, which represents the energy of the system. If we denote as $\{\cdot,\cdot\}$ the Poisson bracket defined on the set of functions of $\mathcal{S}$ and associated to the tensor chosen we can write the vector field representing the dynamics in an intrinsic way as

$$X_h = \{h, \cdot\} \tag{1}$$

That is a brief summary of the mathematical description of a classical system. What about a quantum one? The usual approaches to Quantum Mechanics present a situation quite different to the above. The standard presentations, split the description in two "pictures", one where the primary object are the physical states (the Schrödinger picture) and one where the main objects are the physical observables (the Heisenberg picture). Let us review very quickly both of them from the perspective above:

- In the Schrödinger picture of Quantum Mechanics,

  - the states of the physical system are considered to belong to a Hilbert space $\mathcal{H}$, or rather, to the corresponding projective space, i.e. the space of complex rays in $\mathcal{H}$, since all the points differing by a phase are considered physically equivalent, and the norm of the states must be equal to one, since it is probabilistic in nature.
  - On the other hand, the physical magnitudes are modelled as self-adjoint operators defined on $\mathcal{H}$, i.e., modulo the complex unit, the set of observables is identified with the Lie algebra $\mathfrak{u}(\mathcal{H})$ of the unitary group $U(\mathcal{H})$ associated to the Hilbert space $\mathcal{H}$.
  - The pairing is defined as the quadratic function

$$\mathcal{O} \times \mathcal{S} \to \mathbb{R}; \qquad (A, |\psi\rangle) \mapsto \frac{\langle\psi|A\psi\rangle}{\langle\psi|\psi\rangle},$$

    even if the measure process is still a challenging problem (see [50, 51] and references therein).

– Dynamics is introduced on $\mathcal{H}$ via the Schrödinger equation, defining the evolution as the solutions of the differential equation:

$$i\hbar\frac{\partial|\psi(t)\rangle}{\partial t} = H|\psi(t)\rangle, \tag{2}$$

where H is the Hermitian operator which represents the energy of the system.

- In the Heisenberg picture of Quantum Mechanics, that we can present following the algebraic approach by Segal [46] or Haag and Kastler [36], we find that:
  - The physical magnitudes are the primary object and are supposed to define the real part of a $\mathbb{C}^*$–algebra $\mathcal{A}$ (see [33] for a classical presentation of the concept),
  - the states of the physical system are defined as positive linear functionals ρ on $\mathcal{A}$, normalized by the condition

$$\mathrm{Tr}\rho = 1$$

  - The pairing is defined via the trace operation (see [34] for the theorem proving the result in general)

$$\mathcal{O}\times\mathcal{S}\to\mathbb{R}; \qquad (A,\rho)\mapsto \mathrm{Tr}(\rho A)$$

  - Dynamics is introduced on $\mathcal{A}$ via the Heisenberg equation, defining the evolution as the solutions of the differential equation:

$$i\hbar\frac{\partial A(t)}{\partial t} = (A(t)H - HA(t)), \tag{3}$$

where again H denotes the Hamiltonian operator.

We can notice then that the approaches to Classical and Quantum Mechanics are quite different in many aspects, the most striking one being the linear structure which is present in the Hilbert space $\mathcal{H}$ and which is considered usually as one of the most relevant aspects of the formalism. There are also suggestive similarities, as has been noted often (see [31, 32, 41, 49]) but they have been approached mainly from the algebraic point of view. Our goal in this paper is to describe an alternative description of Quantum Mechanics which is formally analogue to the description of nonrelativistic Classical Mechanics from a geometrical perspective. We will also discuss the main advantages of this new approach, and the most significative differences. We also present two applications to physically relevant examples: the ability to discuss independence of quantum observables (we will use the concept in the context of entanglement witnesses) and a Hamiltonian description of Ehrenfest equations for molecular systems, which allows, for instance, to define a simple

measure, which is preserved by the dynamics, and which allows us to formulate a rigorous extension to Statistical Mechanics (see [2, 4]).

The structure of the paper is as follows. In Section 2 we introduce the geometrical construction for a quantum mechanical system on a pure state for both the Schrödinger and the Heisenberg pictures, and prove that they are actually related by the momentum mapping of the action of the unitary group on the Hilbert space. Both approaches are then equivalent and we are able to define the equivalence explicitly. Section 3 is devoted to the analysis of the mixed states: we will see how we can use the geometrical structures of the dual of the Lie algebra of the unitary group of the Hilbert space, to endow the set with tensorial objects which are analogue to the ones introduced in the case of pure states. Finally, the last two sections present two simple applications where the geometrical formalism introduced provide us with tools which have no analogue in the usual description of Quantum Mechanics. In particular, in Section 4 we introduce a notion of independence of operators which is not available in the usual framework because of the lack of a consistent non-commutative calculus. We exemplify it by proving the independence of two entanglement witnesses defined on mixed states and used vastly in Quantum Information Theory. Finally, Section 5 presents a recent application of the geometric formalism introduced to define a Hamiltonian formalism for the Ehrenfest description of mixed quantum-classical systems (used often to describe, in an approximate way, molecular systems). We will see how the symplectic description we introduce for quantum dynamics allows us to combine the description of a quantum system with the description of a classical system and couple their dynamics together.

2 Geometric formulation of Quantum Mechanics

As we just mentioned, the aim of this section is simply to provide a tensorial characterization of Quantum Mechanics which is similar to the description of geometric Classical Mechanics. We will proceed step-by-step and study the construction first at the level of a pure-state description and later at a general level. Therefore, the first sections refer mainly to the Schrödinger representation, even if we will discuss some aspects of the Heisenberg approach also.

2.1 Representation of pure states

To introduce the real manifold point of view, we start by replacing the Hilbert space $\mathcal{H}$ with its realification $\mathcal{H}_{\mathbb{R}} := M_Q$. In this realification process the complex structure on $\mathcal{H}$ will be represented by a tensor J on M_Q as we will see.

The natural identification is then provided by choosing a basis $\{|z_k\rangle\}$ in $\mathcal{H}$ and splitting the corresponding coordinates into their real and imaginary parts:

$$|\psi\rangle = \sum_k \psi_k |z_k\rangle \qquad \psi_k \to \psi_k^R + i\psi_k^I$$

Then,

$$\{\psi_1, \cdots, \psi_n\} \in \mathcal{H} \mapsto \{\psi_1^R, \cdots, \psi_n^R, \psi_1^I, \cdots \psi_n^I\} \equiv (\Psi_R, \Psi_I) \in \mathcal{H}_{\mathbb{R}}.$$

Under this transformation, the Hermitian product becomes, for $\psi^1, \psi^2 \in \mathcal{H}$

$$\langle (\Psi_R^1, \Psi_I^1), (\Psi_R^2, \Psi_I^2) \rangle = (\langle \Psi_R^1, \Psi_R^2 \rangle + \langle \Psi_I^1, \Psi_I^2 \rangle) + i(\langle \Psi_R^1, \Psi_I^2 \rangle - \langle \Psi_I^1, \Psi_R^2 \rangle).$$

To consider $\mathcal{H}_{\mathbb{R}}$ just as a real differential manifold, the algebraic structures available on $\mathcal{H}$ must be converted into tensor fields on $\mathcal{H}_{\mathbb{R}}$. Consider first the tangent and cotangent bundles $T\mathcal{H}$ and $T^*\mathcal{H}$ and the following structures:

- The complex structure of $\mathcal{H}$ is translated into a tensor

  $$J : M_Q \to M_Q,$$

  satisfying $J(\Psi_R, \Psi_I) = (-\Psi_I, \Psi_R)$ for any point $(\Psi_R, \Psi_I) \in M_Q$. It is immediate to verify that in this case

  $$J^2 = -\mathbb{I}.$$

- The linear structure available in M_Q is encoded in the vector field Δ

  $$\Delta : M_Q \to TM_Q \quad \psi \mapsto (\psi, \psi).$$

- With every vector we can associate a vector field

  $$X_\psi : M_Q \to TM_Q \quad \phi \to (\phi, \psi)$$

  These vector fields are the infinitesimal generators of the vector group M_Q acting on itself.

- The Hermitian tensor $\langle \cdot, \cdot \rangle$ defined on the complex vector space $\mathcal{H}$, can be written in geometrical terms as

  $$\langle X_{\psi_1}, X_{\psi_2} \rangle(\phi) = \langle \psi_1, \psi_2 \rangle.$$

  On the "real manifold" the Hermitian scalar product may be written as

  $$\langle \psi_1, \psi_2 \rangle = g(X_{\psi_1}, X_{\psi_2}) + i\,\omega(X_{\psi_1}, X_{\psi_2}),$$

  where g is now a symmetric tensor and ω a skew-symmetric one.

The properties of the Hermitian product ensure that:

- the symmetric tensor is positive definite and non-degenerate, and hence defines a Riemannian structure on the real vector manifold.
- the skew-symmetric tensor is also non degenerate, and is closed with respect to the natural differential structure of the vector space. Hence, the tensor is a symplectic form (see also [42])

As the inner product is sesquilinear, it satisfies

$$\langle \psi_1, i\psi_2 \rangle = i\langle \psi_1, \psi_2 \rangle, \qquad \langle i\psi_1, \psi_2 \rangle = -i\langle \psi_1, \psi_2 \rangle.$$

This implies

$$g(X_{\psi_1}, X_{\psi_2}) = \omega(JX_{\psi_1}, X_{\psi_2}).$$

We also have that $J^2 = -\mathbb{I}$, and hence that the triple (J, g, ω) defines a Kähler structure (see [25, 27]). This implies, among other things, that the tensor J generates both finite and infinitesimal transformations which are orthogonal and symplectic.

The choice of the basis also allows us to introduce adapted coordinates for the realified structure:

$$\langle z_k, \psi \rangle = (q_k + ip_k)(\psi),$$

and write the geometrical structures introduced above as:

$$J = \partial_{p_k} \otimes dq_k - \partial_{q_k} \otimes dp_k \quad g = dq_k \otimes dq_k + dp_k \otimes dp_k \quad \omega = dq_k \wedge dp_k$$

Note 1. *If we represent the points of $\mathcal{H}$ by using complex coordinates we can write the Hermitian structure by means of $z_n = q^n + ip_n$:*

$$h = \sum_k d\bar{z}_k \otimes dz_k,$$

where of course

$$\langle X_{\psi_1} | X_{\psi_2} \rangle = h(X_{\psi_1}, X_{\psi_2}),$$

the vector fields now being the corresponding ones on the complex manifold.

In an analogous way we can consider a contravariant version of these tensors. The coordinate expressions with respect to the natural basis are:

- the Riemannian structure $G = \sum_{k=1}^{n} \left(\frac{\partial}{\partial qk} \otimes \frac{\partial}{\partial q^k} + \frac{\partial}{\partial p_k} \otimes \frac{\partial}{\partial p_k} \right)$,
- the Poisson tensor $\Omega = \sum_{k=1}^{n} \left(\frac{\partial}{\partial q^k} \wedge \frac{\partial}{\partial p_k} \right)$
- while the complex structure has the form

$$J = \sum_{k=1}^{n} \left(\frac{\partial}{\partial p_k} \otimes dq^k - \frac{\partial}{\partial q^k} \otimes dp_k \right)$$

2.1.1 Example I: the Hilbert space of a two level quantum system

For a two levels system we will consider an orthonormal basis on $\mathbb{C}^2$, say $\{|e_1\rangle, |e_2\rangle\}$. We introduce thus a set of coordinates

$$\langle e_j|\psi\rangle = z^j(\psi) = q^j(\psi) + ip_j(\psi) \qquad j = 1, 2.$$

In the following we will use z^j or q^j, p_j omitting the dependence in the state ψ as it is usually done in differential geometry.

The set of physical states is not equal to $\mathbb{C}^2$, since we have to consider the equivalence relation given by the multiplication by a complex number i.e.

$$\psi_1 \sim \psi_2 \Leftrightarrow \psi_2 = \lambda\psi_1 \qquad \lambda \in \mathbb{C}_0 = \mathbb{C} - \{0\}.$$

And besides, the norm of the state must be equal to one. These two properties can be encoded in the following diagram:

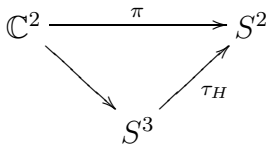

where S^2 and S^3 stand for the two and three dimensional spheres, and the projection τ_H is the Hopf fibration. The projection π is associating each vector with the one-dimensional complex vector space to which it belongs. Thus we see how this projection factorizes through a projection onto S^3 and a further projection given by the Hopf fibration, which is a $U(1)$–fibration.

The Hermitian inner product on $\mathbb{C}^2$ can be written in the coordinates z_1, z_2 as

$$\langle\psi|\psi\rangle = \bar{z}_j z^k \langle e_k|e_j\rangle = \bar{z}_j z^j.$$

Equivalently we can write it in real coordinates q, p and obtain:

$$\langle\psi|\psi\rangle = p_1^2 + p_2^2 + (q^1)^2 + (q^2)^2$$

We can also obtain these tensors in contravariant form if we take as starting point the Hilbert space $\mathcal{H} = \mathbb{C}^2$. If we repeat the steps above, we obtain the two contravariant tensors:

$$G = \frac{\partial}{\partial q^k} \otimes \frac{\partial}{\partial q^k} + \frac{\partial}{\partial p_k} \otimes \frac{\partial}{\partial p_k} \qquad \Lambda = \frac{\partial}{\partial q^k} \wedge \frac{\partial}{\partial p_k}.$$

Other tensors encode the complex vector space structure of $\mathcal{H} = \mathbb{C}^2$:

- the dilation vector field $\Delta = q^1 \frac{\partial}{\partial q^1} + p_1 \frac{\partial}{\partial p_1} + q^2 \frac{\partial}{\partial q^2} + p_2 \frac{\partial}{\partial p_2}$,
- and the complex structure tensor $J = dp_1 \otimes \frac{\partial}{\partial q^1} - dq^1 \otimes \frac{\partial}{\partial p_1} + dp_2 \otimes \frac{\partial}{\partial q^2} - dq^2 \otimes \frac{\partial}{\partial p_2}$.

2.2 The complex projective space

Another important aspect of the Hilbert space description of Quantum Mechanics is the study of the global phase of the state. It is a well known fact that physical states are independent of the global phase of the element of the Hilbert space that we choose to represent them. In the formulation as a real vector space, we can represent the multiplication by a phase on the manifold M_Q as a transformation whose infinitesimal generator is written as:

$$\Gamma = \sum_k \left(p_k \frac{\partial}{\partial q^k} - q^k \frac{\partial}{\partial p_k} \right). \tag{4}$$

The meaning of this vector field is simple to understand if we realize that a phase change changes the angle of the complex number representing the state, when considered in polar form (i.e. in polar coordinates $\{r^i, \theta^i\}_{i=1,\cdots,n}$, Eq. (4) becomes just

$$\Gamma = \sum_k \frac{\partial}{\partial \theta^k}.$$

Then, from a geometrical point of view we can use Eq. (4) in two ways:

- Computing its integral curves, which are the different states which are obtained from an initial one by a global phase multiplication.
- Acting with the vector field on functions of M_Q (which will represent our observables) providing us with the effect of the global phase transformation on the observables.

We can also consider another important vector field, which encodes the linear space structure of the tangent bundle TM_Q. In order to avoid singularities let us eliminate the zero section of the bundle TM_Q and denote the resulting space by T_0M_Q. We remind the reader that M_Q is just the realification of a complex vector space and, as such, we can encode its linear structure in the dilation vector field, which reads:

$$\Delta : M_Q \to T_0 M_Q; \qquad \psi \mapsto (\psi, \psi) \tag{5}$$

In the coordinate system (q^k, p_j), it takes the form

$$\Delta = q^k \frac{\partial}{\partial q^k} + p_k \frac{\partial}{\partial p_k} \tag{6}$$

We are particularly interested in the relation of the vector fields Δ and Γ. In particular:

Lemma 1. *Δ and Γ define a foliation on the manifold M_Q.*

Proof. It is simple to relate Δ with Γ via the complex structure, in the form:

$$\Gamma = J(\Delta). \tag{7}$$

Then it is straightforward to prove that both vector fields commute. □

We thus have an integrable distribution defined on the manifold M_Q. We can thus define the corresponding quotient manifold identifying the points which belong to the same orbit of the generators Γ and Δ. Notice that, from the physical point of view, this corresponds to the identification of points in the same ray of the Hilbert space.

Definition 1. *The resulting quotient manifold, denoted as $\mathcal{P}$, defined as*

$$\pi : M_Q \to \mathcal{P} \tag{8}$$

is called the ***complex projective space*** *and its points represent the physical pure states of a quantum system. We will denote by $[\psi]$ the point in $\mathcal{P}$ which is the image by π of a point $\psi \in M_Q$:*

$$\mathcal{P} \ni [\psi] := \pi(\psi) \qquad \psi \in M_Q \tag{9}$$

2.3 The observables

Our aim now is to provide a representation of the physical magnitudes, such as the energy or the angular momentum, in terms of the geometric objects introduced in the previous section. There are several possibilities, but we will consider only the simplest one from the mathematical point of view, and, at the same time, the most meaningful one from a physical point of view.

We know that in the usual formulation of Quantum Mechanics, physical observables are represented by linear operators on the Hilbert space $\mathcal{H}$, which are self-adjoint with respect to the inner product. The information which is physically relevant, though, corresponds to the expectation value associated to each observable (the pairing we introduced in the introduction), at each normalized state $|\psi\rangle \in \mathcal{H}$:

$$A \mapsto f_A(\psi) = \frac{1}{2}\langle\psi|A\psi\rangle \qquad |\psi\rangle \in \mathcal{H} \quad \langle\psi|\psi\rangle = 1 \tag{10}$$

If we think in the point $|\psi\rangle$ as an element of the differentiable manifold M_Q instead, the function f_A turns out to be a quadratic function defined on M_Q. For arbitrary operators, the function f_A is complex-valued. Hermitian operators give rise thus to quadratic real valued functions. We will denote:

Definition 2. *We will represent as $\mathcal{F}(M_Q)$ the set of all possible quadratic functions on M_Q and as $\mathcal{F}_{\mathbb{R}}(M_Q)$ the subset of real functions associated to the set of Hermitian operators.*

An interesting issue is how to characterize, by using the quadratic functions $\mathcal{F}(M_Q)$, the algebraic structures the set of operators in endowed with and which are physically relevant, for instance, in Heisenberg approach

2.3.1 The algebraic structures

We know that on the set $\mathrm{End}(\mathcal{H})$ there are three relevant ones:

- an associative product

$$\cdot : \mathrm{End}(\mathcal{H}) \times \mathrm{End}(\mathcal{H}) \to \mathrm{End}(\mathcal{H}) \qquad (A, B) \mapsto AB \tag{11}$$

- its symmetric part

$$\circ : \mathrm{End}(\mathcal{H}) \times \mathrm{End}(\mathcal{H}) \to \mathrm{End}(\mathcal{H}) \qquad (A, B) \mapsto A \circ B = AB + BA \tag{12}$$

  which defines a structure called **Jordan algebra** (see [38, 40]). The definition is as follows:

  Definition 3. *A commutative algebra $(\mathcal{A}, \circ)$ over a field $\mathbb{K}$ is called a **Jordan algebra** if*

$$(x \circ y) \circ (x \circ x) = x \circ (y \circ (x \circ x)) \qquad \forall x, y \in \mathcal{A}$$

  It can be easily proved that $(\mathrm{End}(\mathcal{H}, \circ)$ defines a Jordan algebra.

- and its skew-symmetric part,

$$[\cdot, \cdot] : \mathrm{End}(\mathcal{H}) \times \mathrm{End}(\mathcal{H}) \to \mathrm{End}(\mathcal{H}) \qquad (A, B) \mapsto [A, B] := -i(AB - BA) := -i[A, B]_-, \tag{13}$$

  which defines a Lie algebra structure on $\mathrm{End}(\mathcal{H})$, where we recall that

  Definition 4. *A **Lie algebra** is a vector space $\mathfrak{g}$ over a field $\mathbb{K}$ endowed with a bilinear operation $[\cdot, \cdot]$, which is skewsymmetric and satisfies the Jacobi identity, i.e.,*

$$[x, [y, z]] + [z, [x, y]] + [y, [z, x]] = 0 \qquad \forall x, y, z \in \mathfrak{g}.$$

  Notice that we introduce the imaginary unit in order to make it an inner operation in the subspace of Hermitian operators.

The Jordan and the Lie structures can be combined together to define a Lie-Jordan structure (see [40]):

Definition 5. *A **Lie-Jordan algebra** is a real vector space $\mathcal{L}$ endowed with a Jordan structure $\circ$ and a Lie structure $[\cdot, \cdot]$ which satisfy:*

- *the Lie bracket defines derivations of the Jordan product, i.e. $[a, b \circ c] = [a, b] \circ c + b \circ [a, c]$ for all $a, b, c \in \mathcal{L}$*
- *the associator of the Jordan structure can be obtained from the Lie bracket, i.e. for all $a, b, c \in \mathcal{L}$, $(a \circ b) \circ c - a \circ (b \circ c) = \hbar^2 [b, [c, a]]$ where $\hbar \in \mathbb{R}$.*

The set of physical magnitudes is the subset of $\mathrm{End}(\mathcal{H})$ defined by Hermitian operators. Modulo a multiplication by the imaginary unit, that subset corresponds to $\mathfrak{u}(\mathcal{H})$, the Lie algebra of the unitary group $U(\mathcal{H})$. Being a linear subspace, we can restrict easily the three operations above to the set, and define the corresponding operations on the Lie algebra. Moreover, $\mathfrak{u}(\mathcal{H})$ may be identified with its dual $\mathfrak{u}^*(\mathcal{H})$ by the (regular) scalar product defined as

$$\langle\cdot|\cdot\rangle : \mathfrak{u}(\mathcal{H}) \times \mathfrak{u}(\mathcal{H}) \to \mathbb{R}; \qquad \langle A|B\rangle = \frac{1}{2}\mathrm{Tr}AB, \quad \forall A, B \in \mathfrak{u}(\mathcal{H}).$$

The corresponding isomorphism

$$\zeta : \mathfrak{u}(\mathcal{H}) \to \mathfrak{u}^*(\mathcal{H}) \tag{14}$$

allows us to export the geometric and algebraic structures existing in each space, into the other. We can therefore consider the canonical Lie-Poisson structure of the dual $\mathfrak{u}^*(\mathcal{H})$ as a tensor on the space of observables (and therefore we can consider Hamiltonian dynamics), or extend the Jordan structure defined on $\mathfrak{u}(\mathcal{H})$ (since it is contained in $\mathrm{End}(\mathcal{H})$) into its dual.

In particular we can define two tensors

$$[R(\hat{A}, \hat{B})](\xi) = \langle \xi, A \circ B\rangle_{\mathfrak{u}^*} = \mathrm{Tr}(\xi(AB + BA)) \qquad \forall A, B \in \mathfrak{u}(\mathcal{H}) \tag{15}$$

and

$$[\Lambda(\hat{A}, \hat{B})](\xi) = \langle \xi, [A, B]\rangle_{\mathfrak{u}^*} = -i\mathrm{Tr}(\xi(AB - BA)) \qquad \forall A, B \in \mathfrak{u}(\mathcal{H}). \tag{16}$$

where we represent as $\hat{A}$ and $\hat{B}$ the linear functions defined on $\mathfrak{u}^*$ which correspond to the elements $A.B \in \mathfrak{u}(\mathcal{H})$ respectively. Notice that these R is the tensor defined on $\mathfrak{u}(\mathcal{H})$ by the operation defined in Eq. (12) when restricted to $\mathfrak{u}(\mathcal{H}) \subset \mathrm{End}(\mathcal{H})$ and transferred to $\mathfrak{u}^*(\mathcal{H})$ via the isomorphism ζ. On the other hand, the tensor Λ is the tensor defining the Lie-Poisson structure on $\mathfrak{u}^*(\mathcal{H})$. Notice that these two tensors are the geometric objects which directly encode Heisenberg formalism, which is defined on $\mathfrak{u}(\mathcal{H})$ in a natural way, or, via the isomorphism ζ, on $\mathfrak{u}^*(\mathcal{H})$.

Having defined contravariant tensors on M_Q to encode in a Kähler structure the Hermitian product of the Hilbert space, it makes sense to consider the action of those objects on the set of functions. It is immediate to verify that the tensors allow us to implement, at the level of quadratic functions, the three structures above

Lemma 2. *Consider two functions $f_A, f_B \in \mathcal{F}(M_Q)$. Then, the action of the tensors G and Ω define inner operations which encode the algebraic structures of the set of linear operators on the Hilbert space $\mathcal{H}$:*

$$G(df_A, df_B) = \{f_A, f_B\}_+ = f_{A\circ B} \qquad \Omega(df_A, df_B) = \{f_A, f_B\} = f_{[A,B]} \tag{17}$$

If we combine both tensors, we are able to reproduce, at the level of $\mathcal{F}(M_Q)$, the identity:

$$AB = \frac{1}{2}(AB + BA) + \frac{1}{2}(AB - BA) = \frac{1}{2}A \circ B + \frac{i}{2}[A, B],$$

which becomes a new binary operation on $\star : \mathcal{F}(M_Q) \times \mathcal{F}(M_Q) \to \mathcal{F}(M_Q)$:

$$f_A \star f_B := f_{AB} = \frac{1}{2}\{f_A, f_B\}_+ + \frac{i}{2}\{f_A, f_B\}. \tag{18}$$

Considering the three operations introduced so far, we can reproduce completely the algebraic structures of the space of operators on $\mathcal{H}$. We can summarize them in the following result:

Theorem 1. *The set of quadratic functions $\mathcal{F}(M_Q)$ endowed with the product $\star$ and the complex conjugation turns out to be a $\mathbb{C}^*$–algebra. The construction is tensorial since it is built on the pair of tensors G and Ω defined on M_Q.*

The conclusion thus is that we are able to reconstruct, at the level of $\mathcal{F}(M_Q)$, all the structures necessary to implement Heisenberg formalism. From that point of view, $\mathcal{F}(M_Q)$ can be considered to be the geometrical framework of Heisenberg's formalism, and the tensors G and Λ the geometrical structures to encode the dynamics and the indetermination relations.

2.3.2 Example II: the algebraic structures for a two level quantum system

Let us continue the analysis of the case of a two level quantum system that we began in Example 2.1.1. By using the Pauli matrices

$$\left\{\sigma_0 = \begin{pmatrix} 1 & 0 \\ 0 & 1 \end{pmatrix}, \sigma_1 = \begin{pmatrix} 0 & 1 \\ 1 & 0 \end{pmatrix}, \sigma_2 = \begin{pmatrix} 0 & -i \\ i & 0 \end{pmatrix}, \sigma_3 = \begin{pmatrix} 1 & 0 \\ 0 & -1 \end{pmatrix}\right\}$$

as Hermitian operators to construct functions $\langle\psi|A|\psi\rangle$, we obtain the real quadratic functions

$$(q^1)^2 + p_1^2 + (q^2)^2 + p_2^2, \quad q^1q^2 + p_1p_2, \quad q^1p_2 - p_1q^2, \quad (q^1)^2 + p_1^2 - ((q^2)^2 + p_2^2).$$

It is not difficult now to compute the Poisson brackets of these quadratic functions to find that they are the Hamiltonian for the infinitesimal generators of the $\mathfrak{u}(2)$ algebra. We may also compute explicitly the Jordan brackets, as for instance

$$\{(q^1)^2 + p_1^2 + (q^2)^2 + p_2^2, q^1q^2 + p_1p_2\}_+ = 4(q^1q^2 + p_1p_2).$$

Similar results are obtained with the other functions. The result we want to point out is

Lemma 3. *The function* $(q^1)^2 + p_1^2 + (q^2)^2 + p_2^2$ *acts, with respect to the Jordan bracket, as the identity operator except for a normalization factor.*

We also find

$$\{q^1q^2 + p_1p_2, q^1q^2 + p_1p_2\}_+ = 4((q^1)^2 + p_1^2 + (q^2)^2 + p_2^2).$$

And analogously for the other quadratic functions. We have

Lemma 4. *The product of all functions (in the family above) with themselves produce a multiple of the quadratic isotropic function.*

We also can obtain easily

$$\{q^1q^2 + p_1p_2, q^1p_2 - p_1q^2\}_+ = 0 = \{q^1q^2 + p_1p_2, (q^1)^2 + p_1^2 - ((q^1)^2 + p_1^2)\}_+$$

The additional relevant property is that the Hamiltonian vector field are Killing vectors. In terms of brackets this amounts to:

$$\{f, \{g, h\}_+\} = \{\{f, g\}, h\}_+ + \{g, \{f, h\}\}_+$$

This condition, plus the compatibility between the Jordan and the Poisson brackets

$$\{\{f, g\}_+, h\}_+ - \{f, \{g, h\}_+\}_+ = \hbar^2\{g, \{h, f\}\}$$

where $\hbar \in \mathbb{R}$ represents the Planck constant, imply that the two brackets combined define a Lie-Jordan algebra.

In particular, by considering generic quadratic functions of two complex coordinates, we find a complex valued quadratic function whose real and imaginary parts are quadratic functions of the previous type. All in all, the result is:

Lemma 5. *Complex valued quadratic functions close on a* $\mathbb{C}^*$*–algebra with respect to the Hermitian bracket.*

Thus we have found that Hermitian operators are associated with Hamiltonian vector fields which are also Killing. As a matter of fact, this property characterizes functions on $\mathbb{C}^2$ which are associated with Hermitian operators.

2.3.3 Functions on the projective space and their algebraic structures

It is important to notice that the functions defined by Eq. (10) correspond to expectation values of physical observables when restricted to the suitable set of points. But in order to represent true physical magnitudes, they must correspond to functions which are constant

along the fibers of the fibration $\pi : M_Q \to \mathcal{P}$. Those functions, meaningful from a physical point of view, correspond to

$$e_A = \frac{\langle\psi|A\psi\rangle}{\langle\psi|\psi\rangle} \tag{19}$$

These are thus functions on M_Q which are in one-to-one correspondence with the functions on the projective space $\mathcal{P}$. Obviously, they are no longer quadratic; but this is a natural property taking into account that the projective space $\mathcal{P}$ has lost the linear structure of M_Q to become just a differentiable manifold.

Nonetheless, it is still possible to reconstruct the algebraic structures we introduced above by defining a pair of suitable tensors. Consider then the action of the tensors Ω and G on the set of functions of the form given by Eq. (69). We know that the functions are projectable under $\pi : M_Q \to \mathcal{P}$, but it is simple to understand that the product is not, since the tensors are derivations of degree 2, i.e., the Lie derivative of the tensors with respect to the dilation vector field Δ defined in Eq. (5) is

$$\mathcal{L}_\Delta G = -2G; \qquad \mathcal{L}_\Delta \Omega = -2\Omega.$$

Thus, in order to make it projectable, we must rescale it by a factor of degree two, and define for instance:

$$\{e_A, e_B\}_\mathcal{P}(\psi) := G_\mathcal{P}(de_A, de_B)(\psi) = \langle\psi|\psi\rangle\{e_A, e_B\}_+ \tag{20}$$

$$\{e_A, e_B\}_\mathcal{P} := \Omega_\mathcal{P}(de_A, de_B) = \langle\psi|\psi\rangle\{e_A, e_B\} \tag{21}$$

2.3.4 Example III: the projective space for a two level quantum system

Extending the example presented in Sections 2.1.1 and 2.3.2, we can consider now the corresponding projective space and the corresponding tensors. It is important to remark that while forms can not be projected, contravariant tensor fields can. This is the reason why we introduced the contravariant tensors Λ and G. Thus by considering

$$G = \frac{\partial}{\partial q^1} \otimes \frac{\partial}{\partial q^1} + \frac{\partial}{\partial p_1} \otimes \frac{\partial}{\partial p_1} + \frac{\partial}{\partial q^2} \otimes \frac{\partial}{\partial q^2} + \frac{\partial}{\partial p_2} \otimes \frac{\partial}{\partial p_2},$$

we can define a projectable tensor as:

$$\begin{aligned} G_\mathcal{P} &= \langle\psi|\psi\rangle G - \Gamma \otimes \Gamma - \Delta \otimes \Delta = \\ &= ((q^1)^2 + (q^2)^2 + p_1^2 + p_2^2)\left(\frac{\partial}{\partial q^1} \otimes \frac{\partial}{\partial q^1} + \frac{\partial}{\partial p_1} \otimes \frac{\partial}{\partial p_1} + \frac{\partial}{\partial q^2} \otimes \frac{\partial}{\partial q^2} + \frac{\partial}{\partial p_2} \otimes \frac{\partial}{\partial p_2}\right) - \\ &\sum_{lm}\left(p_l\frac{\partial}{\partial q^l} - q^l\frac{\partial}{\partial p_l}\right) \otimes \left(p_m\frac{\partial}{\partial q^m} - q^m\frac{\partial}{\partial p_m}\right) - \sum_{lm}\left(q^l q^m \frac{\partial}{\partial q^l} \otimes \frac{\partial}{\partial q^m} + p_l p_m \frac{\partial}{\partial p_l} \otimes \frac{\partial}{\partial p_m}\right) \end{aligned} \tag{22}$$

Analogously we can introduce

$$\Omega_{\mathcal{P}} = \langle\psi|\psi\rangle\Omega - \Gamma\otimes\Delta - \Delta\otimes\Gamma = ((q^1)^2 + (q^2)^2 + p_1^2 + p_2^2)\left(\frac{\partial}{\partial q^1}\wedge\frac{\partial}{\partial p^1} + \frac{\partial}{\partial q^2}\wedge\frac{\partial}{\partial p^2}\right) -$$
$$-\sum_{lm}\left(p_l\frac{\partial}{\partial p_l} + q^l\frac{\partial}{\partial q^l}\right)\otimes\left(p_m\frac{\partial}{\partial q^m} - q^m\frac{\partial}{\partial p_m}\right) - \sum_{lm}\left(p_l\frac{\partial}{\partial q^l} - q^l\frac{\partial}{\partial p_l}\right)\otimes\left(p_l\frac{\partial}{\partial p_l} + q^l\frac{\partial}{\partial q^l}\right) = \tag{23}$$

The next step is to consider the projectable quadratic functions. If we consider the basis of the Hermitian operators given by the Pauli matrices, we find:

$$e_{\sigma_0} = 1 \qquad e_{\sigma_1} = \frac{q^1q^2 + p_1p_2}{(q^1)^2 + (q^2)^2 + p_1^2 + p_2^2}$$

$$e_{\sigma_2} = \frac{q^1p_2 - p_1q^2}{(q^1)^2 + (q^2)^2 + p_1^2 + p_2^2} \qquad e_{\sigma_3} = \frac{(q^1)^2 + p_1^2 - (q^2)^2 - p_2^2}{(q^1)^2 + (q^2)^2 + p_1^2 + p_2^2}$$

We find that only the functions associated with $\{\sigma_1, \sigma_2, \sigma_3\}$ define non-trivial functions on the complex projective space. Of course, their associated vector fields generate the algebra of $SU(2)$.

We can compute now the action of the tensor $G_{\mathcal{P}}$ on these functions and obtain:

$$G_{\mathcal{P}}(de_{\sigma_0}, df) = 0 \qquad \forall f$$

$$G_{\mathcal{P}}(de_{\sigma_1}, de_{\sigma_1}) = e_0 - 4e_{\sigma_1}^2$$

$$G_{\mathcal{P}}(de_{\sigma_2}, de_{\sigma_2}) = e_0 - 4e_{\sigma_2}^2$$

$$G_{\mathcal{P}}(de_{\sigma_3}, de_{\sigma_3}) = 4(e_0 - e_3^2)$$

$$G_{\mathcal{P}}(de_{\sigma_1}, de_{\sigma_2}) = -4(e_{\sigma_1}e_{\sigma_2})$$

In an analogous way, other products can be computed. We obtain thus:

Lemma 6. *The action of $G_{\mathcal{P}}$ on the set of projectable functions corresponds to*

$$G_{\mathcal{P}}(de_A, de_B) = e_{A\circ B} - e_A.e_B.$$

This implies that for $A = B$ we have

$$G_{\mathcal{P}}(e_A, e_B) = e_{A^2} - e_A^2,$$

i.e. we find the variance, the quadratic deviation from the mean value.

As a conclusion we obtain the physical origin of the construction:

Corollary 1. *$G_{\mathcal{P}}$ is directly related to the indetermination relations.*

2.3.5 Characterizing the physical magnitudes

The final issue is to be able to identify which quadratic functions are actually related to physical magnitudes. In principle, there may exist quadratic functions on M_Q which are not associated to any physical magnitude. The complete characterization requires to take into account both tensorial objects. Indeed, the fact that the two algebraic structures (Jordan and Poisson) of the set $\mathrm{End}(\mathcal{H})$ are compatible and define a Lie-Jordan structure, ensures that the Hamiltonian vector fields, besides preserving the Poisson structure, preserve also the symmetric structure and therefore are Killing vector fields. We can characterize completely those vector field associated to physical magnitudes, precisely because of that property:

Proposition 1 ([27]). *The Hamiltonian vector field X_f (defined as $X_f = \hat{\Omega}(df)$) is a Killing vector field for the Riemannian tensor G if and only if f is a quadratic function associated with an Hermitian operator A, i.e. there exists $A = A^\dagger$ such that $f = f_A$.*

2.3.6 The spectral information

Finally, we can consider the problem of how to recover the eigenvalues and eigenvectors of the operators at the level of the functions of M_Q. We consider the expectation value functions associated to the operators as:

$$A \mapsto e_A(\psi) = \frac{\langle \psi | A\psi \rangle}{\langle \psi | \psi \rangle}.$$

Then,

- eigenvectors correspond to the critical points of functions e_A, i.e.

  $$de_A(\psi_a) = 0 \text{ if and only if } \psi_a \text{ is an eigenvector of } A.$$

  We notice that the invariance of e_A under multiplication by a phase $U(1)$ implies that critical points form a circle on the sphere of normalized vectors if the eigenvalue is not degenerate.

- the corresponding eigenvalue is recovered by the value $e_A(\psi_a)$

Thus we can conclude that the Kähler manifold (M_Q, J, ω, g) contains all the information of the usual formulation of Quantum Mechanics on a complex Hilbert space.

Up to now we have concentrated our attention on states and observables. If we consider observables as generators of transformations, i.e. we consider the Hamiltonian flows associated to the corresponding functions, the invariance of the tensor G implies that the evolution is actually unitary. It is, therefore, natural, to consider the action of the unitary group on the realification of the complex vector space.

2.4 The momentum map: geometrical structures on $\mathfrak{u}^*(\mathcal{H})$

The unitary action of $U(\mathcal{H})$ on $\mathcal{H}$ induces a symplectic action on the symplectic manifold (M_Q, ω). By using the association

$$F : M_Q \times \mathfrak{u}(\mathcal{H}) \to \mathbb{R} \quad (\psi, A) \mapsto \frac{1}{2}\langle\psi|iA\psi\rangle = f_{iA}(\psi),$$

we find, with $F_A := f_{iA} : M_Q \to \mathbb{R}$, that

$$\{F(A), F(B)\} = iF([A, B]).$$

Thus if we fix ψ, we have a mapping $F(\psi) : \mathfrak{u}(\mathcal{H}) \to \mathbb{R}$. With any element $\psi \in \mathcal{H}$ we associate an element in $\mathfrak{u}^*(\mathcal{H})$. The previous map defines a momentum map (see [43])

$$\mu : \mathcal{H} \to \mathfrak{u}^*(\mathcal{H}) \qquad \mu(\psi) = |\psi\rangle\langle\psi|, \tag{24}$$

which provides us with a symplectic realization of the natural Poisson manifold structure available in $\mathfrak{u}^*(\mathcal{H})$.

Analogously, we can consider the projected action:

$$F_{\mathcal{P}} : \mathcal{P} \times \mathfrak{u}(\mathcal{H}) \to \mathbb{R} \qquad ([\psi], A) \mapsto e_{iA}(\pi^{-1}([\psi])). \tag{25}$$

In the following we will omit the imaginary unit when referring to the function unless it is necessary.

Again,

$$F_{\mathcal{P}}([\psi]) : \mathfrak{u}(\mathcal{H}) \to \mathbb{R},$$

associates an element of the dual space $\mathfrak{u}^*(\mathcal{H})$ with any point $[\psi] \in \mathcal{P}$. This yields the momentum map corresponding to the action (25) that we can write:

$$\mu_{\mathcal{P}} : \mathcal{P} \to \mathfrak{u}^*(\mathcal{H}) \qquad \mu_{\mathcal{P}}([\psi]) = \frac{|\psi\rangle\langle\psi|}{\langle\psi|\psi\rangle} := \rho_\psi \tag{26}$$

Therefore, we have proved:

Lemma 7. *The projective space* $\mathcal{P}$ *is in one-to-one correspondence with the subset* $\mathcal{D}^1(\mathcal{H}) \subset \mathfrak{u}^*(\mathcal{H})$ *of elements which are rank-one projectors, i.e., with the subset of elements* $\{\rho_k\}$ *which satisfy*

$$\rho_k^2 = \rho_k \qquad \mathrm{Tr}\rho_k = 1 \tag{27}$$

If we denote the linear function on $\mathfrak{u}^*(\mathcal{H})$ associated with the element $iA \in \mathfrak{u}(\mathcal{H})$ by $\hat{A}$, we have

$$\mu^*(\hat{A}) = f_A. \tag{28}$$

Analogously, for the projected action we have

$$\mu^*_{\mathcal{P}}(\hat{A}) = e_A. \tag{29}$$

It is possible to show that the contravariant tensor fields on M_Q associated with the Hermitian structure are μ–related with a complex tensor on $\mathfrak{u}^*(\mathcal{H})$:

$$\mu_*(G + i\Omega) = R + i\Lambda.$$

Clearly the tensors representing the algebraic structures on each set are related by:

$$G(\mu^*\hat{A}, \mu^*\hat{B}) + i\Omega(\mu^*\hat{A}, \mu^*\hat{B}) = \mu^*(R(\hat{A}, \hat{B}) + i\Lambda(\hat{A}, \hat{B})),$$

and analogously

$$G_{\mathcal{P}}(\mu^*_{\mathcal{P}}\hat{A}, \mu^*_{\mathcal{P}}\hat{B}) + i\Omega_{\mathcal{P}}(\mu^*_{\mathcal{P}}\hat{A}, \mu^*_{\mathcal{P}}\hat{B}) + \mu^*_{\mathcal{P}}\hat{A} \circ \mu^*_{\mathcal{P}}\hat{B} = \mu^*_{\mathcal{P}}(R(\hat{A}, \hat{B}) + i\Lambda(\hat{A}, \hat{B})).$$

2.5 The dynamics

At this stage, we can incorporate dynamics into the picture. Although several approaches are possible, we will consider just the simplest one. Thus, we will consider the definition of a dynamical system on M_Q instead of on $\mathcal{P}$, aiming to construct the geometrical analogue of Schrödinger equation. In a similar way, we will discuss the analogue of Heisenberg equation by using the tensors which we have constructed on $\mathfrak{u}^*(\mathcal{H})$.

Consider then the Poisson structures defined by the tensor Ω (defined by Eq. (17)) on the set of quadratic functions and the tensor Λ defined by Equation and the function associated to the Hamiltonian operator:

$$f_H(\psi) = \frac{1}{2}\langle\psi|H\psi\rangle.$$

- We can consider now the one-parameter family of diffeomorphisms associated with the corresponding Hamiltonian vector field:

  $$X_H = \hbar^{-1}\Omega(df_H, \cdot). \tag{30}$$

  This object is, by construction, a vector field defined on the manifold M_Q. This vector field encodes Schrödinger equation in our geometric language, as we can see immediately.

  Let us consider again the simplest quantum situation defined on $\mathbb{C}^n$. As a real manifold, $M_Q \sim \mathbb{R}^{2n}$. Consider then a Hamiltonian $H : \mathbb{C}^n \to \mathbb{C}^n$ which is usually written as a matrix:

  $$H = \begin{pmatrix} H_{11} & H_{12} & \dots & H_{1n} \\ \vdots & \vdots & \dots & \vdots \\ H_{n1} & H_{n2} & \dots & H_{nn} \end{pmatrix}.$$

If we consider it as a matrix on the real vector space M_Q, it reads:

$$H = \begin{pmatrix} H_{q^1q^1} & H_{q^1p_1} & H_{q^1q^2} & H_{q^1p_2} & \dots & H_{q^1q^n} & H_{q^1p_n} \\ H_{p_1q^1} & H_{p_1p_1} & H_{p_1q^2} & H_{p_1p_2} & \dots & H_{p_1q^n} & H_{p_1p_n} \\ \vdots & \vdots & \vdots & \vdots & \dots & \vdots & \vdots \\ H_{q^nq^1} & H_{q^np_1} & H_{q^nq^2} & H_{q^np_2} & \dots & H_{q^nq^n} & H_{q^np_n} \\ H_{p_nq^1} & H_{p_np_1} & H_{p_nq^2} & H_{p_np_2} & \dots & H_{p_nq^n} & H_{p_np_n} \end{pmatrix}.$$

The function f_H in $\mathcal{F}(M_Q)$ becomes thus:

$$f_H = \frac{1}{2}\left(q^1, p_1, q^2, p_2, \dots, q^n, p_n\right) \begin{pmatrix} H_{q^1q^1} & H_{q^1p_1} & H_{q^1q^2} & H_{q^1p_2} & \dots & H_{q^1q^n} & H_{q^1p_n} \\ H_{p_1q^1} & H_{p_1p_1} & H_{p_1q^2} & H_{p_1p_2} & \dots & H_{p_1q^n} & H_{p_1p_n} \\ \vdots & \vdots & \vdots & \vdots & \dots & \vdots & \vdots \\ H_{q^nq^1} & H_{q^np_1} & H_{q^nq^2} & H_{q^np_2} & \dots & H_{q^nq^n} & H_{q^np_n} \\ H_{p_nq^1} & H_{p_np_1} & H_{p_nq^2} & H_{p_np_2} & \dots & H_{p_nq^n} & H_{p_np_n} \end{pmatrix} \begin{pmatrix} q^1 \\ p_1 \\ q^2 \\ p_2 \\ \vdots \\ q^n \\ p_n \end{pmatrix},$$

where the matrix above is symmetric because H is Hermitian, since we have:

$$\begin{aligned} H_{q^kq^k} &= H_{kk} = H_{p_kp_k}, \\ H_{q^kp_k} &= 0 = H_{p_kq^k}, \\ H_{q^jq^k} &= \mathrm{Re}(H_{jk}) = H_{p_jp_k}, \\ H_{q^jp_k} &= -\mathrm{Im}(H_{jk}) = -H_{p_jq^k}. \end{aligned}$$

Then, the Hamiltonian vector field turns out to be:

$$X_H = \hbar^{-1} \sum_k \left(\frac{\partial f_H}{\partial p_k}\frac{\partial}{\partial q^k} - \frac{\partial f_H}{\partial q^k}\frac{\partial}{\partial p_k} \right).$$

And its integral curves are precisely the expression of Schrödinger equation when we write it back in complex terms:

$$\begin{aligned} \dot{q}^1 &= \hbar^{-1}(H_{p_1q^1}q^1 + H_{p_1p_1}p_1 + \ldots + H_{p_1q^n}q^n + H_{p_1p_n}p_n), \\ \dot{p}_1 &= -\hbar^{-1}H_{q^1q^1}q^1 + H_{q^1p_1}p_1 + \ldots + H_{q^1q^n}q^n + H_{q^1p_n}p_n), \\ &\vdots \\ \dot{q}^n &= \hbar^{-1}(H_{p_nq^1}q^1 + H_{p_np_1}p_1 + \ldots + H_{p_nq^n}q^n + H_{p_np_n}p_n), \\ \dot{p}_n &= -\hbar^{-1}(H_{q^nq^1}q^1 + H_{q^np_1}p_1 + \ldots + H_{q^nq^n}q^n + H_{q^np_n}p_n). \end{aligned}$$

We can write these equations as:

$$\frac{d}{dt}\begin{pmatrix} q^1 \\ p_1 \\ q^2 \\ p_2 \\ \vdots \\ q^n \\ p_n \end{pmatrix} = -\hbar^{-1}\mathbf{J}\begin{pmatrix} H_{q^1q^1} & H_{q^1p_1} & H_{q^1q^2} & H_{q^1p_2} & \dots & H_{q^1q^n} & H_{q^1p_n} \\ H_{p_1q^1} & H_{p_1p_1} & H_{p_1q^2} & H_{p_1p_2} & \dots & H_{p_1q^n} & H_{p_1p_n} \\ \vdots & \vdots & \vdots & \vdots & \dots & \vdots & \vdots \\ H_{q^nq^1} & H_{q^np_1} & H_{q^nq^2} & H_{q^np_2} & \dots & H_{q^nq^n} & H_{q^np_n} \\ H_{p_nq^1} & H_{p_np_1} & H_{p_nq^2} & H_{p_np_2} & \dots & H_{p_nq^n} & H_{p_np_n} \end{pmatrix}\begin{pmatrix} q^1 \\ p_1 \\ q^2 \\ p_2 \\ \vdots \\ q^n \\ p_n \end{pmatrix},$$

where

$$\mathbf{J} = \begin{pmatrix} 0 & -1 & 0 & 0 & \dots & 0 & 0 \\ 1 & 0 & 0 & 0 & \dots & 0 & 0 \\ \vdots & \vdots & \vdots & \vdots & \dots & \vdots & \vdots \\ 0 & 0 & 0 & 0 & \dots & 0 & -1 \\ 0 & 0 & 0 & 0 & \dots & 1 & 0 \end{pmatrix};$$

or, equivalently,

$$\dot{\psi}(q,p) = -\hbar^{-1}\mathbf{J}H\psi(q,p),$$

where

$$\psi(q,p) = \begin{pmatrix} q^1 \\ p_1 \\ q^2 \\ p_2 \\ \vdots \\ q^n \\ p_n \end{pmatrix} \tag{31}$$

is the real space representation of the state vector and $\mathbf{J}$ the complex structure. This is precisely the real space expression of Schrödinger equation.

The most significative result is then:

Theorem 2. *Schrödinger equation defines a Hamiltonian vector field on M_Q.*

- On the set $\mathfrak{u}^*(\mathcal{H})$, dynamics is introduced directly as the Hamiltonian vector field associated to the operator H, or, isomorphically, as the derivation

$$\hat{X}_H = \hbar^{-1}\{\hat{H}, \cdot\} = \Lambda(d\hat{H}, \cdot)$$

where $\hat{H}$ is the linear function on $u^*(\mathcal{H})$ which corresponds to the operator $H \in \mathfrak{u}(\mathcal{H})$. This vector field is representing Heisenberg formalism of quantum dynamics. If we write the expression of the corresponding flow we obtain:

$$\frac{d\hat{A}(t)}{dt} = \hbar^{-1}\{\hat{H}, \hat{A}\}. \tag{32}$$

We could also see that the integral curve above can be represented, isomorphically, on the set $\mathcal{F}(M_Q)$, as

$$\hbar \frac{d}{dt} f_A(t) = \{f_H, f_A\} = \Omega(df_H, df_A). \tag{33}$$

The most significative result is then:

Theorem 3. *Heisenberg equation defines a Hamiltonian vector field on* $\mathfrak{u}^*(\mathcal{H})$.

- By our geometric construction is possible to prove, easily, that both formalisms are equivalent. Indeed, by direct computation, we can prove that the momentum map μ is equivariant with respect to the unitary action $U(\mathcal{H}) \times \mathcal{H} \to \mathcal{H}$ (as it is $\mu_{\mathcal{P}}$ with respect to $U(\mathcal{H}) \times \mathcal{P} \to \mathcal{P}$) and the co-adjoint action of $U(\mathcal{H})$ on $\mathfrak{u}^*(\mathcal{H})$. Both vector fields are therefore related via the momentum mapping given by Eq. (24), i.e.,

$$\mu_*(X_H) = \hat{X}_H \tag{34}$$

The conclusion is then:

Theorem 4. *The dynamics of a closed quantum system is Hamiltonian with respect to the canonical Poisson tensors defined on* M_Q *or* $\mathfrak{u}^*(\mathcal{H})$. *Besides, both Hamiltonian vector fields are related by the momentum mapping* μ *associated to the canonical action of the unitary group* $U(\mathcal{H})$.

3 The space of density states

3.1 General considerations

We know that the manifold $\mathcal{P}$ is not enough to represent all the possible physical states of a system. Given one point $\psi_k \in \mathcal{H} - \{0\}$ which is associated to a point $[\psi_k] \in \mathcal{P}$ and corresponds then via the momentum mapping $\mu_{\mathcal{P}}$ to the rank-one projector ρ_{ψ_k}, we know that

$$\rho_{\psi_k}(A) := \langle A \rangle = \mathrm{Tr}(\rho_{\psi_k} A) \qquad \forall A \in i\mathfrak{u}(\mathcal{H}) \tag{35}$$

This implies that the action on the physical magnitude can be written as

$$\rho_{\psi_k}(A) = \frac{\langle \psi_k | A \psi_k \rangle}{\langle \psi_k | \psi_k \rangle} = e_A(\psi_k). \tag{36}$$

But, as we know, arbitrary convex combinations of rank-one projectors also define admissible physical states.

Definition 6. *The **set of density states** $\mathcal{D}(\mathcal{H})$ of the system corresponds to the subset of $\mathfrak{u}^*(\mathcal{H})$ obtained by convex combinations of rank-one projectors, i.e.,*

$$\mathcal{D}(\mathcal{H}) = \left\{ \rho = \sum_k p_k \rho_k |\ \ p_k \geq 0, \sum_j p_j = 1, \rho_k \in \mathcal{D}^1(\mathcal{H}) \right\} \tag{37}$$

Equivalently, we can consider the following definition: an element $\rho \in \mathfrak{u}^*(\mathcal{H})$ is a density operator if and only if

$$\mathrm{Tr}\rho = 1, \qquad \rho \geq 0. \tag{38}$$

This is the most general set containing the possible states of a quantum system defined on a Hilbert space $\mathcal{H}$, even if it can be presented in different ways (see [12, 34]).

We can also construct the set following the second characterization, following [35]. First, we introduce the space of all non-negatively defined operators, i.e. the space of all those $\rho \in \mathfrak{gl}(\mathcal{H})$ which can be written in the form

$$\rho = T^\dagger T \quad T \in \mathfrak{gl}(\mathcal{H}).$$

We will denote by $\mathcal{PH}$ this space of operators, which is a convex cone in $\mathfrak{u}^*(\mathcal{H})$. By imposing the condition $\mathrm{Tr}\rho = 1$ we select in $\mathcal{PH}$ the convex body of density states $\mathcal{D}(\mathcal{H})$. We have then the sequence

$$\mathcal{D}(\mathcal{H}) \subset \mathcal{PH} \subset \mathfrak{u}^*(\mathcal{H}).$$

We will also consider non-negative Hermitian operators and density states of rank k (defined as those operators which have k non-vanishing eigenvalues) and denote the corresponding spaces as $\mathcal{P}^k(\mathcal{H})$ and $\mathcal{D}^k(\mathcal{H})$ respectively. The complex projective space is in one-to-one correspondence with $\mathcal{D}^1(\mathcal{H})$. Indeed, any state in $\mathcal{D}(\mathcal{H})$ can be written as a convex combination of distinct states $\rho = \lambda\rho_1 + (1-\lambda)\rho_2$, with $0 \leq \lambda \leq 1$. We will call **extremal states** those which can not be written in this form (i.e. as convex combination of two ρ_1 and ρ_2). The extremal states are thus given by $\mathcal{D}^1(\mathcal{H})$.

Under this framework, it is natural to consider the following $\mathrm{GL}(\mathcal{H})$–action:

$$\mathrm{GL}(\mathcal{H}) \times \mathfrak{u}^*(\mathcal{H}) \to \mathfrak{u}^*(\mathcal{H}) \quad (T, \xi) \mapsto T\xi T^\dagger.$$

Then:

1. The Hermitian operators ξ_1 and ξ_2 belong to the same GL–orbit if and only if they have the same number K_+ of positive eigenvalues and the same number K_- of negative eigenvalues (counted with multiplicities).

2. Any GL–orbit intersecting the positive cone $\mathcal{PH}$ is contained in $\mathcal{PH}$; so that $\mathcal{PH}$ is stratified by the GL–orbits. These GL–orbits in $\mathcal{PH}$ are determined by the rank of the operator, i.e. they are exactly $\mathcal{P}^k(\mathcal{H})$.

3. When we restrict to the space of density states by imposing the condition $\mathrm{Tr}\rho = 1$, this GL–action will not preserve the states. It is however possible to define a new action that maps $\mathcal{D}(\mathcal{H})$ into itself by setting

$$\mathrm{GL}(\mathcal{H}) \times \mathcal{D}(\mathcal{H}) \to \mathcal{D}(\mathcal{H}) \quad (T, \rho) \mapsto \frac{T\rho T^\dagger}{\mathrm{Tr}(T\rho T^\dagger)}.$$

This action does preserve the rank of ρ and then the following proposition holds true:

Proposition 2. *The decomposition of the convex body of density states $\mathcal{D}(\mathcal{H})$ into orbits of the $\mathrm{GL}(\mathcal{H})$–action $\rho \mapsto \frac{T\rho T^\dagger}{\mathrm{Tr}(T\rho T^\dagger)}$ is exactly the stratification*

$$\mathcal{D}(\mathcal{H}) = \bigcup_{k=1}^{n} \mathcal{D}^k(\mathcal{H}),$$

into states of a given rank.

The boundary of the convex body of density states consists of states of rank lower than n, i.e. $\partial\mathcal{D}(\mathcal{H}) = \bigcup_{k=1}^{n-1} \mathcal{D}^k(\mathcal{H})$, and each stratum is a smooth submanifold in $\mathfrak{u}^*(\mathcal{H})$. However, the boundary $\partial\mathcal{D}(\mathcal{H})$ is not smooth (for $n > 2$). For $n = 2$, the set of density states is diffeomorphic to a 3-dimensional ball, as we will see later, while its boundary corresponds to the set of rank-one projectors $\mathcal{D}^1(\mathbb{C}^2)$, which are represented on the 3-dimensional ball by the surface 2-dimensional sphere, which is, of course, a smooth manifold.

From a dynamical point of view, we can summarize the geometrical picture of the evolution in the following theorem:

Theorem 5. *Every smooth curve $\gamma : \mathbb{R} \to \mathfrak{u}^*(\mathcal{H})$ through the convex body of density states is tangent, at every point, to the stratum to which it belongs, i.e.*

$$\gamma(t) \in \mathcal{D}^k(\mathcal{H}) \Rightarrow T\gamma(t) \in T_{\gamma(t)}\mathcal{D}^k(\mathcal{H}).$$

Once this property is known, we can use the fact that the set is contained in the set $\mathfrak{u}^*(\mathcal{H})$, and restrict the geometrical objects to it. In particular, we can consider the restriction of the Poisson tensor Λ and this allows to define a Hamiltonian vector field by

$$\frac{d\hat{\rho}(t)}{dt} = \hbar^{-1}\{\hat{H}, \hat{\rho}\} = \hbar^{-1}\Lambda(d\hat{H}, d\hat{\rho}), \tag{39}$$

or analogously as

$$\hbar\frac{df_\rho(t)}{dt} = \{f_H, f_\rho\} = \Omega(df_H, df_\rho) \tag{40}$$

if we use the tensor Ω defined on M_Q. This unitary dynamics associated with a Hermitian Hamiltonian H is known as **von Neumann equation**.

3.2 Example: States of a two level system

3.2.1 The geometrical objects

We will consider in some detail two examples. The first one is the two level system with carrier space $\mathcal{H} = \mathbb{C}^2$. We consider $\mathfrak{u}(2)$ and $\mathfrak{u}^*(2)$ and choose again as a basis the Pauli matrices:

$$\sigma_0 = \begin{pmatrix} 1 & 0 \\ 0 & 1 \end{pmatrix} \quad \sigma_1 = \begin{pmatrix} 0 & i \\ -i & 0 \end{pmatrix} \quad \sigma_2 = \begin{pmatrix} 0 & 1 \\ 1 & 0 \end{pmatrix} \quad \sigma_3 = \begin{pmatrix} 1 & 0 \\ 0 & -1 \end{pmatrix}$$

We can introduce coordinate functions with respect to them:

$$y_\mu(A) = \frac{1}{2}\mathrm{Tr}\sigma_\mu A.$$

In these coordinates, a generic Hermitian matrix A can be written as

$$A = y_0\sigma_0 + y_r\sigma_r$$

The corresponding Poisson brackets for the canonical Lie-Poisson structure on the dual of the Lie algebra read:

$$\{y_0, y_a\} = 0 \quad \{y_a, y_b\} = 2\epsilon_{abc}y_c.$$

The expression of the Poisson tensor thus becomes:

$$\Lambda = 2\left(y_1\frac{\partial}{\partial y_2}\wedge\frac{\partial}{\partial y_3} + y_2\frac{\partial}{\partial y_3}\wedge\frac{\partial}{\partial y_1} + y_3\frac{\partial}{\partial y_1}\wedge\frac{\partial}{\partial y_2}\right)$$

It is also possible to construct the Riemann-Jordan tensor in the form:

$$R = \frac{\partial}{\partial y_0}\otimes_s\left(y_1\frac{\partial}{\partial y_1} + y_2\frac{\partial}{\partial y_2} + y_3\frac{\partial}{\partial y_3}\right) + y_0\left(\frac{\partial}{\partial y_0}\otimes\frac{\partial}{\partial y_0} + \frac{\partial}{\partial y_1}\otimes\frac{\partial}{\partial y_1} + \frac{\partial}{\partial y_2}\otimes\frac{\partial}{\partial y_2} + \frac{\partial}{\partial y_3}\otimes\frac{\partial}{\partial y_3}\right)$$

where $\otimes_s$ means the symmetrized tensor product.

In order to characterize the rank of the tensors, we can consider the distributions associated by them to the coordinate functions, i.e., the distributions generated as

$$\mathfrak{h} = \mathrm{span}\left(\Lambda(dy_j)\right) \qquad \mathfrak{r} = \mathrm{span}\left(R(dy_j)\right) \quad j = 0, 1, 2, 3 \tag{41}$$

It is easy to see that the Hamiltonian distribution is generated by

$$H_1 = y_3\frac{\partial}{\partial y_2} - y_2\frac{\partial}{\partial y_3}, \quad H_2 = y_1\frac{\partial}{\partial y_3} - y_3\frac{\partial}{\partial y_1}, \quad H_3 = y_2\frac{\partial}{\partial y_1} - y_1\frac{\partial}{\partial y_2},$$

while the distribution associated with the Riemann-Jordan tensor is

$$X_0 = y^a\frac{\partial}{\partial y^a} + y^0\frac{\partial}{\partial y^0} \quad X_a = y^a\frac{\partial}{\partial y^0} + y^0\frac{\partial}{\partial y^a}$$

It is clear that X_0 is central and $\{X_a\}$ are boosts of a four dimensional Lorentz group, therefore their commutator will provide us with the Lie algebra of the rotation group:

$$[X_a, X_b] = y^a \frac{\partial}{\partial y^b} - y^b \frac{\partial}{\partial y^a}.$$

From the analysis of the dimension of these distributions at each point, we find that:

Lemma 8. *The rank of Λ is zero if $y_1^2 + y_2^2 + y_3^2 = 0$ and the rank is equal to 2 if $y_1^2 + y_2^2 + y_3^2 > 0$.*

The situation is richer with R:

Lemma 9. *The rank of R is*

- *zero if $y_0^2 + y_1^2 + y_2^2 + y_3^2 = 0$*
- *two if $y_0 = 0$ and $y_1^2 + y_2^2 + y_3^2 > 0$.*
- *three for $y_0^2 = y_1^2 + y_2^2 + y_3^2$*
- *four if $y_0^2 \neq y_1^2 + y_2^2 + y_3^2$*

3.2.2 The space of density states in two dimensions

As we have already seen in the previous sections the set of states is identified with a subset of $\mathfrak{u}^*(\mathcal{H})$ satisfying a positivity condition and a normalization condition. In the specific situation we are considering, a generic Hermitian matrix $A = y^0\sigma_0 + y^a\sigma_a$

$$A = \begin{pmatrix} y_0 + y_3 & y_1 - iy_2 \\ y_1 + iy_2 & y_0 - y_3 \end{pmatrix}.$$

We know that A will define a state if and only if

$$\mathrm{Tr}A = 1; \qquad \mu_\pm = y_0 \pm \sqrt{(y_1^2 + y_2^2 + y_3^2)} \geq 0,$$

where $\mu_\pm$ are the two eigenvalues.

Explicitly we have

$$y^0 = \frac{1}{2}, \quad (y_1)^2 + (y_2)^2 + (y_3)^2 \leq \frac{1}{4}.$$

Thus in our parametrization states are determined by points in $\mathbb{R}^4$ on the hyperplane $y^0 = \frac{1}{2}$, and on this three dimensional space are identified by the points in the ball of radius $\frac{1}{2}$. When referring to states we replace A with ρ and write:

$$\rho = \begin{pmatrix} \frac{1}{2} + y_3 & y_2 + iy_1 \\ y_2 - iy_1 & \frac{1}{2} - y_3 \end{pmatrix}. \tag{42}$$

Then,

$$\mathcal{D}(\mathbb{C}^2) = \left\{ \mathfrak{u}(2) \ni \rho = \begin{pmatrix} \frac{1}{2} + y_3 & y_2 + iy_1 \\ y_2 - iy_1 & \frac{1}{2} - y_3 \end{pmatrix} \Big| \ (y_1)^2 + (y_2)^2 + (y_3)^2 \leq \frac{1}{4} \right\} \qquad (43)$$

The pure states corresponding to the vector $(z_1, z_2) \in \mathbb{C}^2$ with unit norm $z_1\bar{z}_1 + z_2\bar{z}_2 = 1$ has a density state

$$\rho = \begin{pmatrix} \bar{z}_1 \\ \bar{z}_2 \end{pmatrix} \otimes (z_1, z_2) = \begin{pmatrix} z_1\bar{z}_1 & \bar{z}_1 z_2 \\ \bar{z}_2 z_1 & z_2\bar{z}_2 \end{pmatrix}.$$

Within the previous parametrization we find

$$y_3 = \frac{1}{2}(z_1\bar{z}_1 - z_2\bar{z}_2), \quad y_1 = \mathrm{Im}(\bar{z}_1 z_2), \quad y_2 = \mathrm{Re}(\bar{z}_1 z_2),$$

and for these points the inequality is saturated thus implying that they lie on the surface of the ball of radius $\frac{1}{2}$. These points on the surface sphere, are in one-to-one correspondence with the unit rays in $\mathbb{C}^2$ and the map is given by the momentum map associated with the symplectic action of $U(2)$ on $\mathcal{P} \sim \mathbb{CP}^1$.

For any generic $\rho \in \mathcal{D}$ there exist pure states ρ_1 and ρ_2 and a positive number $0 \leq \lambda \leq 1$ such that $\rho = \lambda\rho_1 + (1-\lambda)\rho_2$. The decomposition of an arbitrary density state ρ corresponding to some point in the ball, as a convex sum of two pure states

$$\xi_1 = \frac{|\psi_1\rangle\langle\psi_1|}{\langle\psi_1, \psi_1\rangle}$$

and

$$\xi_2 = \frac{|\psi_2\rangle\langle\psi_2|}{\langle\psi_2, \psi_2\rangle},$$

is given geometrically by drawing a straight line through ρ: the states ξ_1 and ξ_2 are the intersections of the line with the sphere. Evidently this decomposition may be done in a two parameter family of ways, filling the disc which has as boundary the yellow circle in Figure 1.

As a subset of $\mathfrak{u}^*(2)$, the ball of the density states is foliated by symplectic leaves associated with the coadjoint action of $U(2)$, which coincide also with the orbits of the $SU(2)$ group. As we know that the rank of the matrices will be preserved, the analysis of these orbits may also be done by considering the orbits passing through diagonal matrices, in other terms

$$\rho = S \begin{pmatrix} a & 0 \\ 0 & b \end{pmatrix} S^\dagger \quad a + b = 1 \quad a \geq 0, \quad b \geq 0 \qquad S \in SU(2).$$

We should keep in mind that these orbits will also correspond to the corresponding dynamical evolution for unitary dynamics, and therefore is physically meaningful.

We visualize the situation with the help of Figure 2. The red segment connecting $(\frac{1}{2}, \frac{1}{2})$ with $(1, 0)$ (or equivalently the dashed green one, connecting with $(0, 1)$) parametrizes the

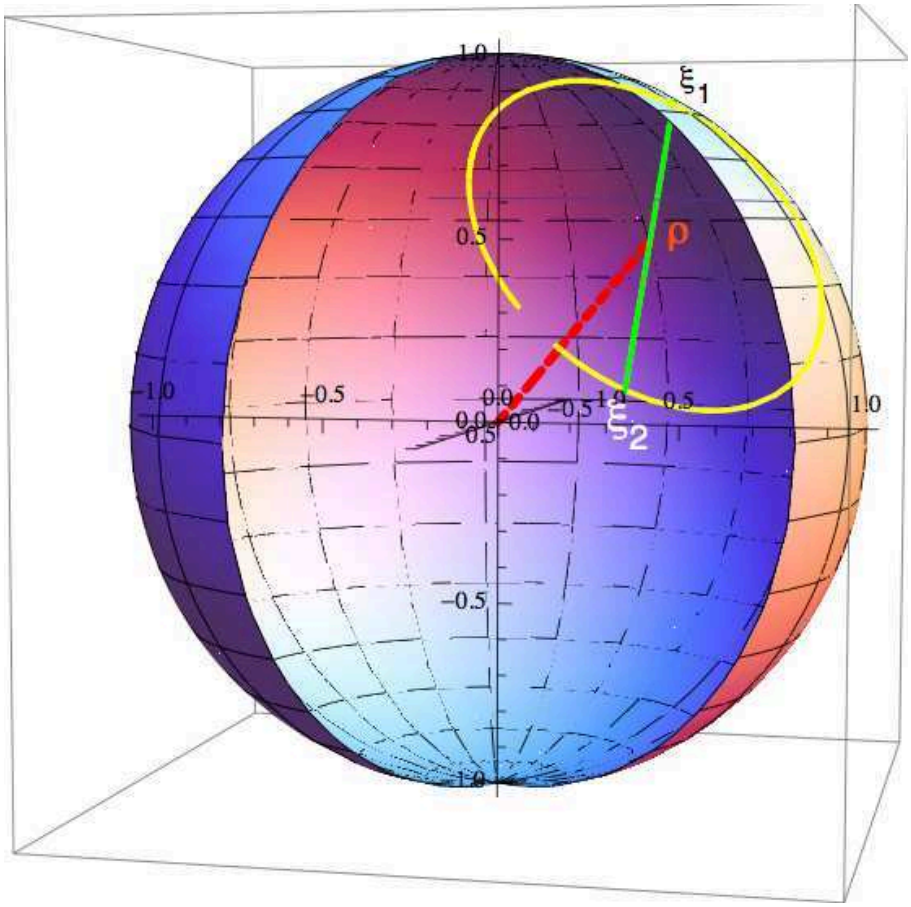

Figure 1.— Bloch sphere and state ρ corresponding to the point $(\frac{1}{2}, \frac{1}{2}, \frac{1}{2})$. This state can be written as the sum of the two extremal states in infinitely many ways, each one corresponding to the diameters of the yellow circle. The diameter corresponding to the pair of states ξ_1 and ξ_2 is depicted in green.

family of two dimensional spheres. The point $(\frac{1}{2}, \frac{1}{2})$ coincides with the center of the Bloch sphere (Figure 1) and represents the maximally mixed state and $(1, 0)$ (or $(0, 1)$) belongs to the outmost sphere of pure states.

3.3 Example: States of a three level system

Now $\mathcal{H} = \mathbb{C}^3$. The states are normalized positive 3×3 matrices inside $\mathfrak{u}^*(3)$. We first consider the geometrical tensors defined by means of the momentum map construction.

3.3.1 The choice of the basis

We choose a basis for $\mathfrak{u}(3)$ given by the Gell-Mann matrices

$$\lambda_1 = \begin{pmatrix} 0 & 1 & 0 \\ 1 & 0 & 0 \\ 0 & 0 & 0 \end{pmatrix} \quad \lambda_2 = \begin{pmatrix} 0 & -i & 0 \\ i & 0 & 0 \\ 0 & 0 & 0 \end{pmatrix} \quad \lambda_3 = \begin{pmatrix} 1 & 0 & 0 \\ 0 & -1 & 0 \\ 0 & 0 & 0 \end{pmatrix}$$

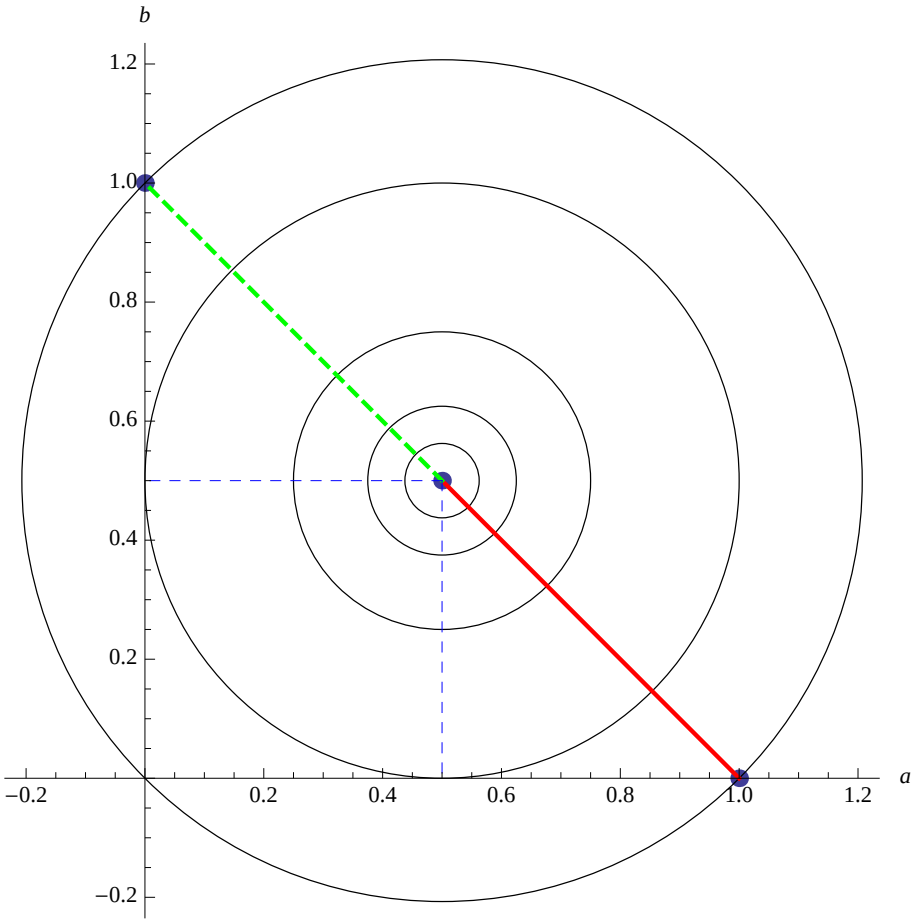

Figure 2.— Set of orbits of the group $SU(2)$ acting on the (a, b) plane

$$\lambda_4 = \begin{pmatrix} 0 & 0 & 1 \\ 0 & 0 & 0 \\ 1 & 0 & 0 \end{pmatrix} \quad \lambda_5 = \begin{pmatrix} 0 & 0 & -i \\ 0 & 0 & 0 \\ i & 0 & 0 \end{pmatrix} \quad \lambda_6 = \begin{pmatrix} 0 & 0 & 0 \\ 0 & 0 & 1 \\ 0 & 1 & 0 \end{pmatrix}$$

$$\lambda_7 = \begin{pmatrix} 0 & 0 & 0 \\ 0 & 0 & -i \\ 0 & i & 0 \end{pmatrix} \quad \lambda_8 = \frac{1}{\sqrt{3}} \begin{pmatrix} 1 & 0 & 0 \\ 0 & 1 & 0 \\ 0 & 0 & -2 \end{pmatrix} \quad \lambda_0 = \sqrt{\frac{2}{3}} \begin{pmatrix} 1 & 0 & 0 \\ 0 & 1 & 0 \\ 0 & 0 & 1 \end{pmatrix}.$$

These matrices satisfy the scalar product relation

$$\mathrm{Tr}\lambda_\mu \lambda_\nu = 2\delta_{\mu\nu}.$$

Their commutation and anti-commutation relations are written in terms of the anti-symmetric structure constants and symmetric d–symbols $d_{\mu\nu\rho}$. We find

$$[\lambda_\mu, \lambda_\nu] = 2iC_{\mu\nu\rho}\lambda_\rho \quad [\lambda_\mu, \lambda_\rho]_+ = 2\sqrt{\frac{2}{3}}\lambda_0\delta_{\mu\nu} + 2d_{\mu\nu\rho}\lambda_\rho.$$

The numerical values turn out to be

$$C_{123} = 1, \qquad C_{458} = C_{678} = \frac{\sqrt{3}}{2}, \quad C_{147} = -C_{156} = C_{246} = C_{257} = C_{345} = -C_{367} = \frac{1}{2}$$

The values of these symbols show the different embeddings of $SU(2)$ into $SU(3) \subset U(3)$. For the other coefficients we have

$$d_{jj0} = -d_{0jj} = -d_{j0j} = \sqrt{\frac{2}{3}} \quad j = 1, \cdots, 8$$

$$-d_{888} = d_{8jj} = d_{jj8} = d_{j8j} = \frac{1}{\sqrt{3}} \quad j = 1, 2, 3$$

$$d_{8jj} = d_{jj8} = d_{j8j} = -\frac{1}{2\sqrt{3}} \quad j = 4, 5, 6, 7$$

$$d_{3jj} = d_{jj3} = d_{j3j} = \frac{1}{2} \quad j = 4, 5 \qquad d_{3jj} = d_{jj3} = d_{j3j} = -\frac{1}{2} \quad j = 6, 7$$

$$d_{146} = d_{157} = d_{164} = d_{175} = -d_{247} = d_{256} = d_{265} = -d_{274} = \frac{1}{2}$$

$$d_{416} = -d_{427} = d_{461} = -d_{472} = d_{517} = d_{526} = d_{562} = d_{571} = \frac{1}{2}$$

$$d_{614} = d_{625} = d_{641} = d_{652} = d_{715} = -d_{724} = d_{751} = -d_{742} = \frac{1}{2}$$

3.3.2 The tensors

The scalar product induced on vectors on $\mathbb{R}^8$ will be invariant under the action of $SO(8)$. It is now possible to write the Poisson tensor

$$\Lambda = 2C_{\mu\nu\rho} y^\rho \frac{\partial}{\partial y^\mu} \wedge \frac{\partial}{\partial y^\nu}$$

and the Riemann-Jordan tensor

$$R = \frac{\partial}{\partial y^0} \otimes_s y^\mu \frac{\partial}{\partial y^\mu} + y^0 \frac{\partial}{\partial y^r} \otimes \frac{\partial}{\partial y^r} + d_{\mu\nu\rho} y^\mu \frac{\partial}{\partial y^\nu} \otimes_s \frac{\partial}{\partial y^\rho}.$$

Now the analysis of the various distributions is more cumbersome, however it is easy to identify a few elements:

$$R(dy^0) = y^\mu \frac{\partial}{\partial y^\mu},$$

which is the dilation vector field on $\mathbb{R}^9$; while $R(dy^r) = y^r \frac{\partial}{\partial y^0} + y^0 \frac{\partial}{\partial y^r} + d_{\mu\nu r} y^\mu \frac{\partial}{\partial y^\nu}$, where it is possible to identify a boost structure plus a correction due to the d–symbols. In any case the union of the Hamiltonian distribution and the Riemannian-Jordan distribution generates $\mathrm{GL}(3, \mathbb{C})$.

3.3.3 Describing the density matrices

The indices appearing in the non-null structure constants are identifying the corresponding λ–matrices whose pairwise commutators define $SU(2)$–subgroups. It is now possible to introduce coordinate functions

$$y^\mu(A) = \frac{1}{2} \mathrm{Tr} \lambda_\mu A.$$

In these coordinates, a generic Hermitian matrix A can be written as

$$A = y^0\lambda_0 + y^r\lambda_r$$

The trace condition

$$\mathrm{Tr}\rho = 1 \Leftrightarrow y_0 = \frac{1}{\sqrt{6}}$$

allows to identify this subset as a subset of the vector space of $\mathbb{R}^8$ corresponding to the dual space of the Lie algebra of $SU(3)$. To identify the set of density matrices, we can consider those points satisfying

$$\mathrm{Tr}\rho^2 \leq \mathrm{Tr}\rho = 1.$$

If we write the states in terms of the λ–matrices, we have

$$\rho = \frac{1}{3}\mathbb{I}_3 + \sum_{j=1}^{8} y_j\lambda_j,$$

with

$$\sum_{j=1}^{8} y_j^2 \leq \frac{1}{2}$$

Extremal states (pure states) are in one-to-one correspondence with the minimal symplectic orbit of the unitary group according to the coadjoint action and corresponds to $\mathbb{CP}^2$, the complex projective space of $\mathbb{C}^3$. They are defined from vectors $(z_1, z_2, z_3) \in \mathbb{C}^3$ with the normalization condition $z_1\bar{z}_1 + z_2\bar{z}_2 + z_3\bar{z}_3 = 1$ as

$$\begin{pmatrix} z_1\bar{z}_1 & \bar{z}_1 z_2 & \bar{z}_1 z_3 \\ \bar{z}_2 z_1 & z_2\bar{z}_2 & \bar{z}_2 z_3 \\ \bar{z}_3 z_1 & z_3\bar{z}_2 & \bar{z}_3 z_3 \end{pmatrix}$$

Previous inequalities are saturated by these matrices.

Under conjugation with $S \in SU(3)$, any matrix A can be written as

$$A = S \begin{pmatrix} a & 0 & 0 \\ 0 & b & 0 \\ 0 & 0 & c \end{pmatrix} S^\dagger \quad a \geq 0, b \geq 0, c \geq 0, \;\; a + b + c = 1, \quad s \in SU(3).$$

By using this "radial-angular" parametrization of states, we may study the structure of this union of symplectic orbits by considering the family of diagonal matrices with the positivity condition (elements of a positive Weyl chamber in the Abelian Cartan subalgebra). The hyperplane $\mathrm{Tr}\rho = 1$ identifies a triangle (the blue one in Figure 3) with the intersection with positive axes (Oa, Ob, Oc); i.e. in the positive octant.

Each internal point of the triangle corresponds to a 6–dimensional symplectic orbit, out of which we may consider convex combinations, excepting the vertices of the triangle where

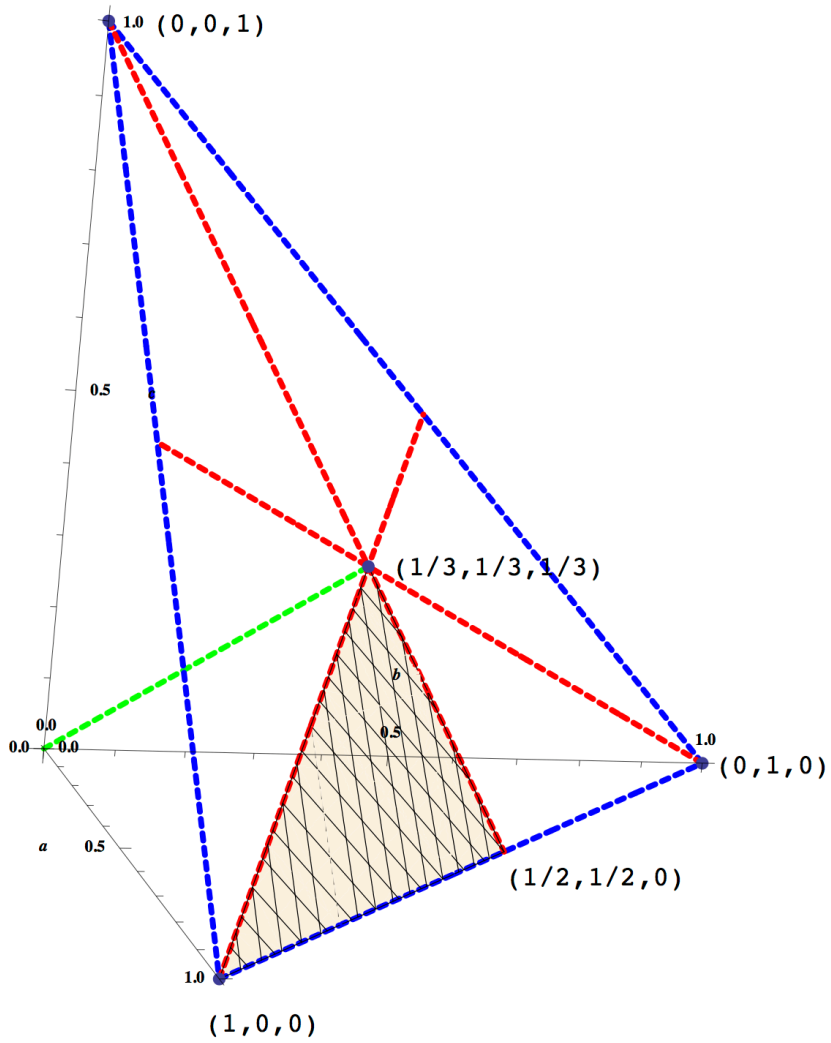

Figure 3.— Representaton of the orbits of $SU(3)$ on the simplex of diagonal density matrices in three dimensions

it is 4–dimensional. Due to the action of $SU(3)$ containing the action of the discrete Weyl group, the symplectic orbits are actually parametrized by the smaller triangle (colored in Figure 3). When $a = b = c = \frac{1}{3}$ we have the "maximally mixed state" which play a crucial role when we consider composite systems and entangled states (the orbit passing through this point degenerates to a zero dimensional orbit). On the boundary of the blue triangle the rank of ρ is either 1 (in the vertex, which represent the pure states) or 2 (on the segment, which represent the mixtures of two of the three levels). For a generic point, the orbits are diffeomorphic to $SU(3)/U(1) \times U(1)$. It appears quite clearly that the set of states is a stratified manifold characterized by the rank of the state.

4 Application I: Describing entanglement

4.1 Generalities

Entanglement is a property of composite physical systems which plays a very important role in many different phenomena, but in particular, it has become a crucial issue of quantum computation and quantum information theory. Despite the growing interest in recent years, it was already discussed by Schrödinger and the "founding fathers" of quantum theory in the early years (see [44, 45]).

Roughly speaking, entanglement is the concept dual to separability.

Definition 7. *Let $|\psi\rangle$ be state of a Hilbert space $\mathcal{H} = \mathcal{H}_1 \otimes \mathcal{H}_2$ of a bipartite system. Then, $|\psi\rangle$ is said to be* **separable** *if there exists a pair of states $|\psi_1\rangle \in \mathcal{H}_1$ and $|\psi_2\rangle \in \mathcal{H}_2$ satisfying that $|\psi\rangle = |\psi_1\rangle \otimes |\psi_2\rangle$. A system which is not separable, it is said to be* ***entangled****.*

But entanglement exhibits many interesting properties, for instance the fact that there is a gradation in the level of entanglement of the different states. Thus we can measure the entanglement of a state by using physical magnitudes. These different observables are called **entanglement witnesses**.

It is known that the set of pure states is completely clasified, from the point of view of entanglement, with just one observable. The usual choices are the **concurrence** of the state, the **von Neumann entropy** of one of its partial traces (i.e. the entropy of the density state $\rho_1 = \mathrm{Tr}_2\rho_\psi$ or of $\rho_2 = \mathrm{Tr}_1\rho_\psi$, where $\rho_\psi = |\psi\rangle\langle\psi|$).

Definition 8. *The concurrence of a density matrix $\rho \in \mathcal{D}(\mathcal{H})$ is defined as*

$$C(\rho) = \max(0, 2\lambda_{max}(\hat{\rho}) - \mathrm{Tr}(\hat{\rho}))$$

where $\hat{\rho}$ corresponds to

$$\hat{\rho} = \sqrt{(\sigma_2 \otimes \sigma_2)\rho^*(\sigma_2 \otimes \sigma_2)\rho}$$

and $\lambda_{max}(\hat{\rho})$ stands for its largest eigenvalue.

Definition 9. *The von Neumann entropy of a density matrix $\rho \in \mathcal{D}(\mathcal{H})$ is defined as*

$$S(\rho) = \mathrm{Tr}\rho\log(\rho). \tag{44}$$

When the density matrix corresponds to a pure state the function above vanishes. Thus we define the corresponding entropy as the value of the function on the partial trace over one of the subsystems:

$$S(\rho_\psi) = \mathrm{Tr}\rho_1\log(\rho_1) \qquad \rho_1 = \mathrm{Tr}_1\rho_\psi \tag{45}$$

If the state ρ_ψ is separable and we can find $\rho_{\psi_a} \in \mathcal{D}^1(\mathcal{H}_1)$ and $\rho_{\psi_b} \in \mathcal{D}^1(\mathcal{H}_2)$ such that

$$\rho_\psi = \rho_{\psi_a} \otimes \rho_{\psi_b};$$

the corresponding partial traces satisfy:

$$\begin{cases} \rho_1 = \rho_{\psi_a} \Rightarrow S(\rho_1) = S(\rho_{\psi_a}) = 0 \\ \rho_2 = \rho_{\psi_b} \Rightarrow S(\rho_2) = S(\rho_{\psi_b}) = 0 \end{cases},$$

because both partial states are pure. If the state ρ is entangled, though, the partial trace yields a density state for the subsystem which is a mixed state. Therefore, the corresponding von Neumann entropy is different from zero. But it is simple to verify that, in the case of pure states, both functions provide the same information, since they are functionally dependent.

Analogously, we can define a simpler operator containing similar information:

Definition 10. *The linear entropy of a density matrix $\rho \in \mathcal{D}(\mathcal{H})$ is defined as*

$$S_L(\rho) = \frac{4}{3}\left(1 - \mathrm{Tr}\rho^2\right). \tag{46}$$

4.2 Entanglement of pure states

For pure states, the three functions provide the same information, as we can simply verify in a simple case:

Example 1. *Let us consider a simple example. Assume $\mathcal{H} = \mathbb{C}^2 \otimes \mathbb{C}^2$ and consider a family of pure states in the form:*

$$|\psi\rangle = \cos(\alpha)\begin{pmatrix}1\\0\end{pmatrix} \otimes \begin{pmatrix}1\\0\end{pmatrix} + \sin(\alpha)\begin{pmatrix}0\\1\end{pmatrix} \otimes \begin{pmatrix}0\\1\end{pmatrix} \tag{47}$$

We can evaluate the concurrence for this state and obtain:

$$C(|\psi\rangle) = \sin(2\alpha).$$

On the other hand, we can construct the density state associated to $|\psi\rangle$ and evaluate the corresponding partial trace:

$$\rho_\psi = |\psi\rangle\langle\psi| = \begin{pmatrix} \cos^2\alpha & 0 & 0 & \cos\alpha\sin\alpha \\ 0 & 0 & 0 & 0 \\ 0 & 0 & 0 & 0 \\ \cos\alpha\sin\alpha & 0 & 0 & \sin^2\alpha \end{pmatrix} \Rightarrow \rho_1 = \mathrm{Tr}_2\rho_\psi = \begin{pmatrix} \cos^2\alpha & 0 \\ 0 & \sin^2\alpha \end{pmatrix}.$$

Thus, the corresponding von Neumann entropy reads:

$$S(\rho_1) = \cos^2\alpha\log(\cos^2\alpha) + \sin^2\alpha + \log(\sin^2\alpha) \tag{48}$$

But it is simple to verify that both quantities are functionally dependent, since a direct representation as that of Figure 4 of the three functions prove that, excepting the normalization, both entropy functions and the square of the concurrence behave exactly in the same way.

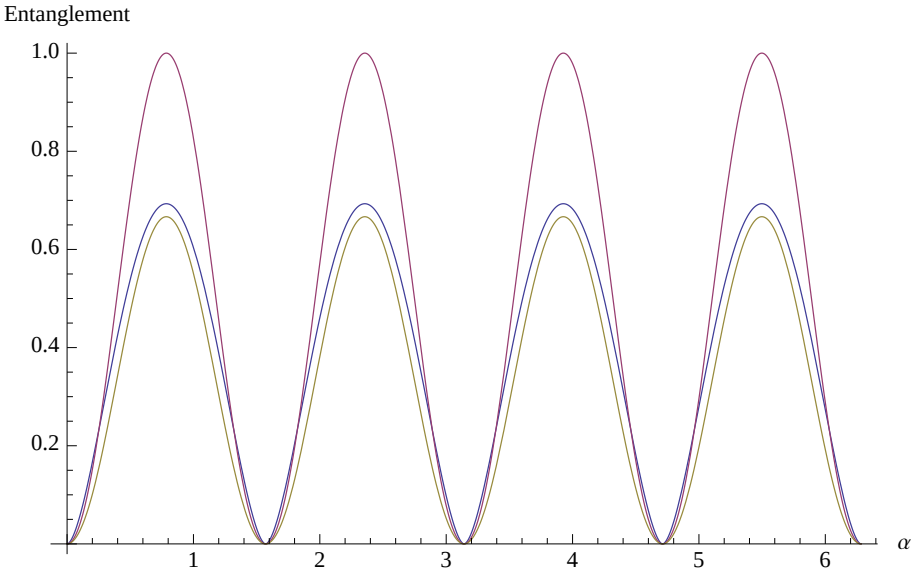

Figure 4.— Representation of the square of the concurrence, the linear entropy and the von Neumann entropy for a pure state

The reason for this is the following result:

Theorem 6. *Let $\mathcal{H} = \mathcal{H}_1 \otimes \mathcal{H}_2$ of dimensions $n_1 \leq n_2$. Given any state $|\psi\rangle \in \mathcal{H}$, there exists orthonormal sets $\{|v_j\rangle\}$ for $\mathcal{H}_1$ and a basis $\{|w_k\rangle\}$ for $\mathcal{H}_2$ such that*

$$|\psi\rangle = \sum_{j=1}^{n_1} \alpha_j |v_j\rangle \otimes |w_j\rangle \qquad \alpha_j > 0. \tag{49}$$

*This is the **Schmidt decomposition of the pure state** $|\psi\rangle$. The number of non-vanishing coefficients in the decomposition is called the **Schmidt rank**.*

Therefore, it is trivial to prove from here that the Schmidt coefficient encodes completely the degree of entanglement of pure states:

Theorem 7. *A pure state $|\psi\rangle \in \mathcal{H}$ is separable if and only if its Schmidt rank is equal to one.*

Thus, we can easily understand the system of the previous example, since the family of states defined in Equation (47) has Schmidt rank equal to 2.

4.3 Entanglement of mixed states

On the other hand, if we consider the case of mixed states, the situation is not that simple. In general, it is necessary to consider more than one entanglement witness in order to completely characterize the state of the system. One interesting question arises thus: how can we characterize the independence of the different observables we use?

In the framework of classical mechanics this question is simple to answer. Given two physical magnitudes, which are represented by two functions f_1, f_2 on phase-space, they are said to be independent at a point $p \in M$ if their exterior differentials satisfy

$$(df_1 \wedge df_2)(p) \neq 0$$

The usual approach to Quantum Mechanics, in terms of Hilbert spaces or $\mathbb{C}^*$–algebras does not allow a similar treatment of the analogous quantum problem. We lack of a noncommutative differential calculus allowing to define a "noncommutative" exterior differential translating the previous definition to the quantum setting.

But the geometrical formalism we introduced in the previous sections allows us to look at the problem from a different perspective. Treating the quantum state space as a real differential manifold, we do have a differential calculus at our disposal: the usual differential calculus of real manifolds.

Consider the Hilbert space $\mathcal{H}$ and an operator A. We know that we can associate with A the quadratic function

$$A \to f_A(\psi) = \frac{1}{2}\langle\psi|A|\psi\rangle \qquad \psi \in \mathcal{H}.$$

In the geometric description of Quantum Mechanics we read from the set of quadratic functions the algebraic structures the set of operators is endowed with:

- the associative product of operators is translated into the nonlocal product $\star$,
- the Lie algebra defined by the commutator is translated into the Poisson algebra defined by the tensor Λ
- the Jordan algebra given by the anticommutator is translated into the Jordan algebra defined by the tensor G

But the geometric description also includes a pointwise algebra $(f_A.f_B)(\psi) = f_A(\psi)f_B(\psi)$, which is commutative, and whose differential calculus is the standard one. This is the algebraic structure with respect to which we define the differential algebra we are interested in:

Definition 11. *Two observables A and B are said to be* **independent** *if their associated functions satisfy*

$$df_A \wedge df_B \neq 0 \text{ on a dense submanifold of } \mathcal{H}$$

Example 2. *Now we will test this formalism with a particular example. Consider for instance the family of density states defined by the matrices:*

$$\rho_t = \begin{pmatrix} 0 & 0 & 0 & 0 \\ 0 & a & \frac{1}{2}ce^{i\phi}, 0 & \\ 0 & \frac{1}{2}ce^{-i\phi} & b & 0 \\ 0 & 0 & 0 & 1-a-b \end{pmatrix}$$

Such a matrix represents a density state provided that

$$0 \leq a+b \leq 1 \quad 0 \leq c \leq 1 \quad 4ab \geq c$$

This is clearly a 4–dimensional submanifold $\mathcal{S}$ of $\mathcal{D}(\mathbb{C}^4)$ and therefore much simpler to handle than the full space. We can take an adapted basis for it, considering the matrices

$$\begin{pmatrix} 0 & 0 & 0 & 0 \\ 0 & 1 & 0 & 0 \\ 0 & 0 & 0 & 0 \\ 0 & 0 & 0 & -1 \end{pmatrix}, \begin{pmatrix} 0 & 0 & 0 & 0 \\ 0 & 0 & 0 & 0 \\ 0 & 0 & 1 & 0 \\ 0 & 0 & 0 & -1 \end{pmatrix}, \begin{pmatrix} 0 & 0 & 0 & 0 \\ 0 & 0 & 1 & 0 \\ 0 & 1 & 0 & 0 \\ 0 & 0 & 0 & 0 \end{pmatrix}, \begin{pmatrix} 0 & 0 & 0 & 0 \\ 0 & 0 & i & 0 \\ 0 & -i & 0 & 0 \\ 0 & 0 & 0 & 0 \end{pmatrix}$$

We can use the four real numbers $\{a, b, c, \phi\}$ as adapted coordinates on that submanifold.

Now we can evaluate the three functions above on these states. As we already know the expression of the Jordan and the Poisson bracket we can also obtain the corresponding Hamiltonian and gradient vector fields. And besides, we can also study the independence of the functions by evaluating the expressions of

$$dS \wedge dC \quad dS_L \wedge dC,$$

where d represents the exterior differential of the differentiable structure defined on $\mathfrak{u}^*(\mathcal{H})$.

Let us thus proceed:

- *The value of the different functions is easy to obtain. We have*

  Von neumann entropy reads,

$$\begin{aligned} 2S(\rho_t) = &-2(-1+a+b)\log[1-a-b]+ \\ &\left(a+b-\sqrt{(a-b)^2+c^2}\right)\log\left[\frac{1}{2}\left(a+b-\sqrt{(a-b)^2+c^2}\right)\right]+ \\ &\left(a+b+\sqrt{(a-b)^2+c^2}\right)\log\left[\frac{1}{2}\left(a+b+\sqrt{(a-b)^2+c^2}\right)\right]. \end{aligned}$$

  The linear entropy S_L corresponds to

$$S_L(\rho_t) = -\frac{2}{3}\left(4\left(a^2+a(-1+b)+(-1+b)b\right)+c^2\right) \tag{50}$$

  Finally, the value of the concurrence is very simple:

$$C(\rho_t) = c \tag{51}$$

- *We can study now the Poisson brackets corresponding to them. It is simple to prove that all three functions commute, i.e.*

$$\{S, S_L\} = \{S, C\} = \{S_L, C\} = 0 \tag{52}$$

This implies that the local transformations generated by them are independent.

- *Finally, we can study the independence of the different functions. This is an important issue, in particular the independence of the von Neumann entropy and the concurrence, because it affects the description of entanglement of general quantum density states. We can prove the following:*

Lemma 10. *The concurrence and the von Neumann entropy of the family of states ρ_t are not indepent in all the space of density states but are independent as observables.*

Proof. We are considering the submanifold of $\mathfrak{u}(\mathcal{H})$ corresponding to the family of density states ρ_t. On this set, the differential of the concurrence is trivial to obtain:

$$dC(\rho_t) = dc. \tag{53}$$

The computation of the differential of the von Neumann entropy is quite more involved. It is evident from the expression above that the functions $\mathcal{S}$ depends on the three variables. But as C depends only on c, we have to consider only the a and b dependence in what regards the computation of $dS \wedge dC$. We compute thus $\frac{\partial S}{\partial a}$ and $\frac{\partial S}{\partial b}$. Now, the condition for (53) to be equal to zero corresponds to

$$\frac{\partial S}{\partial a} = 0 = \frac{\partial S}{\partial b}$$

And these conditions become

$$2\mathrm{Log}[1 - a - b] + \mathrm{Log}\left[ab - \frac{c^2}{4}\right] = 0$$

These equations have a solution on

$$\frac{1}{3} < a < \frac{1}{2}; \qquad b = a; \qquad c = \sqrt{-1 + 4a - 3a^2}$$

Figure 5 presents these functions and the subset where they functionally dependent.

Thus we conclude that there is a nonempty subset of $\mathfrak{u}^*(4)$ where the von Neumann entropy functions and the concurrence function introduced above are not independent. On any point outside this submanifold the two functions are indeed independent, as it can be verified easily from the different behavior in different regions. As the submanifold where the functions are functionally-dependent is clearly not dense in M_Q, we can conclude that the two entanglement witnesses S and C are indeed independent. □

The main advantage of this approach is that, as the dimensions are finite, it is simple to identify what is the number of functions (or observables) which are necessary to unambiguously describe the entanglement of the of density states.

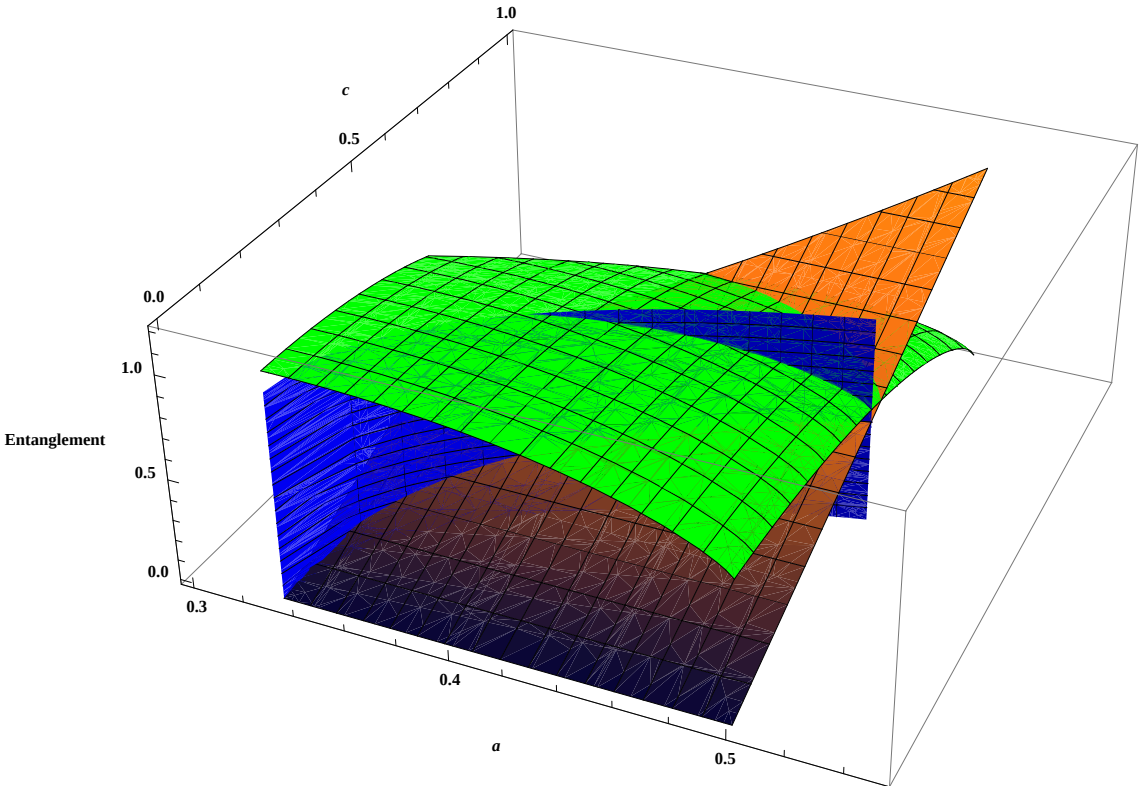

Figure 5.— Representations of the concurrence (in brown) and the von Neumann entropy (in green) in the space parametrized by (a, a, c). In blue, we show the line corresponding to the submanifold where both functions are functionally dependent even if they take different values

5 Application II: Ehrenfest dynamics as a Hamiltonian system

The goal of this section is to summarize some of the results which have been presented in [2, 4] concerning the mathematical description of Mixed Quantum Classical Dynamical (MQCD) systems. We will see how we can combine quantum and classical models by using the tensorial objects we have introduced in the first sections. The combination is possible because, from a formal point of view, those objects are completely analogous to those used in the geometrical description of classical mechanical systems.

5.1 Symplectic description of Classical Mechanics

Let us begin by recalling very quickly the Hamiltonian formulation of classical dynamics. We address the interested reader to a classical reference as [1] for a more detailed presentation.

Let us consider a classical system with phase space M_C. For the sake of simplicity, let us assume that this set is endowed with a vector space structure, i.e., $M_C \sim \mathbb{R}^{2n}$ for n the number of degrees of freedom of the system. In that manifold, there are two types of degrees of freedom: the states of the physical variables describing the position of the system (by "position" we mean any relevant degree of freedom one should consider), and their corresponding momenta. We will use $(\vec{R}, \vec{P})$ as notation to represent these variables.

In what regards the observables, Classical Mechanics uses the set of differentiable functions

$$f : M_C \to \mathbb{R}, \tag{54}$$

assigning the result of the measurement to every point in M_C.

On the set of functions $C^\infty(M_C)$ we introduce an operation, known as Poisson bracket, which allows us to study the effect of symmetry transformations and also the dynamical evolution. The precise definition is as follows:

Definition 12. *A **Poisson bracket**, $\{\cdot,\cdot\}$, is a bilinear operation*

$$\{\cdot,\cdot\} : C^\infty(M_C) \times C^\infty(M_C) \to C^\infty(M_C), \tag{55}$$

which:

- *It is antisymmetric,*

$$\{f, g\} = -\{g, f\}, \qquad \forall f, g \in C^\infty(M_C).$$

- *It satisfies the Jacobi identity, i.e. $\forall f, g, h \in C^\infty(M_C)$:*

$$\{f, \{g, h\}\} + \{h, \{f, g\}\} + \{g, \{h, f\}\} = 0.$$

- *It satisfies the Leibniz rule i.e. $\forall f, g, h \in C^\infty(M_C)$:*

$$\{f, gh\} = \{f, g\}h + g\{f, h\}.$$

A Poisson bracket allows us to introduce the concept of Hamiltonian vector field:

Definition 13. *Given a function $f \in C^\infty(M_C)$ and a Poisson bracket $\{\cdot,\cdot\}$, a vector field, X_f is said to be its **Hamiltonian vector field** if*

$$X_f(g) = \{f, g\}, \qquad \forall g \in C^\infty(M_C).$$

The concept can also be given a tensorial flavor by using a tensor Π, which allows us to define

$$\Pi(df, dg) = \{f, g\} \qquad \forall f, g \in C^\infty(M_C). \tag{56}$$

See [1] for the expression of the conditions to be satisfied by the 2-vector Π.

Example 3. *Let $M_C = \mathbb{R}^2$ with coordinates (R, P). We consider as Poisson bracket*

$$\{f_1, f_2\} = \frac{\partial f_1}{\partial P}\frac{\partial f_2}{\partial R} - \frac{\partial f_1}{\partial R}\frac{\partial f_2}{\partial P}.$$

Then, given $f \in C^\infty(\mathbb{R}^2)$, we can write the corresponding Hamiltonian vector field X_f as

$$X_f = \frac{\partial f(R,P)}{\partial P}\frac{\partial}{\partial R} - \frac{\partial f(R,P)}{\partial R}\frac{\partial}{\partial P}.$$

The geometric formulation of Hamiltonian Mechanics is very often defined on Poisson manifolds, i.e. manifolds endowed with a Poisson bracket on the corresponding space of functions. We will call a **Hamiltonian system** to a triple $(M_C, \{\cdot,\cdot\}, H)$, where $\{\cdot,\cdot\}$ is a Poisson structure on M_C, and dynamics is introduced via the function $H \in C^\infty(M_C)$, that we call the Hamiltonian. One can consider two different formulations of the dynamics:

- One which defines the corresponding Hamiltonian vector field X_H obtained as above

$$X_H(g) = \{H, g\}, \qquad \forall g \in C^\infty(M_C).$$

  The integral curves of the vector field X_H define the solution of the dynamics.

- An analogous formulation can be given in terms of the observables. If we consider now the set of functions of the system, i.e. the set of classical observables which contains, as elements, the functions 'position' and 'momenta' of each particle (i.e. $\vec{R}$ and $\vec{P}$), dynamics is written as the Poisson bracket of the Hamiltonian function H with any other function of the system, i.e.

$$\frac{df}{dt} = \{H, f\}, \qquad \forall f \in C^\infty(M_C). \tag{57}$$

Both approaches are equivalent.

5.2 The set of states of our system

Let us now proceed to combine the geometrical description of Classical Mechanics and Quantum Mechanics. It is immediate to realize that, from a dynamical point of view, both approaches are closely related. Indeed, in both cases there is an intrinsic Poisson structure which allows us to interpret the solutions of the dynamics as the integral curves of Hamiltonian vector fields.

Besides, we know that if we have two classical particles, defined on symplectic manifolds (M_1, ω_1) and (M_2, ω_2), the dynamical description of the system of the two particles is achieved on the manifold $M_1 \times M_2$, with a symplectic structure which is obtained as the sum of both, i.e.,

$$\omega_{12} = \pi_1^*\omega_1 + \pi_2^*\omega_2,$$

where $\pi_1 : M_1 \times M_2 \to M_1$ and $\pi_2 : M_1 \times M_2 \to M_2$ are the canonical projections.

Our goal now is to provide a geometrical framework to represent Ehrenfest equations of a molecular system. Ehrenfest equations represent an approximation for the description of an atomic or molecular system where:

- the nuclei and the inner electrons, are represented as classical systems, called **cores**, coupled to
- the outer electrons which are considered to behave as quantum systems.

The approximation makes sense when the evolution of the degrees of freedom which are assumed to be classical is much slower than the quantum evolution. This implies that we are implicitly assuming that we can disregard the entanglement between the classical and the quantum degrees of freedom. But this fact implies that the complete set of states will be just the cartesian product of the sets of states of the classical and the quantum parts.

Thus, the set of states of the complete system contains:

- First, a Hilbert space $\mathcal{H}$ which contains the states of the set of objects of our system which are described quantum-mechanically. It is the vector space corresponding to the completely antisymmetric representation of the permutation group S_N (i.e. a set of Slater determinants), where N is the number of electrons of the system and each electron lives in a Hilbert space of dimension M. Thus, the dimension of $\mathcal{H}$ will be $N_Q = \binom{M}{N}$. We know that it is a complex vector space, but we choose to consider it as a real vector space with the double of degrees of freedom and denote it as M_Q. Also, in correspondence with the Hilbert space vectors in the usual formalism of quantum mechanics, several states in M_Q represent the same physical state. To consider true physical states one should extract only those corresponding to the projective space, which can be identified with a submanifold of M_Q. A more general approach is to consider the sphere of states with norm equal to one, S_Q, and take into account the phase transformations generated by Eq (4) in a proper way. We will discuss this in the following sections.

- Second, a differentiable manifold M_C (for simplicity we can just consider it to be a vector space), which contains the classical degrees of freedom. We will assume it to be a phase space, and thus it will have an even number of degrees of freedom and it will be endowed with a canonical symplectic structure. Therefore we can also consider a Poisson structure on the set of functions of the manifold M_C.

- Third, we let our state space S be the Cartesian product of both manifolds,

$$\mathcal{S} = M_C \times M_Q.$$

Such a description has important implications: it is possible to consider each subsystem separately in a proper way but it is not possible to entangle the subsystems one with the other. As long as Ehrenfest dynamics disregards this possibility, the choice of the Cartesian product is the most natural one.

Example 4. *If we consider a simple case, where we have one nucleus moving in a three dimensional domain and the electron state is considered to belong to a two-level system, the situation would be:*

$$\Psi = (\vec{R}, \vec{P}, q^1, q^2, p_1, p_2), \qquad (q^1, q^2, p_1, p_2) \in \mathbb{R}^4,$$

where $\vec{R}$ represents the position of the nucleus, and $\vec{P}$ represents its linear momentum. The tetrad (q^1, q^2, p_1, p_2) represents the set of four real coordinates which correspond to the representation of the state of the two-level system on a real vector space (of four 'real' dimensions which corresponds to a two 'complex'-dimensional vector space).

As a conclusion from the example above, we use as coordinates for our states:

- The positions and momenta of the nuclei and electrons of the cores:

$$(\vec{R}, \vec{P}) \in M_C. \tag{58}$$

  We will have $3N_C + 3N_C$ of these, for N_C the number of classical particles of the system.

- The real and imaginary parts of the coordinates of the Hilbert space elements with respect to some basis:

$$(\vec{q}, \vec{p}) \in M_Q. \tag{59}$$

  We will have $N_Q + N_Q$ of these, for N_Q the complex dimension of the Hilbert space $\mathcal{H}$.

5.3 The observables

To represent the physical magnitudes we must consider also the classical-quantum observables from a new perspective. Our observables must be functions defined on the state space $S = M_C \times M_Q$. We can consider also the projections:

$$\pi_C : M_C \times M_Q \to M_C, \quad \pi_C(\vec{R}, \vec{P}, \vec{q}, \vec{p}) = (\vec{R}, \vec{P}) \tag{60}$$

and

$$\pi_Q : M_C \times M_Q \to M_Q, \quad \pi_Q(\vec{R}, \vec{P}, \vec{q}, \vec{p}) = (\vec{q}, \vec{p}). \tag{61}$$

We know from our discussion in the case of a purely quantum system that any function of the form (38) produces an evolution, via the Poisson bracket, which preserves the norm. In the MQCD case, we can easily write the analogue of the vector field (4) by writting:

$$\Gamma_Q = \mathbb{I} \otimes \Gamma. \tag{62}$$

It is simple to see that this object is completely determined by the pullback of the projections π_C and π_Q:

$$\pi_{C*}\Gamma_Q = 0, \qquad \pi_{Q*}\Gamma_Q = \Gamma.$$

This is again the infinitesimal generator of phase transformations for the quantum subsystem, but written at the level of the global state space $M_C \times M_Q$. A reasonable property to be asked to the functions chosen to represent our observables is to be constant under this transformation. From a mathematical point of view we can write such a condition as follows:

Definition 14. *We will define the set of possible physical observables, $\mathcal{O}$, as the set of all C^∞–functions on the set $M_C \times M_Q$ which are constant under phase changes on the quantum degrees i.e.*

$$\mathcal{O} = \{f \in C^\infty(M_C \times M_Q) |\ \Gamma_Q f = 0\}. \tag{63}$$

As we will see later, this choice reflects the fact that, when considered coupled together, the nonlinearity of Classical Mechanics expands also to MQCD.

We would like to remark that because of the choice of the set of states as a Cartesian product of the classical states and the quantum states, we can consider as subsets of the set of observables:

- The set of classical functions: these are functions which depend only on the classical degrees of freedom. Mathematically, they can be written as those functions $f \in \mathcal{O}$ such that there exists a function $f_C \in C^\infty(M_C)$ such that

  $$f = \pi_C^*(f_C);\ \text{i.e. } f(\vec{R}, \vec{P}, \vec{q}, \vec{p}) = f_C(\vec{R}, \vec{P}),$$

  for π_C^* the pullback of the projection π_C. We denote this subset as $\mathcal{O}_C$. An example of a function belonging to this set is the linear momentum of the nuclei.

- The set of **generalized quantum functions**: functions which depend only on the quantum degrees of freedom and which are constant under changes in the global phase. Mathematically, they can be written as those functions $f \in \mathcal{O}$ such that there exists a function $f_Q \in C^\infty(M_Q)$ for which $f = \pi_Q^*(f_Q)$, i.e.

  $$f(\vec{R}, \vec{P}, \vec{q}, \vec{p}) = f_Q(\vec{q}, \vec{p}); \quad \Gamma(f_Q) = 0, \tag{64}$$

for π_Q^* the pullback of the projection π_Q. We denote these functions as $\mathcal{O}_Q$. We have added the adjective "generalized" because this set is too large to represent the set of pure quantum observables. These later functions, should be considered, when necessary, as a smaller subset, which corresponds to the set of functions defined in Eq. (38). We denote this smaller subset as $\mathcal{O}_Q^s$. An example of a function belonging to $\mathcal{O}_Q^s$ is the linear momentum of the electrons.

- A third interesting subset is the set of arbitrary linear combinations of the subsets above, i.e. those functions which may be written as the sum of a purely classical function and a purely quantum one: $f = \pi_Q^*(f_Q) + \pi_C^*(f_C)$, i.e.

$$f(\vec{R}, \vec{P}, \vec{q}, \vec{p}) = f_C(\vec{R}, \vec{P}) + f_Q(\vec{q}, \vec{p}). \tag{65}$$

  We will denote this set as $\mathcal{O}_{C+Q}$. An element of this set of functions is the total linear momentum of the composed system.

We would like to make a final but very important remark. We have not chosen the set of observables as

$$\left\{ f \in C^\infty(M_C \times M_Q) | f = \langle \psi(\vec{q}, \vec{p}), A(\vec{R}, \vec{P}) \psi(\vec{q}, \vec{p}) \rangle \right\}, \tag{66}$$

for $A(\vec{R}, \vec{P})$ a linear operator on the Hilbert space $\mathcal{H}$ depending on the classical degrees of freedom because of two reasons:

- It is evident that the set above is a subset of (63) and thus we are not loosing any of these operators. But it is a well known property that Ehrenfest dynamics is not linear and then if we consider the operator describing the evolution of the system, it can not belong to the set above. We must thus enlarge the set (66).

- We are going to introduce in the next section a Poisson bracket on the space of operators. For that bracket to close a Poisson algebra, we need to consider the whole set (63).

It is important to notice that in the set (63) there are operators which are not representing linear operators for the quantum part of the system and hence the set of properties listed above for the pure quantum case are meaningless for them. But this is a natural feature of the dynamics we are considering, because of its nonlinear nature.

5.4 Geometry and the Poisson bracket on the classical-quantum world

Finally, we must combine the quantum and the classical description in order to provide a unified description of our system of interest. As we assume that both the classical and the quantum subsystems are endowed with Poisson structures, we face the same problem

we have when combining, from a classical mechanics perspective, two classical systems. Therefore it is immediate to conclude that the corresponding Poisson structures can be combined as:

$$\{\cdot,\cdot\} = \{\cdot,\cdot\}_C + \hbar^{-1}\{\cdot,\cdot\}_Q, \tag{67}$$

where the term $\{\cdot,\cdot\}_C$ acts on the degrees of freedom of the first manifold and $\{\cdot,\cdot\}_Q$ acts on the degrees of freedom of the second one.

From a more geometric point of view, this combination is equivalent to define a symplectic tensor on $M_C \times M_Q$ combining the corresponding symplectic structures, ω_C and ω_Q, in the form:

$$\omega = \omega_C + \hbar\omega_Q. \tag{68}$$

Remember that it is always possible to combine two symplectic forms in this way, because of the properties of differential algebra.

Lemma 11. *The tensor* (67) *defines a Poisson structure on* $C^\infty(M_C \times M_Q)$.

Proof It is completely straightforward if we realize that the Poisson tensor is directly related to the form ω which is trivally a symplectic form. □

Notice that the set of pure classical functions $\mathcal{O}_C$ and the set of quantum generalized functions $\mathcal{O}_Q$ are closed under the Poisson bracket. The same happens with the quantum functions $\mathcal{O}_Q^s$ and the set of linear combinations $\mathcal{O}_{C+Q}$. In mathematical terms, what we have is a family of Poisson subalgebras. This property ensures that the description of purely classical or purely quantum systems, or even both systems at once but uncoupled to each other, can be done within the formalism.

Once the Poisson bracket on $M_C \times M_Q$ has been introduced we can express again the constraint we introduced in the definition of the observables in Poisson terms. Thus we find that in a completely analogous way to the pure quantum case, we can prove that

Lemma 12. *The condition in Eq.*(63)

$$\Gamma_Q(f) = 0$$

is equivalent to ask the function f *to Poisson-commute with the function* $f_{\mathbb{I}} = \sum_k((q^k)^2 + p_k^2)$, *i.e.*

$$\Gamma_Q(f) = 0 \Leftrightarrow \{f_{\mathbb{I}}, f\} = 0.$$

5.5 The definition of the dynamics

From the previous sections we know that our formulation of MQCD can be implemented on:

- The manifold which represents the set of states by defining a vector field whose integral curves represent the solutions of the dynamics (equivalent to the Schrödinger picture of standard quantum mechanical systems).

- The set of functions (please note the differences between the classical and the quantum cases) defined on the set of states which represent the set of observables of the system. In this case the Poisson bracket of the functions with the Hamiltonian of the system defines the corresponding evolution (equivalent to the Heisenberg picture of standard quantum mechanical systems).

Remember that both approaches are not disconnected, since they can be easily related either by the momentum mapping or simply by the vector fields::

$$X_H = \{f_H, \cdot\}, \tag{69}$$

where we denote by X_H the vector field which represents the dynamics on the phase space and by f_H the function which corresponds to the Hamiltonian of the complete system.

We can now proceed to our first goal: to provide a Hamiltonian description of Ehrenfest dynamics in terms of a Poisson structure. We thus define the following Hamiltonian system:

- A state space corresponding to the Cartesian product $M_C \times M_Q$.

- A set of operators corresponding to the set of functions $\mathcal{O}$ defined in Eq. (17). On this set, we consider the Poisson bracket defined in Eq. (67) defined on the symplectic vector space $M_C \times M_Q$ with symplectic form (68).

- And finally, the dynamics introduced by the following Hamiltonian function:

$$f_H(\vec{R}, \vec{P}, \vec{q}, \vec{p}) = \sum_J \frac{\vec{P}_J^2}{2M_J} + \langle \psi(\vec{q}, \vec{p}), H_e(\vec{R})\psi(\vec{q}, \vec{p})\rangle, \tag{70}$$

  where H_e is the expression of the electronic Hamiltonian, M_J are the masses of the classical subsystem of the nuclei and $\psi(\vec{q}, \vec{p})$ is the real-space representation of the state ψ analogous to Eq. (31).

As a result, the dynamics of both subsystems are obtained easily. In the Schrödinger picture we obtain:

$$\dot{\vec{R}} = \frac{\partial f_H}{\partial \vec{P}} = M^{-1}\vec{P}, \tag{71}$$

$$\dot{\vec{P}} = -\frac{\partial f_H}{\partial \vec{R}} = -\text{grad}(\langle \psi(\vec{q},\vec{p}), H_e(\vec{R})\psi(\vec{q},\vec{p})\rangle), \tag{72}$$

$$\dot{q}^1 = \hbar^{-1}\frac{\partial f_H}{\partial p_1}, \tag{73}$$

$$\dot{p}_1 = -\hbar^{-1}\frac{\partial f_H}{\partial q^1}, \tag{74}$$

$$\vdots$$

$$\dot{q}^{N_Q} = \hbar^{-1}\frac{\partial f_H}{\partial p_{N_Q}}, \tag{75}$$

$$\dot{p}_{N_Q} = -\hbar^{-1}\frac{\partial f_H}{\partial q_{N_Q}}. \tag{76}$$

This set of equations corresponds exactly with Ehrenfest dynamics.

The final point is to prove the following lemma:

Lemma 13. *The dynamics preserves the set of observables $\mathcal{O}$.*

Proof An observable belongs to $\mathcal{O}$ if it Poisson-commutes with $f_{\mathbb{I}}$. Thus, as $f_H \in \mathcal{O}$, if we consider an observable $f \in \mathcal{O}$, by the Jacobi identity:

$$\{f_{\mathbb{I}}, \{f_H, f\}\} = -\{f, \{f_{\mathbb{I}}, f_H\}\} - \{f_H, \{f, f_{\mathbb{I}}\}\} = 0 \tag{77}$$

□

Example 5. *In the following example we will study a simple toy model in which the coupling of classical and quantum degrees of freedom gives rise to chaotic-like behavior. This behavior has been proven to be related with physical effects such as the change of the degree of purity of the quantum part of the system (see [4]).*

The system consists of a complex two dimensional Hilbert space $M_Q = \mathbb{C}^2$ and a classical 2-D phase space where we define a 1-D harmonic oscillator. Using coordinates (J_θ, θ) for the classical variables (action-angle coordinates for the oscillator) and $\Psi \in \mathbb{C}^2$ we define the following Hamiltonian

$$f_H = J_\theta + \frac{1}{2}\langle\Psi|\sigma_z + \epsilon\cos(\theta)\sigma_x|\Psi\rangle,$$

with σ_x, σ_z the Pauli sigma matrices.

We parametrize the normalized quantum state by

$$|\Psi\rangle = e^{i\alpha}\begin{pmatrix}\sqrt{J_\phi}\\ e^{i\phi}\sqrt{1-J_\phi}\end{pmatrix},$$

α *being the global phase.*

In these variables the Hamiltonian reads

$$f_H = J_\theta + J_\phi + \epsilon\sqrt{J_\phi}\sqrt{1 - J_\phi}\cos(\theta)cos(\phi), \tag{78}$$

where ϵ *measures the coupling of the classical and quantum systems.*

In the limit of vanishing ϵ *the system is integrable and actually linear in these coordinates. However for non vanishing* ϵ *the model becomes non linear and more complicated behavior appears. We can represent the trajectories of the corresponding Hamilton equations, which read:*

$$\begin{cases} \dot{\theta} = 1 \\ \dot{\phi} = \hbar^{-1}\left(1 + \left(-1 + \frac{1}{2\sqrt{J_\phi}}\right)\epsilon\cos(\theta)\cos(\phi)\right) \\ \dot{J}_\theta = -(-1 + \sqrt{J_\phi})\sqrt{J_\phi}\epsilon\cos(\phi)\sin(\theta) \\ \dot{J}_\phi = -\hbar^{-1}\left((-1 + \sqrt{J_\phi})\sqrt{J_\phi}\epsilon\sin(\phi)\cos(\theta)\right) \end{cases} \tag{79}$$

We can see then how the dynamics becomes more complex as the coupling ϵ *increases, the nonlinear effects becoming more and more important. For small values of* ϵ *the trajectory is almost planar and periodic while when it is increased, it becomes more and more complicated.*

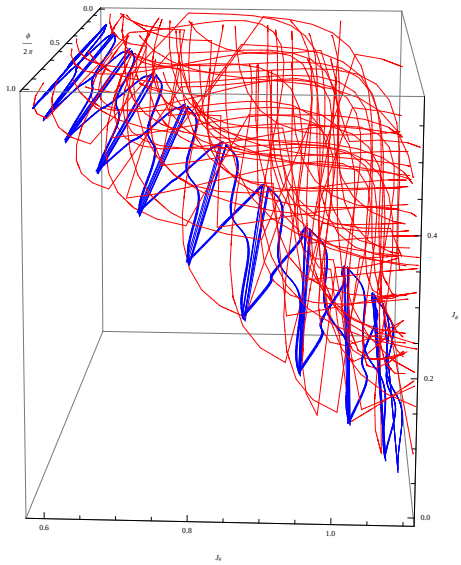

Figure 6.— The plot shows the trajectory with initial conditions $(\theta(0), \phi(0), J_\theta(0), J_\phi(0)) = (0.1, 0.32, 0.6, 0.55)$ on the hyperplane $(\phi/2\pi, J_\theta, J_\phi)$ for $\epsilon = 0.15$ (blue curve) and for $\epsilon = 1.55$ (red curve). For simplicity, we take $\hbar = 1$

References

[1] R. Abraham and J.E. Marsden. *Foundations of Mechanics.* Reading, 1978.

[2] J. L. Alonso, A. Castro, J. Clemente-Gallardo, J. C. Cuchí, P. Echenique, and F. Falceto. Statistics and Nosé formalism for Ehrenfest dynamics. *Journal of Physics A: Mathematical and Theoretical*, 44(39):395004, 2011.

[3] J. L. Alonso, A. Castro, J. Clemente-Gallardo, P. Echenique, J. J. Mazo, V. Polo, a. Rubio, and D. Zueco. Non-adiabatic effects within a single thermally averaged potential energy surface: Thermal expansion and reaction rates of small molecules. *The Journal of Chemical Physics*, 137(22):22A533, 2012.

[4] J. L. Alonso, J. Clemente-Gallardo, J. C. Cuchi, P. Echenique, and F. Falceto. Ehrenfest dynamics is purity non-preserving: A necessary ingredient for decoherence. *The Journal of Chemical Physics*, 137(5):054106, 2012.

[5] J. Anandan. A geometric approach to Quantum Mechanics. *Foundations of Physics*, 21(11):1265–1284, 1991.

[6] J. Anandan and Y. Aharonov. Geometry of quantum evolution. *Physical Review Letters*, 65(14):1697–1700, 1990.

[7] P. Aniello, J. Clemente-Gallardo, G. Marmo, and G. F. Volkert. Classical tensors and quantum entanglement I: pure states. *International Journal of Geometric Methods in Modern Physics*, 07(03):485, 2010.

[8] P. Aniello, J. Clemente-Gallardo, G. Marmo, and G. F. Volkert. Classical tensors and quantum entanglement II: mixed States. *International Journal of Geometric Methods in Modern Physics*, 8(4):853–883, 2011.

[9] A. Ashtekar and T. A. Schilling. Geometrical formulation of Quantum Mechanics. In *On Einstein's Path: Essays in Honor of Engelbert Schucking*, Springer New York, pages 23–65, 1999

[10] A. Benvegnù, N. Sansonetto, and M. Spera. Remarks on geometric Quantum Mechanics. *Journal of Geometry and Physics*, 51(2):229–243, 2004.

[11] A. Bloch. An infinite-dimensional Hamiltonian system on projective Hilbert space. *Transactions AMS*, 302(2):787–796, 1987.

[12] H. P. Breuer and F. Petruccione. *The theory of open quantum systems.* Oxford University Press, 2002.

[13] D. C. Brody and L. Hughston. Geometry of Quantum Statistical Inference. *Physical Review Letters*, 77(14):2851–2854, 1996.

[14] D. C. Brody and L. P. Hughston. Geometric Quantum Mechanics. *Journal of Geometry and Physics*, 38(1):19–53, 2001.

[15] D. C. Brody. Information geometry of density matrices and state estimation. *Journal of Physics A: Mathematical and Theoretical*, 44(25):252002, 2011.

[16] D. C. Brody, D. D. Holm, and D. M. Meier. Quantum splines. *Arxiv*, 1206.2675, 2012.

[17] D. C. Brody, D. W. Hook, and L. P. Hughston. Microcanonical distributions for quantum systems. *Arxiv quant-ph/0506163*, 2005.

[18] D. C. Brody and L. P. Hughston. Statistical geometry in Quantum Mechanics. *Proceedings of the Royal Society A: Mathematical, Physical and Engineering Sciences*, 454(1977):2445–2475, 1998.

[19] V. Cantoni. Generalized "transition probability". *Comm. Math. Phys.*, 44:125–128, 1975.

[20] V. Cantoni. Intrinsic geometry of the quantum-mechanical phase space, Hamiltonian systems and Correspondence Principle. *Rend. Accd. Naz. Lincei*, 62:628–636, 1977.

[21] V. Cantoni. The Riemannian structure on the space of quantum-like systems. *Comm. Math. Phys.*, 56:189–193, 1977.

[22] V. Cantoni. Geometric aspects of Quantum Systems. *Rend. Sem. Mat. Fis. Milano*, 48:35–42, 1980.

[23] V. Cantoni. Superposition of physical states: a metric viewpoint. *Helv. Phys. Acta*, 58:956–968, 1985.

[24] J. F. Cariñena, J. Clemente-Gallardo, and G. Marmo. Geometrization of Quantum Mechanics. *Theoretical and Mathematical Physics*, 152(1):894–903, 2007.

[25] R. Cirelli, P. Lanzavecchia, and A. Manià. Normal pure states of the von Neumann algebra of bounded operator as Kähler manifold. *J. Phys. A: Math Gen*, 15:3829–3835, 1983.

[26] R. Cirelli, P. Lanzavecchia, and A. Manià. Hamiltonian vector fields in Quantum Mechanics. *Nuovo Cimento B*, 79:271–283, 1984.

[27] R. Cirelli, A. Manià, and L. Pizzocchero. Normal pure states of the von Neumann algebra of bounded operator as Kähler manifold. *J. Phys. A: Math Gen*, 31:2891–2903, 1990.

[28] J. Clemente-Gallardo and G. Marmo. The space of density states in geometrical quantum mechanics. In *Differential Geometric Methods in Mechanics and Field Theory*, pages 35–56. Gent University Press, Gent, 2007.

[29] J. Clemente-Gallardo and G. Marmo. Basics of Quantum Mechanics, geometrization and some applications to Quantum Information. *International Journal of Geometric Methods in Modern Physics*, 05:989, 2008.

[30] J. Clemente-Gallardo and G. Marmo. Towards a definition of quantum integrability. *International Journal of Geometric Methods in Modern Physics*, 06(01):129, 2009.

[31] P. A. M. Dirac. On the Analogy Between Classical and Quantum Mechanics. *Rev. Mod. Phys.*, 17(2-3):195–199, 1945.

[32] P. A. M. Dirac. The principles of Quantum Mechanics. *The International Series of Monographs on Physics, Oxford: Clarendon Pres*, 1947.

[33] J. Dixmier and F. Jellett. *C*-algebras*. North-Holland Amsterdam, 1977.

[34] A.M. Gleason. Measures on the closed subspaces of a Hilbert space. *J. of Mathematics and Mechanics*, 6(6):885–893, 1957.

[35] J. Grabowski, M. Kuś, and G. Marmo. Geometry of quantum systems: density states and entanglement. *Journal of Physics A: Mathematical and General*, 38(47):10217–10244, 2005.

[36] R. Haag and D. Kastler. An algebraic approach to Quantum Field Theory. *Journal of Mathematical Physics*, 5(7):848, 1964.

[37] A. Heslot. Quantum mechanics as a classical theory. *Physical Review D*, 31(6):1341–1348, 1985.

[38] P. Jordan, J. Neumann, and E. Wigner. On an algebraic generalization of the quantum mechanical formalism. *The Annals of Mathematics*, 35(1):29–64, 1934.

[39] T. Kibble. Geometrization of Quantum Mechanics. *Communications in Mathematical Physics*, 65(2):189–201, 1979.

[40] N. P. Landsman. *Mathematical topics between Classical and Quantum Mechanics*. Springer Verlag, 1998.

[41] G. W. Mackey. The relationship between classical mechanics and quantum mechanics. *Contemporary Mathematics*, 214:91–110, 1998.

[42] G. Marmo and G. Vilasi. Symplectic Structure and Quantum Mechanics. *Modern Physics Letters B*, 10(12):545–553, 1996.

[43] P. W. Michor. The moment mapping for unitary representations. *Annals of Global Analysis and Geometry*, 8(3):299–313, 1990.

[44] E. Schrödinger Discussion of Probability Relations between Separated Systems. *Math. Proc. Cambridge Phil. Soc.*, 31(4):555-563, 1935.

[45] E. Schrödinger Probability relations between separated systems. *Math. Proc. Cambridge Phil. Soc.*, 32(3):446-452, 1936.

[46] I. E. Segal. Postulates for general Quantum Mechanics. *Annals of Mathematics*, 48(4):930–948, 1947.

[47] M. Spera. On a generalized uncertainty principle, coherent states, and the moment map. *Journal of Geometry and Physics*, 12(3):165–182, 1993.

[48] F. Strocchi. Complex coordinates and Quantum Mechanics. *Reviews of Modern Physics*, 38(1):36–40, January 1966.

[49] J. Von Neumann. *Mathematical principles of Quantum Mechanics*. Princeton University Press, Princeton, 1955.

[50] J. A. Wheeler and W. H. Zurek. *Quantum theory and measurement*. Princeton Univ Press, 1983.

[51] W.H. Zurek. Decoherence, einselection, and the quantum origins of the classical. *Reviews of Modern Physics*, 75(3):715–775, 2003.

Rev. Real Academia de Ciencias. Zaragoza. **67:** 105–111, (2012).
ISSN: 0370-3207

Nonsymmetric metric tensor and anticommutative geometry

Ginés R. Pérez Teruel
e-mail: gipete@alumni.uv.es

Abstract

In the framework of nonsymmetric gravitational theories we consider the equations of motion for matter fields. It is found that the antisymmetric part of the metric is the Pauli matrix in 4 dimensions, suggesting a possible deep relation between spin and geometry. Some arguments about the possibility of building a fermionic space-time instead the ordinary bosonic space-time are discussed.

1 Introduction

The possible extensions of General Relativity is a subject that has experimented a lot of different theoretical approximations since the formulation of the general theory in 1915. For example: Einstein, Schrodinger, Weyl, and many others [1]–[5], tried to unify electromagnetism and gravity using a formalism which defined both, a metric tensor and an affine connection that were non symmetric. This theory, despite its high degree of mathematical elegance did not work, and failed in the attempt to recover some classical results like the Lorentz Force. Years before the formulation of Einstein-Schrodinger theory, Cartan [6, 7], studied how to extend general relativity in order to incorporate torsion(the antisymmetric part of the affine connection). His efforts yields to the conception of space-time with curvature and torsion, unlike usual General Relativity where torsion is zero.

More recently, other physicists like John Moffat [8] have studied in detail the field equations of general theories based in nonsymmetric metric tensors. We will accept this theoretical framework as our starting point, with the aim of investigate the implications for particle physics. In particular, we want to study how the wave equations of the matter fields will be affected by the addition of a non symmetric contribution in the metric tensor. The mathematical discussion that follows provides the result that allow us to identify the Pauli matrix in 4 dimensions with the antisymmetric part of the metric.

2 The line element in General Relativity. Bosonic space-time and fermionic space-time

We begin with the standard definition for the line element in General Relativity:

$$ds^2 = g_{\alpha\beta}(x)dx^\alpha dx^\beta, \tag{1}$$

where the metric tensor is regarded as symmetric.Note that if we add a skew symmetric contribution to the metric tensor, $w_{\alpha\beta}$=$-w_{\beta\alpha}$, the line element remains unchanged due to a simple fact: usual space-time coordinates commute. In such sense, they are bosonic coordinates and represent bosonic degrees of freedom:

$$ds^2 = (g_{\alpha\beta} + w_{\alpha\beta})dx^\alpha dx^\beta = g_{\alpha\beta}dx^\alpha dx^\beta, \tag{2}$$

$$[x^\alpha, x^\beta] = 0 \Longrightarrow dx^\alpha dx^\beta = dx^\beta dx^\alpha. \tag{3}$$

For this reason the term $w_{\alpha\beta}dx^\alpha dx^\beta$ vanishes identically.

We want to generalize (1) for a more general space-time configurations. Let us investigate how the line element in (1) can be extended in situations where the metric tensor is not generally symmetric, and where coordinates do not generally commute. Let us assume the hypothesis that this general expression of the line element is preserved:

$$\begin{aligned} ds^2 = G_{\alpha\beta}dx^\alpha dx^\beta &= (g_{\alpha\beta} + w_{\alpha\beta})(\frac{1}{2}\{dx^\alpha, dx^\beta\} + \frac{1}{2}[dx^\alpha, dx^\beta]) \\ &= \frac{1}{2}g_{\alpha\beta}\{dx^\alpha, dx^\beta\} + \frac{1}{2}w_{\alpha\beta}[dx^\alpha, dx^\beta], \end{aligned} \tag{4}$$

where we have made the following decomposition:

$$dx^\alpha dx^\beta = \frac{1}{2}\{dx^\alpha, dx^\beta\} + \frac{1}{2}[dx^\alpha, dx^\beta] \tag{5}$$

and where the nonsymmetric metric $G_{\alpha\beta}$ consists in the sum of two contributions:

$$G_{\alpha_\beta} = g_{\alpha\beta} + w_{\alpha\beta}, \tag{6}$$

with

$$g_{\alpha\beta} = \tfrac{1}{2}(G_{\alpha\beta} + G_{\beta\alpha}), \tag{7}$$

$$w_{\alpha\beta} = \tfrac{1}{2}(G_{\alpha\beta} - G_{\beta\alpha}). \tag{8}$$

The contravariant tensor $G^{\alpha\beta}$ is defined in terms of the equation

$$G^{\mu\nu}G_{\sigma\nu} = \delta^\mu_\sigma. \tag{9}$$

For usual commutative geometry and bosonic space-time :

$$[dx^\alpha, dx^\beta] \quad = 0, \tag{10}$$

$$\{dx^\alpha, dx^\beta\} \quad = 2dx^\alpha dx^\beta. \tag{11}$$

In this case, the second term in the right side of (4) vanishes, and we recover the usual expression (1), for the line element in General Relativity. But it is more interesting analys what would happen if we consider a fermionic configuration of space-time. This means that at each point exists a chart of coordinates that are Grassman numbers and verify the following relations:

$$\{d\theta^\alpha, d\theta^\beta\} \quad = 0, \tag{12}$$

$$[d\theta^\alpha, d\theta^\beta] \quad = 2d\theta^\alpha d\theta^\beta. \tag{13}$$

Under these conditions, the general line element (4) becomes:

$$ds^2 = G_{\alpha\beta}dx^\alpha dx^\beta = w_{\alpha\beta}d\theta^\alpha d\theta^\beta. \tag{14}$$

Automatically, it arises the question: What is the physical meaning of this construction? Does a fermionic space-time make sense after all? General Relativity is a theory formulated in a purely bosonic space-time where geometry is widely regarded as commutative. Meanwhile, Grassman variables represent fermions, and are present in the path formulation of fermionic fields in quantum field theory. Besides, exist in supersymmetry the superspace where bosonic coordinates are completed with Grassmann numbers, but in a framework where the metric is considered like a symmetric tensor. Given our hypothesis of a general metric with a decomposition in a symmetric and antisymmetric tensors, It seems that the last relations suggest that an unusual type of fermionic fields could be able to feel the antisymmetric part, while bosons and the other ordinary fermions only couple to the symmetric part. Despite the beauty and symmetry of this approach, we will show in the next section that if we accept the possibility of (12) and (13), the formalism leads to the existence of tachyons.

3 The metric tensor and the spin of the particles

In Minkowski space-time, a symmetric metric tensor given with signature $(+,-,-,-)$ we have the Casimir

$$P^\mu P_\mu = g_{\mu\nu}P^\mu P^\nu = m^2. \tag{15}$$

By application of the correspondence principle $P_\mu \rightarrow i\partial_\mu$ we obtain the free Klein Gordon wave equation

$$(g_{\mu\nu}\partial^\mu\partial^\nu + m^2)\phi(x) = 0. \tag{16}$$

Again, we make now the following observation: in the case free, if we add an antisymmetric field $w_{\mu\nu}$ to the metric tensor in (15) the Casimir is not affected by this addition, because $P^\mu P^\nu$ is a purely symmetric object describing bosonic matter. However, when we have interactions, the correspondence principle is modified by inserting covariant derivatives $P^\alpha \to iD^\alpha$ instead of usual derivatives, $P^\alpha \to i\partial^\alpha$. This substitution has the effect of changing the symmetry of $P^\alpha P^\beta$, because $D^\alpha D^\beta$ no longer commutes, and this will generate an additional term involving the antisymmetric part of the metric.

To show this in detail, let us write the Klein-Gordon equation in general curved space-time:

$$(G^{\alpha\beta}(x)D_\alpha D_\beta + m^2)\phi(x) = [(g^{\alpha\beta} + w^{\alpha\beta})(\frac{1}{2}\{D_\alpha, D_\beta\} + \frac{1}{2}[D_\alpha, D_\beta]) + m^2]\phi(x) = 0. \quad (17)$$

By a direct computation of the product in the last equation we obtain:

$$(\frac{1}{2}g^{\alpha\beta}\{D_\alpha, D_\beta\} + \frac{1}{2}w^{\alpha\beta}[D_\alpha, D_\beta] + m^2)\phi(x) = 0. \quad (18)$$

Straightforward manipulations show that the commutator of the covariant derivative can be written as:

$$[D_\alpha, D_\beta]\phi(x) = -(\Gamma^c_{\alpha\beta} - \Gamma^c_{\beta\alpha})\partial_c\phi(x). \quad (19)$$

General Relativity is torsion- free and this means that the Levi-Civita connection is symmetric. In these conditions the last commutator vanishes. Nevertheless, in our analysis this term gives an additional contribution that we shall bear in mind.

Similarly, it can be found an expression for the anti-commutator of the covariant derivatives, but involving the symmetric part of the affine connection:

$$\{D_\alpha, D_\beta\}\phi(x) = 2\partial_\alpha\partial_\beta\phi(x) - (\Gamma^c_{\alpha\beta} + \Gamma^c_{\beta\alpha})\partial_c\phi(x). \quad (20)$$

Eqs. (19) and (20) can be used to write the compact expression for the Klein-Gordon field in curved nonsymmetric space-time. Replacing these relations in (18) we find after straightforward calculations:

$$(g^{\alpha\beta}\partial_\alpha\partial_\beta + m^2)\phi(x) = G^{\alpha\beta}\Gamma^c_{\alpha\beta}\partial_c\phi(x), \quad (21)$$

where

$$\Gamma^c_{\alpha\beta} = \frac{1}{2}(\Gamma^c_{\alpha\beta} + \Gamma^c_{\beta\alpha}) + \frac{1}{2}(\Gamma^c_{\alpha\beta} - \Gamma^c_{\beta\alpha}). \quad (22)$$

The left side of (21) is identical to the corresponding Klein-Gordon equation in General Relativity. The difference lies in the right side: now the metric and the affine connection are not symmetric, but it is worth to note that the form of the equation remains the same.

What about Dirac fields? The explicit and detailed treatment of Dirac fields in a general curved space-time is a much more complicated task (see for instance [9]), but we

only want to take a general picture in order to inquire some aspects of the field $w_{\alpha\beta}$. For this reason, we will not solve the covariant derivative over Dirac fields. We will limit to the task of requiring that the Dirac equation could be expressed as the square root of the Klein-Gordon field.

The Dirac equation in curved space-time can be written as

$$(i\gamma^{\alpha}D_{\alpha} - m)\psi(x) = 0, \tag{23}$$

where $D_{\alpha} = \partial_{\alpha} + \Gamma_{\alpha}$. As we have said before, we make the assumption that the Dirac field in general curved space-time can be expressed as the square root of the Klein-Gordon equation. This allows us to write

$$(-i\gamma^{\alpha}D_{\alpha} - m)(i\gamma^{\beta}D_{\beta} - m)\psi(x) = 0. \tag{24}$$

If we assume $D_{\alpha}\gamma^{\beta} = 0$, which seems a plausible generalization of the condition $\partial_{\alpha}\gamma^{\beta} = 0$ that is verified by the Dirac matrices in a flat space-time, we find

$$(\gamma^{\alpha}\gamma^{\beta}D_{\alpha}D_{\beta} + m^2)\psi(x) = 0. \tag{25}$$

This is nothing but the Klein-Gordon equation in general nonsymmetric curved space-time (17). Thus, we can make the identification

$$\gamma^{\alpha}\gamma^{\beta} = \frac{1}{2}\{\gamma^{\alpha}, \gamma^{\beta}\} + \frac{1}{2}[\gamma^{\alpha}, \gamma^{\beta}] = G^{\alpha\beta} = g^{\alpha\beta} + w^{\alpha\beta}. \tag{26}$$

That provides

$$g^{\alpha\beta} = \frac{1}{2}\{\gamma^{\alpha}, \gamma^{\beta}\}, \tag{27}$$

$$w^{\alpha\beta} = \frac{1}{2}[\gamma^{\alpha}, \gamma^{\beta}]. \tag{28}$$

Equation (27) is a well known result that remit us to the field of Clifford algebra. On the other hand, the commutator of the Dirac matrices transforms as a tensor, and is a clue concept to understand the behavior of the Dirac field under general Lorentz transformations. We suggest a new interpretation of this tensor in the framework of nonsymmetric space-time, where the metric tensor has an antisymmetric part.

With these results in mind let us return to the previous section where we studied the notion of a fermionic space-time of Grassmann coordinates, that couple to the antisymmetric part of the metric tensor in the definition of the general line element(4). Let us begin writing the left side of the Casimir invariant (15), in a flat space-time doted with a nonsymmetric metric $G^{\alpha\beta} = \gamma^{\alpha}\gamma^{\beta}$. Then we have

$$G^{\alpha\beta}p_{\alpha}p_{\beta} = \gamma^{\alpha}\gamma^{\beta}p_{\alpha}p_{\beta}. \tag{29}$$

Making contact now with (12) and (13), for fermionic degrees of freedom

$$\{p_\alpha, p_\beta\} = p_\alpha p_\beta + p_\beta p_\alpha = 0. \tag{30}$$

This allow us to make the substitution: $p_\alpha p_\beta = -p_\beta p_\alpha$ in equation (29) and we have

$$-\gamma^\alpha \gamma^\beta p_\beta p_\alpha. \tag{31}$$

Note that $\gamma^\beta p_\beta$ is nothing but the Dirac equation in momentum space: $\gamma^\beta p_\beta \psi = m\psi$. Therefore, equation (29) provides after a direct computation a global term of $-m^2$, and this means that we are dealing with tachyons.

If we repeat the same reasoning for bosonic commutative variables, the result gives the correct sign for the Casimir invariant.

This result is intriguing. It likely means that we are not allowed to describe usual fermions with anticommutative variables in the external space-time, but only in their own internal vectorial space. Maybe this result is telling us something about tachyons. Tachyons would be Grassman fields that behave in the space-time being able to feel the antisymmetric part of the metric tensor, undetectable for us and the other ordinary matter. Indeed, bosons and the usual fermions that are represented by Grassmann variables in their internal spinor space, are all associated with standard bosonic coordinates when they move in the space-time.

In any case, this last result only questions the assumptions of the equations (12) and (13), but says nothing about the validity of nonsymmetrical gravitational theories.

4 Discussion

In this paper we have explored an alternative approach which combines some insights of nonsymmetrical gravitational theories with concepts of noncommutative geometry. In this approach, we have discussed that the inclusion of an antisymmetric part in the metric tensor has some interesting consequences when is considered the possibility of extend the conception of bosonic space-time with coordinates that do not commute. We have postulated a generalization for the invariant line element in General relativity, which puts bosonic and fermionic coordinates on an equal footing. Bosonic degrees of freedom couple to the symmetric part of the metric, while unusual fermionic degrees of freedom would do the same but with the other part.

Nevertheless, these assumptions lead to the wrong sign for the square of the mass in the Casimir invariant, which means that tachyons arise inevitably when we describe these unusual type of fermions. In other words: Grassman coordinates in a nonsymmetric space-time represent degrees of freedom that behave like tachyons.

On the other hand, it has been studied in some detail the wave equations for matter fields in the framework of nonsymmetric gravitational theories, suggesting a possible new

interpretation for the commutator of the Dirac matrices, which emerges naturally as the antisymmetric part of the metric tensor.

Until now, it has not been found any experimental evidence of the nonsymmetric nature of the metric tensor. But we point out that if these nonsymmetric theories of gravity are finally found to be a correct description of nature, then such identification of the antisymmetric part of the metric tensor with the commutator of the gamma matrices could be naturally established as a theoretical consequence.

References

[1] A. Einstein, *Sitzunsberg. Preuss. Akad. Wiss(Berlin)* 32, (1923)

[2] A. Einstein, *Sitzunsberg. Preuss. Akad. Wiss(Berlin)* 137, (1 923)

[3] A. S. Eddington, *The Mathematical Theory of Relativity*(Cambridge Univ. Press, 1924)

[4] E. Schrodinger, *Proc. R. Ir. Acad.* A 51, 163 (1947)

[5] E. Schrodinger, *Space-Time Structure* (Cambridge Univ. Press,1950)

[6] E. Cartan, *Comp. Rend. Acad. Sci. (Paris)* 174, 593 (1922)

[7] E. Cartan, *Ann. Ec. Norm. Sup.* 40, 25 (1923)

[8] J. Moffat, *Nonsymmetric Gravitational Theory.* Phys. Lett. B 355: 447-452 (1995)

[9] H. A. Weldon, *Fermions without Vierbeins in Curved Space-Time* Phys. Rev. D 63 104010 (2001)

[10] H. Weyl, *Space, Time, Matter* (Methuen, 1922)

Nota Necrológica
Enrique Meléndez Andreu

Es difícil recoger en unas pocas palabras toda una vida dedicada a la investigación y la docencia, como ha sido el caso del Prof. Enrique Meléndez, pero voy a intentar hacerlo.

El profesor Meléndez nació en Zaragoza el 17 de julio de 1933, en 1955 se licenció en Ciencias Químicas por la Universidad de Valladolid y en 1962 obtuvo el título de "Docteur en Sciences Physiques" por la Universidad de La Sorbona en París que refrendó posteriormente en 1963 con el de "Doctor en Químicas" por la Universidad de Valladolid.

Su trayectoria profesional se desarrolló primero en París (1956–1964) como Investigador en el C.N.R.S., volviendo a continuación a España como Investigador en el Instituto Alonso Barba de Química Orgánica del C.S.I.C. en Madrid (1964–1968). Posteriormente fue Profesor Agregado en la Cátedra de Química Farmacéutica de la Universidad de Barcelona (1968–1974) y finalmente fue Catedrático de Química Orgánica en la Universidad de Zaragoza (1974–2003) donde desarrolló su labor docente e investigadora hasta su jubilación.

Fue uno de los fundadores del grupo de Química Orgánica, creado en 1967, del que fue su primer secretario y que cuenta actualmente con 650 socios. Asimismo fue presidente de la Sociedad Española de Química Terapéutica entre 1985 y 1989. A pesar de ser químico por su fuerte interacción con la investigación en Medicina fue elegido académico numerario de la Real Academia de Medicina de Zaragoza.

Ingresó como académico numerario de la Real Academia de Ciencias Exactas, Físicas, Químicas y Naturales de Zaragoza en febrero de 1982, cuando leyó su discurso de ingreso titulado "Cristales Líquidos". En 1990 fue elegido como Presidente cargo que ostentó hasta 1996.

En el discurso de contestación a su discurso de ingreso el Profesor Gutiérrez Losa enumeró los méritos del Profesor Meléndez y quiero recordar algunas de sus palabras que indican muy claramente la importancia de su labor en nuestra Universidad: *"Por eso cuando en 1974 accede a la Cátedra de Química Orgánica en nuestra Facultad de Ciencias... Enrique Meléndez trae consigo no sólo el entusiasmo y la inquietud que siempre le caracterizaron, sino también un bagaje científico (teórico y práctico) considerable. En sólo siete años de estancia en esta Universidad, el Prof. Meléndez ha reestructurado las*

enseñanzas dependientes del Departamento de Química Orgánica de acuerdo con el nuevo plan de estudios y ha marcado, con trazo firme, nuevas líneas de investigación orientadas principalmente al estudio de heterociclos, a la preparación de nuevos aminoácidos y al complejo y sugestivo campo de los cristales líquidos, precisamente el tema elegido por él para su disertación en este lugar".

Figure 1.— El Profesor Enrique Meléndez Andreu (en el centro de la segunda fila) con motivo de su incorporación al *Senatrus Científico* en 2006, con el Rector Pétriz, el Decano Elipe y el Presidente de la Real Academia, Horacio Moll.

Este entusiasmo por la Química Orgánica, en todas sus facetas, lo supo transmitir a sus discípulos. Así de los 19 doctorandos del Prof. E. Meléndez en la Universidad de Zaragoza, 16 han seguido una trayectoria vinculada a la docencia y a la investigación en la Universidad y en el Consejo Superior de Investigaciones Científicas. De hecho entre sus discípulos se cuenta con nueve catedráticos de Química Orgánica, un catedrático de Química Física, un profesor titular de Química Orgánica y un profesor de investigación y cuatro investigadores del Consejo Superior de Investigaciones Científicas.

El Profesor Enrique Meléndez era un excelente docente. Todos los que tuvimos la suerte de asistir a sus clases recordamos con admiración y cariño como llegaba siempre puntual, con su bata blanca siempre remangada, y comenzaba a hablar de forma clara y concisa, a la vez que iba rellenando una pizarra que al cabo de un tiempo aparecía ante nuestros ojos como un fantástico esquema de todo lo que se había tratado hasta

el momento. Siempre hemos comentado la perfección de las pizarras tanto en cuanto a calidad de contenido como a la estética de las mismas.

Otro punto a resaltar era la combinación de respeto y afabilidad que tenía en el trato con todos sus alumnos y estudiantes, era muy fácil hablar con él pero no lo era el tutearlo, el usted salía de forma espontánea.

Tal y como indicaba el Profesor Gutiérrez Losa en 1974 llegó el Prof. E. Meléndez a la Universidad de Zaragoza. Su antecesor el Prof. Barluenga se acababa de trasladar a la Universidad de Oviedo con casi todos sus discípulos, por lo que el Profesor Meléndez tuvo que empezar con estudiantes con la carrera recién acabada. En aquel momento los laboratorios de Química Orgánica estaban en condiciones bastante precarias, el material era muy escaso y era necesario reciclar y aprovechar al máximo los disolventes. El profesor Meléndez, en un período de tiempo relativamente corto, dotó a los laboratorios de la infraestructura necesaria, tanto en material como en equipos, para realizar los trabajos de investigación.

Finalmente en 1987 se constituyó el Dpto. de Química Orgánica y como primer firmante del acta de constitución el profesor Meléndez fue nombrado director del mismo.

La estancia doctoral y postdoctoral en Francia del profesor Meléndez le hizo tener una concepción de la Universidad y de la Investigación muy diferente a la que se tenía en nuestro país en el mismo período, dejando una gran libertad a sus doctorandos y valorando positivamente sus opiniones e iniciativas. De hecho, en el primer año de su estancia en Zaragoza, y a pesar de las penurias económicas de la cátedra, puso en marcha dos líneas de investigación completamente diferentes, una basada en compuestos con actividad farmacológica mediante la síntesis de nuevos aminoácidos y otra en nuevos materiales de tipo cristal líquido. Estas dos líneas, en campos tan diferentes, comenzaron utilizando los mismos compuestos de partida en lo que denominaron en el grupo como "química de estantería", lo que da idea de la imaginación y capacidad del Profesor Meléndez. Posteriormente se incorporó una tercera línea de investigación basada en derivados heterocíclicos. De estas tres líneas iniciales han derivado los seis grupos de investigación del actual Departamento de Química Orgánica.

Para conseguir estos resultados tan rápidamente se apoyó en sus excelentes relaciones con investigadores de gran prestigio a nivel nacional e internacional. En muchas ocasiones estos investigadores no dudaban en venir a Zaragoza a ser sometidos a sesiones maratonianas con todos los doctorandos del Profesor Meléndez. Destacan entre ellos el Profesor José Elguero del CSIC y el Profesor Félix Serratosa de la Universidad de Barcelona y del CSIC, dos de los químicos orgánicos españoles más prestigiosos a nivel internacional y el Prof. Lionel Liébert del CNRS en el centro de excelencia de Orsay (Francia), pionero en el estudio de los cristales líquidos.

Su visión de la investigación era muy amplia y entendió claramente la importancia de la colaboración entre físicos y químicos en el campo de los Materiales Avanzados donde se necesita una visión multidisciplinar. Así, a raíz de una de las primeras publicaciones de nuestro grupo en el campo de los cristales líquidos ferroeléctricos, en 1984 estableció contacto con un grupo de la Universidad del País Vasco en Lejona (Vizcaya). Tras los primeros contactos esta colaboración, que todavía se mantiene, ha dado lugar a más de una decena de proyectos coordinados nacionales e internacionales y a casi un centenar de publicaciones conjuntas.

Otro hito importante para nuestra Universidad fue su participación en la negociación con el CSIC para la creación del Instituto de Ciencia de los Materiales de Aragón (ICMA-1985). Este Instituto Mixto de Investigación entre la Universidad de Zaragoza y el CSIC ha tenido y tiene una gran relevancia en el desarrollo de la investigación de nuestra comunidad.

Su inquietud por todo lo relacionado con nuestra Facultad hizo que tras su jubilación siguiera participando en las actividades académicas, siendo uno de los primeros miembros de Senatus científico de nuestra Facultad.

Es importante resaltar, además de su indudable vocación por la Química, su gran conocimiento y pasión por el arte, fundamentalmente pintura y música clásica. Conoció a muchos y famosos pintores coetáneos, de hecho logró una excelente colección de pinturas y era asiduo a los conciertos (fundamentalmente si eran de calidad) que tenían lugar en nuestra ciudad.

Finalmente quiero hacer especial hincapié en su gran pasión por la naturaleza y la montaña, especialmente por el Valle de Tena, del que provenía su padre, y en el que pasó excelentes momentos paseando, pescando, buscando setas o simplemente, contemplando la naturaleza.

En resumen, un excelente profesor y una excelente persona, que ha contribuido de forma importante al desarrollo científico de nuestro país y que ha dejado una huella muy marcada en todos los que lo conocieron.

José Luis Serrano
Académico numerario

ACTIVIDADES DE LA REAL ACADEMIA DE CIENCIAS EXACTAS, FÍSICAS, QUÍMICAS Y NATURALES DE ZARAGOZA EN EL AÑO 2012

Sesiones:

En el año 2012 la Real Academia de Ciencias de Zaragoza celebró tres sesiones, una de ellas con motivo de la entrega de Premios de Investigación.

Las sesiones tuvieron lugar los días 16 de mayo, 17 de octubre y 7 de noviembre. Esta última fue la mencionada sesión de entrega de Premios de Investigación 2011-2012.

La Real Academia de Ciencias de Zaragoza participó también el 18 de octubre en la Sesión solemne de apertura de curso de las academias de Aragón y el 24 de noviembre en la Solemne Sesión conjunta de las Academias de Aragón para conmemorar el V Centenario de Miguel Servet.

El 26 de septiembre la Real Academia de Ciencias de Zaragoza organizó un acto académico en memoria del Académico Enrique Meléndez Andreu, quien fue Presidente de la misma desde 1990 hasta 1996.

Publicaciones de la Academia:

La Academia ha publicado el volumen 66 de la Revista de la Academia de Ciencias de Zaragoza, y el volumen 38 de la serie Monografías de la Real Academia de Ciencias, con el título de *"A special tribute to Professor Monique Madaune-Tort"*.

Organización de Congresos y Conferencias:

La Academia ha organizado en 2012, entre otros, los siguientes eventos:

- Conferencia de la Profesora Laurence BOUQUIAUX, de la Universidad de Lieja (Bélgica) el día 18 de abril con el título *"The Leibniz Newton Controversy"*.
- Conferencia el 9 de mayo de José Manuel Blecua, Director de la Real Academia Española titulada: *"Camino de las palabras hacia el diccionario"*.
- Conferencia a cargo de Dr. Miguel Andériz López, con el título *"Bases biomatemáticas del estudio de los factores de riesgo en medicina"*.

- La Academia ha colaborado en el *XIV Encuentro de Invierno Geometría, Mecánica y Teoría de Control* celebrado en Zaragoza los días 6 y 7 de febrero

- Colaboración en la organización conjunta con la Facultad de Ciencias de los Ciclos de Conferencias *Cita con la Ciencia* y *Espacio Facultad 2011-2012*.

Por último, dentro de la habitual participación de Académicos en numerosos congresos nacionales e internacionales, y en conferencias en el ámbito de la difusión de la ciencia, cabe destacar las siguientes actuaciones:

- El Académico Alberto Elduque ha sido conferenciante invitado en los congresos *Workshop on Exceptional Algebras and Groups* (Ottawa, Canadá, abril de 2012), *International Workshop on Groups, Rings, Lie and Hopf Algebras II* (Bonne Bay, Newfoundland, Canadá, agosto de 2012), y *DAG days: The Freudenthal-Tits Magic Square* (Gante, Bélgica, en octubre de 2012).

  Ha sido también miembro del Comité Científico del *II Encuentro Conjunto Real Sociedad Matemática Española - Sociedad Matemática Mexicana* (Torremolinos, Málaga, enero de 2012), de la Escuela CIMPA *Algebraic structures, their representations and applications in geometry and nonassociative models* (Cartagena de Indias, Colombia, marzo de 2012) y del congreso *Lie and Jordan Algebras, their Representations and Applications-V* (Belem, Brasil, julio de 2012).

  Además ha impartido las siguientes conferencias y cursos: *Lie algebras: Killing-Cartan classification*, mini-curso de 8 horas en la CIMPA School *Algebraic structures, their representations and applications in geometry and nonassociative models*, Cartagena, Colombia, en marzo de 2012, *Conways's rational tangles*, en Memorial University of Newfoundland (St. John's, Canadá, julio de 2012), *Lie theory*, curso de verano de 30 horas en la Memorial University of Newfoundland (St. John's, Canadá, julio–agosto de 2012, *A Freudenthal-Tits Supermagic Square*, en la Universidade da Beira Interior (Portugal), octubre de 2012, *Gradings on simple Lie algebras* en el Seminario de *Álgebra y Combinatoria* del ICMAT, Madrid, noviembre de 2012. *Symmetric composition algebras and exceptional simple Lie algebras*, Colloquium Talk en la Universidad de Uppsala (Suecia), en diciembre de 2012.

- El Académico Eladio Liñán fue el organizador de los actos conmemorativos y de la exposición que tuvieron lugar en Zaragoza con motivo del 150 aniversario del hallazgo del yacimento de Murero (Zaragoza) que fue el primer yacimento paleontológico declarado Bien de Interés Cultural (BIC) en España.

- El Académico Pablo J. Alonso fue miembro del comité científico de la *XI reunión nacional del GIRSE* y *1ª reunión conjunta ARPE-GERPE-GIRSE)* (GIRSE=Gruppo

Italiano di Risonanza di Spin Elettronico, ARPE=Association française de Résonance Paramagnétique Électronique, GERPE=Grupo Español de Resonancia Paramagnética Electrónica.

- El Académico Antonio Elipe ha sido miembro del Comité Científico de los siguientes congresos: *1st IAA Conference on Dynamics, Control and Space Systems*. Porto, Portugal. 19–21 marzo; *XIII Jornadas de trabajo en mecánica celeste*. Zaragoza, 18–19 junio; y *Maths and Chemistry*, Zaragoza, 20–22 junio.

  En colaboración con la ACPUA (Agencia de Calidad y Prospectiva Universitaria de Aragón) ha organizado las jornadas *La Calidad en los Centros Universitarios de la Defensa: Una garantía de futuro*, celebradas en Zaragoza los días 7 y 8 de noviembre.

- El Secretario José F. Cariñena formó parte del Comité Organizador de los *XIV Encuentros de Invierno Mecánica, Geometría y Teoría de control*, 6 y 7 de febrero y del *Thematic Day: Geometric Structures in Mechanics"* el 8 de febrero, en Zaragoza. Fue también miembro del Comité Científico del Congreso *Mathematical Structures in Quantum Systems and applications* en Benasque, julio 8-14.

Varios Académicos han colaborado en cursos propios en la Universidad de la Experiencia que organiza la Universidad de Zaragoza.

Premios de investigación 2012

Se concedieron los Premios de Investigación 2011-2012 de la Academia correspondientes a las secciones de Exactas y Físicas. En la sección de Exactas el premio fue para el Profesor Luis Rández García y en la de Físicas al Doctor Jesus Clemente Gallardo. Los premiados expusieron sendos trabajos de investigación en la sesión celebrada el 7 de noviembre y se les hizo entrega del Premio de Investigación 2012. Los trabajos de investigación con los títulos respectivos de *"Optimization of spatial and temporal discretization schemes for Computational Aero-Acoustics problems"* y *"The geometrical formulation of Quantum Mechanics"*, se publican en este volumen **67** de la Revista de la Real Academia.

Se ha iniciado el proceso para los Premios 2012-2013 en las Secciones de Químicas y Naturales.

Distinciones y Nombramientos a Académicos.

La Junta de Gobierno de la Sociedad Española de ptica decidió nombrar Socio de Honor de SEDOPTICA al Académico Miguel A. Rebolledo por su labor en favor del desarrollo de la ptica española.

El Académico D. Antonio Elipe fue nombrado *Cadete Honorífico* por la Academia General Militar.

Otros datos.

La Real Academia de Ciencias de Zaragoza, en contra de lo sucedido hasta el momento, este año no ha recibido subvencióna para su funcionamiento del Ministerio de Educación y Ciencia a través del programa de apoyo a las Reales Academias asociadas al Instituto de España.

Se ha continuado poniendo al día la página web de la Academia, cuya dirección es `http://acz.unizar.es`

Zaragoza, diciembre de 2012

REVISTA DE LA REAL ACADEMIA DE CIENCIAS EXACTAS, FÍSICAS, QUÍMICAS Y NATURALES DE ZARAGOZA

Abstract

La Revista de la Real Academia de Ciencias publishes original research contributions in the fields of Mathematics, Physics, Chemistry and Natural Sciences. All the manuscripts are peer reviewed in order to assess the quality of the work. On the basis of the referee's report, the Editors will take the decision either to publish the work (directly or with modifications), or to reject the manuscript.

1 Normas generales de publicación

1.1 Envío de los manuscritos.

Para su publicación en esta Revista, los trabajos deberán remitirse a

Académico-Director de Publicaciones
Revista de la Academia de Ciencias
Universidad de Zaragoza
50009 Zaragoza

o bien electrónicamente a la cuenta `elipe@unizar.es`.

La Revista utiliza el sistema de *offset* de edición, empleando el texto electrónico facilitado por los autores, que deberán cuidar al máximo su confección, siguiendo las normas que aquí aparecen.

Los autores emplearán un procesador de texto. Se recomienda el uso de LaTeX, para el que se han diseñado los estilos `academia.sty` y `academia.cls` que pueden obtenerse directamente por internet en `http://acz.unizar.es` o por petición a la cuenta de correo electrónico: `elipe@unizar.es`.

1.2 Dimensiones

El texto de los trabajos, redactados en español, inglés o francés, no deberá exceder de 16 páginas, aunque se recomienda una extensión de 6 a 10 páginas como promedio. El texto de cada página ocupará una caja de 16×25 cm., con espacio y medio entre líneas.

2 Presentación del trabajo.

Los trabajos se presentarán con arreglo al siguiente orden: En la primera página se incluirán los siguientes datos:

a) Título del trabajo: Conciso, pero ilustrativo, con mayúsculas.

b) Autor: Nombre y apellidos del autor o autores, con minúscula.

c) Centro: Centro donde se ha realizado, con su dirección postal.

d) Abstract: En inglés y con una extensión máxima de 200 palabras.

e) Texto

A) Los encabezamientos de cada sección, numerados correlativamente, serán escritos con letras **minúsculas** en negrita. Los encabezamientos de subsecciones, numerados en la forma 1.1, 1.2, ..., 2.1, 2.2, ..., se escribirán en *cursiva*.

B) Las fórmulas estarán centradas y numeradas correlativamente.

C) Las referencias bibliogáficas intercaladas en el texto, deben ser fácilmente identificables en la lista de refencias que aparecerá al final del artículo, bien mediante un número, bien mediante el nombre del autor y año de publicación.

D) Las figuras y tablas, numeradas correlativamente, se intercalarán en el texto. Las figuras se enviarán en formato EPS, o que se pueda convertir a éste con facilidad. Los apéndices, si los hay, se incluirán al final del texto, antes de la bibliografía.

G) Las referencias bibliográficas de artículos deberán contener: Autor: año de publicación, "Título del artículo", *revista* **número**, páginas inicial–final. En el caso de libros, deberá incluirse: Autor: año de publicación, *Título del libro*. Editorial, lugar de publicación.

3 Notas finales

Por cada trabajo publicado, se entregarán al autor o autores un total de 25 separatas. La Revista permite la inclusión de fotografías o figuras en color, con un coste adicional que correrá a cargo de los autores.

Antonio Elipe
Académico Editor

RELACIÓN DE REVISTAS NACIONALES QUE RECIBE EN INTERCAMBIO LA BIBLIOTECA DE LA ACADEMIA DE CIENCIAS

ACTA BOTANICA BARCINONENSIS
ACTA QUIMICA COMPOSTELANA - Departamento de Química Analítica
AFINIDAD - Revista Química Teórica y Aplicada
ANALES DE BIOLOGIA - Sección de Biología General (Murcia)
ANALES DEL JARDIN BOTANICO DE MADRID
ANALES DE LA REAL ACADEMIA DE DOCTORES
ANALES DE LA UNIVERSIDAD DE MURCIA
ANALES DE CIENCIAS - Facultad de Ciencias (Químicas y Matemáticas) (Murcia)
ANALES SECCION DE CIENCIAS - Colegio Universitario de Girona
ANUARIO DEL OBSERVATORIO ASTRONOMICO - Madrid.
BELARRA. SOCIEDAD MICOLOGICA. Baracaldo.
BLANCOANA - Col. Univ. "Santo Reino" Jaén
BOLETIN DA ACADEMIA GALEGA DE CIENCIAS - (Santiago de Compostela)
BOLETIN DE LA ASOCIACION HERPETOLOGICA ESPAÑOLA
BOLETIN GEOLOGICO Y MINERO
BOTANICA COMPLUTENSIS - Madrid
BUTLLETI DEL CENTRO D'HISTORIA NATURAL DE LA CONCA DE BARBARA
COLLECTANEA BOTANICA - (Barcelona)
COLLECTANEA MATEMATICA - (Barcelona)
ESTUDIO GENERAL - Revista Colegio Universitario (Girona)
EXTRACTA MATHEMATICAE - Universidad de Extremadura
FACULTAD DE CIENCIAS EXPERIMENTALES DE JAEN. Monografías.
FOLIA BOTANICA MISCELANEA - Departamento de Botánica (Barcelona)
GACETA DE LA REAL SOCIEDAD MATEMÁTICA ESPAÑOLA
INDICE ESPAÑOL DE CIENCIA Y TECNOLOGIA -
INSTITUTO GEOLOGICO Y MINERO DE ESPAÑA
INVESTIGACION E INFORMACION TEXTIL Y DE TENSIOACTIVIVOS (C.S.I.C.) - Barcelona
LACTARIUS.- BOL. DE LA ASOCIACION MICOLOGICA - Jaén
LUCAS MALLADA - Inst. Est. Altoaragoneses.

MEMORIAS DE LA REAL ACADEMIA DE CIENCIAS Y ARTES DE BARCELONA
MISCELANEA ZOOLOGICA - Museo Zoológico - Ayuntamiento de Barcelona
NATURALIA BAETICA - Jaén
PIRINEOS
PUBLICACIONES PERIODICAS DE LA BIBLIOTECA DEL MUSEU DE ZOOLOGIA - (Barcelona)
REBOLL.- Bull. Centro d'Historia Natural de la Conca de Barbera.
REVISTA DE LA ACADEMIA CANARIA DE CIENCIAS
REVISTA REAL ACADEMIA GALEGA DE CIENCIAS
REVISTA DE BIOLOGIA DE LA UNIVERSIDAD DE OVIEDO
REVISTA ESPAÑOLA DE FÍSICA
REVISTA ESPAÑOLA DE FISIOLOGIA - Pamplona
REVISTA ESPAÑOLA DE HERPETOLOGIA
REVISTA IBERICA DE PARASITOLOGIA
REVISTA MATEMATICA COMPLUTENSE - (Madrid)
REVISTA DE OBRAS PUBLICAS
REVISTA DE LA REAL ACADEMIA DE CIENCIAS EXACTAS, FISICAS Y NATURALES DE MADRID – Matemáticas
REVISTA DE LA REAL ACADEMIA DE CIENCIAS - QUIMICA - Madrid
RUIZIA - Monografías del Jardín Botánico (Madrid)
SCIENCIA GERUNDENSIS
STUDIA GEOLOGICA SALMANTICENSIA - Universidad de Salamanca
TRABAJOS DE GEOLOGIA - Universidad de Oviedo
TREBALLS DEL CENTRE D'HISTORIA NATURAL DE LA CONCA DE BARBERA.
TREBALLS DE L'INSTITUT BOTANIC DE BARCELONA
TREBALLS DEL MUSEU DE ZOOLOGIA DE BARCELONA
ZOOLOGIA BAETICA. UNIVERSIDAD DE GRANADA.

RELACIÓN DE REVISTAS INTERNACIONALES QUE RECIBE EN INTERCAMBIO LA BIBLIOTECA DE LA ACADEMIA DE CIENCIAS

ACADEMIA NACIONAL DE CIENCIAS - Córdoba. Argentina
ACADEMY OF NATURAL SCIENCES OF PHILADELFIA
ACCADEMIA NAZIONALE DEI LINCIEI - Notiziario
ACCADEMIA UDINESE DI SCIENZI LETTERS ED ARTI.
ACTA ENTOMOLOGICA MUSEI NATIONALIS PRAGAE
ACTA FAUNISTICA ENTOMOLOGICA MUSEI NATIONALIS - Pragae
ACTA GEOLOGICA POLONICA - Warszawa
ACTA MATHEMATICA HUNGARICA
ACTA MATEMATICA SINICA - New Series China
ACTA MUSEI NATIONALI PRAGAE
ACTA ORNITHOLOGICA - Polska Akademia Nauk Warszawa
ACTA PHYSICA - Academia Scientarum Hungaricae
ACTA SOCIETATIS ENTOMOLOGICA BOHEMOSLOVACA
ACTA UNIVERSITATIS - Series: Mathematics and Informatic – University of Nis – Yugoeslavia
ACTA ZOOLOGICA FENNICA
AGRONOMIA LUSITANICA - Est. Agr. Nac. Sacavem - Portugal
AKADEMIE DER WISSENSCHAFTEN
ANALES DE LA ACADEMIA NACIONAL DE CIENCIAS EXACTAS, FISICAS Y NATURALES DE BUENOS AIRES
ANALES DE LA ESCUELA NACIONAL DE CIENCIAS BIOLOGICAS. México
ANALES DE LA SOCIEDAD CIENTIFICA ARGENTINA
ANALES DE LA ESCUELA NACIONAL DE CIENCIAS BIOLOGICAS - México
ANIMAL BIODIVERSITY CONSERVATION
ANNALEN DES NATURHISTORICHEN MUSEUMS IN WIEN
ANNALES ACADEMIA SCIENTARUM FENNICAE - Serie A - I Matematica - Helsinke
ANNALES ACADEMIA SCIENTARUM FENNICAE - Serie A - II Chemica - Helsinke
ANNALES ACADEMIA SCIENTARUM FENNICAE - III Geologica Geografica - Helsinke
ANNALES ACADEMIA SCIENTARUM FENNICAE - Serie A - IV Physica - Helsinke
ANNALES HISTORICO NATURALES - Musei Nationalis Hungarici

ANNALES DE L'INSTITUT FOURIER - Université de Grenoble
ANNALES DE L'INSTITUT FOURIER - Gap
ANNALES DE LA SOCIETE SCIENTIFIQUE - Serie I - Science Mathematiques Physiques Bruxelles
ANNALES UNIVERSITATIS MARIA CURIE - Sectio A Mathemat. - Sklodowska
ANNALES UNIVERSITATIS MARIA CURIE - Sklodowska - Sectio AA Chemica. Lublin.
ANNALES UNIVERSITATIS MARIA CURIE - Sklodowska - Sectio AAA Physica. Lublin.
ANNALES ZOOLOGICI FENNICI - Helsinki
ANNALI DELLA FACOLTA DE AGRARIA - Universita de Pisa
ANNALI DEL MUSEO CIVICO DI STORIA NATURALE "Giacomo Doria"
ARBOLES Y SEMILLAS DEL NEOTROPICO - Museo Nac. de Costa Rica
ARCHIVIO GEOBOTANICO - Univ de Pavía.
ATTI DELLA ACCADEMIA NAZIONALE DEI LINCEI. RENDICONTI LINCEI - Matematica e Applicacioni - Roma
ATTI DELLA ACCADEMIA NAZIONALE DEI LINCEI. RENDICONTI LINCEI - Scienze Fisiche e Naturali - Roma
ATTI DELLA ACCADEMIA DI SCIENZE, LETTERE E ARTI DI UDINE
ATTI DELL'INSTITUTO BOTANICO E DEL LABORATORIO CRITTOGRAMICO DELL'UNIVERSITA DI PAVIA
BAYERISCHE AKADEMIE DR WISSENSCHAFTEN - Munchen
BEITRAGE ZUR FORSCHUNSTECHOLOGIE - Akademie Verlag Berlin
BOLETIM DA SOCIEDADE PARANAENSE DE MATEMATICAS - Paraná
BOLETIM DA SOCIEDADES PORTUGUESA DE CIENCIAS NATURALES - Lisboa
BOLETIN DE LA REAL ACADEMIA DE CIENCIAS FISICAS, MATEMATICAS Y NATURALES - Caracas
BOLETIN DE LA ACADEMIA DE CIENCIAS - Córdoba. Argentina.
BOLETIN BIBLIOGRAFICO DE LA ESCUELA NACIONAL DE CIENCIAS BIOLÓGICAS - México
BOLETIN DEL MUSEO NAC. DE COSTA RICA.
BOLETIN DE LA SOCIEDAD MATEMATICA MEXICANA
BOTANY UNIV. OF CALIFORNIA PUBLICATIONS.
BRENESIA - Museo Nacional de Costa Rica
BULGARIAN ACADEMY OF SCIENCES - Scientific Information - CENTRE MATHEMATICAL AND PHYSICAL SCIENCES
BULGARIAN JOURNAL OF PHYSICS
BULLETIN OF THE AMERICAN MATHEMATICAL SOCIETY - Providence
BULLETIN DE LA CLASSE DE SCIENCES - Academie Royale de Belgique - Bruxelles
BULLETIN OF THE GEOLOGICAL INSTITUTION OF THE UNIVERSITY UPSALA

BULLETIN OF THE JSME (Japan Society of Mechanical Engineers)
BULLETIN DE LA SOCIETE SCIENTIFIQUE DE BRETAGNE - Rennes
CALIFORNIA AGRICULTURE - University of California
CIENCIAS TECNICAS FISICAS Y MATEMATICAS. Academia de Ciencias. Cuba.
COLLOQUIUM MATHEMATICUM - Warszawa
COMMENTATIONES MATHEMATICAE - Ann. So, Mathematicae Polonese
COMPTES RENDUS DE L'ACADEMIE BULGARE DE SCIENCES - Sofia
DARWINIANA REV. INST. BOTANICA DARWINION - República Argentina
DORIANA - Supplementa agli Annali del Museo Civico di Storia Naturale "G. Doria" - Cenova
ESTUDOS, NOTAS E TRABALHOS DO SERVIC DE FOMENTO MINERO - Portugal
ESTUDOS, NOTAS E TRABALHOS, DIECCIÓ GERAL DE GEOLOGIA E MINAS - Porto
FILOMAT - FACTA UNIVERSITATIS - Univ. af Nis.
FÍSICA DE ONDAS ACÚSTICAS Y ELECTROMAGNÉTICAS LINEALES - Acad. Búlgara de las Ciencias
FOLIA ANATOMICA UNIVERSITATIS CONIMBRIGENSIS - Coimbra
FOLIA ZOOLOGICA - Czechoslovak Academy of Sciences
FUNCTIONS ET APPROXIMATIC COMMENTARI MATHEMATICI - Poznań
GLASNIK MATEMATICKI - Zagreb
IBC - INFORMAZIONI - Rivista Bimestrale Inst. Beni. Artistic. - Regione Emilis-Romagna
INSTITUTO DE MATEMATICA - Univ. Nac. del Sur - Bahia Blanca - Argentina
INSTITUTO NACIONAL DE INVESTIGAÇAO AGRARIA - Estaçao AGRONOMICA NACIONAL OEIRAS INSTITUTO SUPERIOR TÉCNICO DE CIENFUEGOS
INTERNATIONAL TIN RESEARCH INSTITUTE
JAHRBUCH DER AKADEMIE DER WISSENSCHAFTEN IN GÖTTINGEN.
JOURNAL OF THE AMERICAN ACADEMY OF ARTS AND SCIENCES - Daedalus
JOURNAL OF THE BULGARIAN ACADEMY OF SCIENCES
JOURNAL OF THE LONDON MATHEMATICAL SOCIETY
JOURNAL OF NON-CRYSTALLINE SOLIDS - Amsterdam
LESTURAS MATEMATICAS - Colombia
MATHEMATICA BALKANICA
MATHEMATICA MONTISNIGRA
MEMORABILIS ZOOLOGICA
MEMORANDA SOCIETATIS PROFAUNA ET FLORA FENNICA - Helsingfors
MEMORIAS DA ACADEMIA DAS CIENCIAS DE LISBOA (Classe de Ciencias)
MITTEILUNGEN AUS DEN ZOOLOGISCHEN MUSEUM IN BERLIN

MONOGRAFIAS DE LA ACADEMIA NACIONAL DE CIENCIAS EXACTAS, FISICAS Y NATURALES DE BUENOS AIRES
NACHRICHTEN DER AKADEMIE DER WISSENSCHAFTEN IN GUTTINGEN - II Matemáticas y Física
NATURAL HISTORY MUSEUM UNIV. OF KANSAS.
NEOTROPICO - Museo Nacional de Costa Rica
NETHERLANDS JOURNAL OF ZOOLOGY
NONLINEARITY - Inst. Physics and London Math. Soc
NOTAS DE ALGEBRA Y ANALISIS - Ins. de Matematica - Univ. Atac. del Sur. Bahia Blanca
NOTULAE NATURAE
NUCLEAR ENERGY -Bulgarian Academy of Sciences
OCCASIONAL PAPERS OF THE CALIFORNIA ACADEMY OF SCIENCES - San Francisco
PHILIPPINE JOURNAL OF SCIENCES - Manila
POLISH ACADEMY OF SCIENCES. INSTITUTE OF MATHEMATICA
POLSKA AKADEMIE NAUK-PRACE GEOLOGICZNE
POLSKA AKADEMIE NAUK-PRACE MINERALOGICZNE
PORTUGALIA PHYSICA - Sociedade Portuguesa de Física
PROCEEDINGS OF THE ACADEMY OF NATURAL SCIENCES OF PHILADELPHIA
PROCEEDINGS OF THE CALIFORNIA ACADEMY OF SCIENCES
PROCEEDINGS OF THE LONDON MATHEMATICAL SOCIETY
PROCEEDINGS OF THE ROCHESTER ACADEMY OF SCIENCES
PROCEEDINGS OF THE ROYAL SOCIETY OF LONDON - A: Mathematical and Physical Sciences
PROCEEDINGS OF THE ROYAL SCOIETY OF EDINBURGH - Section A (Mathematical and Physical Sciences)
PROCEEDINGS OF THE ROYAL SOCIETY OF QUEENSLAND
PUBLICACIONES FUNDAMENTALES DE LA ACADEMIA DE CIENCIAS DE SOFIA
PUBLICATION DE L'INSTITUT DE RECHERCHE MATHEMATIQUE AVANCEE - Strasbourg
PUNIME MATEMATIKE - Prishtine
QUADERNI DELL' ACADEMIA UDINESA.
QUATERLY OF APPLIED MATHEMATICS
REVISTA CUBANA DE FISICA
REVISTA COLOMBIANA DE MATEMÁTICAS

REVISTA DE LA FACULTAD DE INGENIERIA QUIMICA- Univ. Nal. del Litoral - Argentina
REVISTA TRIMESTRAL DEL INTERNATIONAL TIN RESEARCH INSTITUTE
REVISTA UNIVERSIDAD NACIONAL DE LA PLATA - Argentina
REVISTA DE LA UNION MATEMATICA ARGENTINA
REZIMEA ABSTRACS - POGDORICA
SCIENCE BULLETIN - University of Kansas
SCIENTIFIC PAPERS NAT. HISTORY MUSEUM. The University Kansas.
SEARCH AGRICULTURAL ITHACA NEW YORK
SENCKENBERGIANA BIOLOGICA - Frankfurt
SENCKENBERGIANA LETHAEA - Frankfurt
SMITHSONIAN CONTRIBUTIONS TO PALEONTOLOGY
SPECTRUM - Akademie der Wissenschaften der DDR
STUDIA GEOLOGICA POLONICA - Polska Akademy Nauk Warsovia
SUT JOURNAL OF MATHEMATICS - Science University of Tokio
T. KOSCIUSZKI TECHNICAL - Univesity of Cracow
UNIVERSIDAD NACIONAL DE LA PLATA - Notas del museo de la Plata
UNIVESITY OF THE STATE OF NEW YORK - Bulletin
UNIVERSITY OF KANSAS PALEONTOLOGICAL CONTRIBUTIONS
VERTEBRATOLOGICKE ZPRAVY CESKOLOVENSKA AKADEMIE BRNO
ZBORNIK RADOVA FILOZOFSKOG - Fakulteta u Nisu-Serija Matematika
ZBORNIK - Acta Musei Nationalis - Pragae
ZOOLOGICA POLONIAE
ZPRAVY USEB (Vertebralogy zpravy) - Brno - Checoslovaquia